AD-A058 807 NEWCASTLE-UPON-TYNE UNIV (ENGLAND) F/G 11/2
THE ROLE OF ADDITIVES IN THE DENSIFICATION OF NITROGEN CERAMICS--ETC(U)
NOV 77 K H JACK DA-ERO-76-G-067
UNCLASSIFIED NL
1 OF 2
AD A058 807

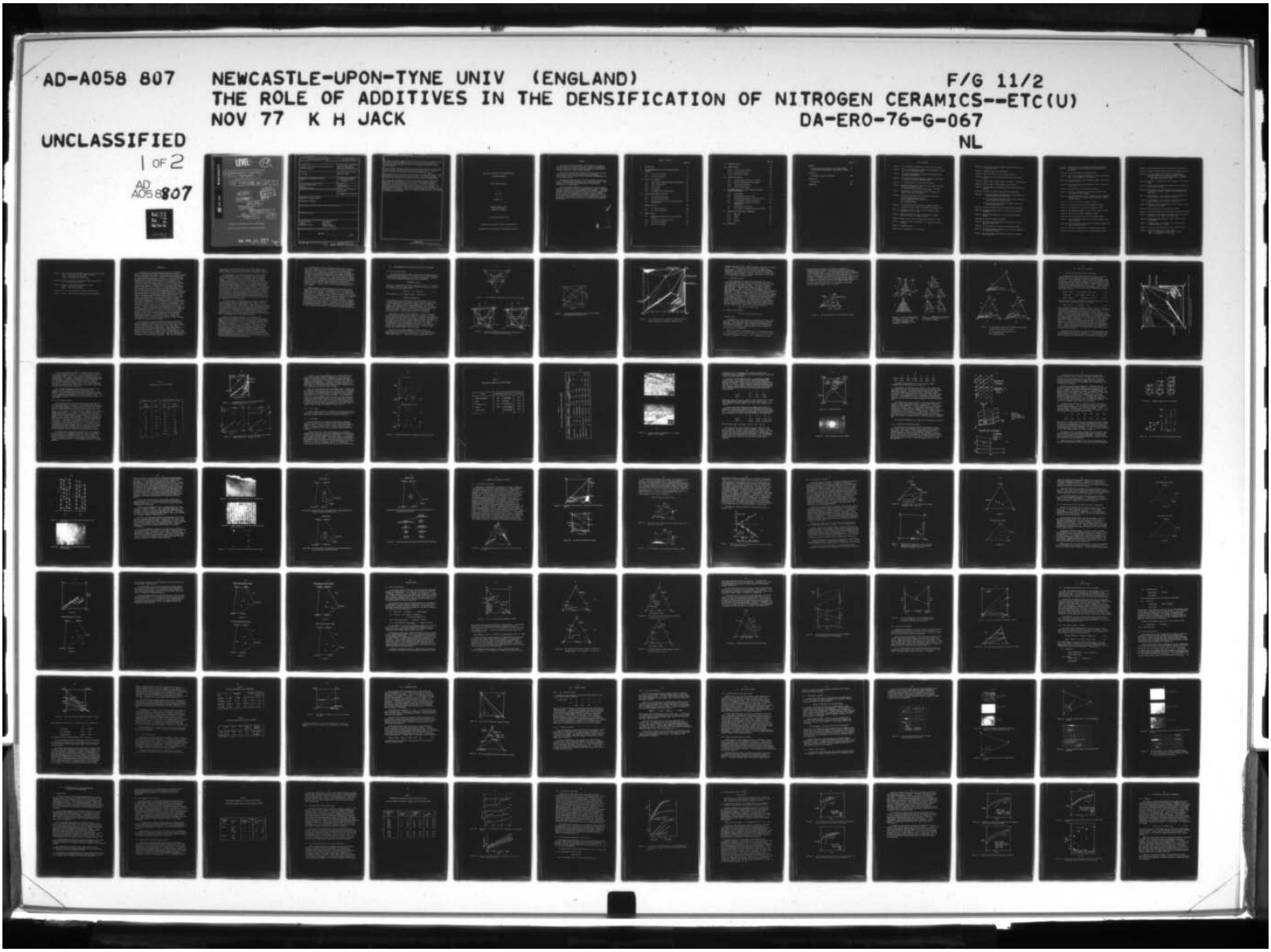

LEVEL II

12 SC

6 THE ROLE OF ADDITIVES IN THE Ddensification OF NITROGEN CERAMICS.

9 Final Technical Report. Apr - Oct 77,

by

10 K.H. JACK

11 NOV [redacted] 77

12 123p.

EUROPEAN RESEARCH OFFICE
United States Army
London W. 1, England

16 1T161102BH57

15 Grant Number DAERO-76-G-067

17 94

University of Newcastle upon Tyne, United Kingdom

UNCLASSIFIED
SECURITY CLASSIFICATION OF THIS PAGE (When Data Entered)

REPORT DOCUMENTATION PAGE		READ INSTRUCTIONS BEFORE COMPLETING FORM
1. REPORT NUMBER	2. GOVT ACCESSION NO.	3. RECIPIENT'S CATALOG NUMBER
4. TITLE (and Subtitle) THE ROLE OF ADDITIVES IN THE DENSIFICATION OF NITROGEN CERAMICS		5. TYPE OF REPORT & PERIOD COVERED FINAL TECHNICAL REPORT APRIL 77 - OCTOBER 77 6. PERFORMING ORG. REPORT NUMBER
7. AUTHOR(s) K. H. JACK		8. CONTRACT OR GRANT NUMBER(s) DAERO-76-G-067
9. PERFORMING ORGANIZATION NAME AND ADDRESS UNIVERISTY OF NEWCASTLE-UPON-TYNE U.K.		10. PROGRAM ELEMENT, PROJECT, TASK AREA & WORK UNIT NUMBERS 6.11.02A-1T161102BH57-04 00-596
11. CONTROLLING OFFICE NAME AND ADDRESS U.S.A. R&S GROUP (EUR) BOX 65 FPO NEW YORK 09510		12. REPORT DATE OCTOBER 1977 13. NUMBER OF PAGES 120
14. MONITORING AGENCY NAME & ADDRESS(if different from Controlling Office)		15. SECURITY CLASS. (of this report) UNCLASSIFIED 15a. DECLASSIFICATION/DOWNGRADING SCHEDULE

16. DISTRIBUTION STATEMENT (of this Report)
APPROVED FOR PUBLIC RELEASE

DISTRIBUTION UNLIMITED

17. DISTRIBUTION STATEMENT (of the abstract entered in Block 20, if different from Report)

18. SUPPLEMENTARY NOTES

19. KEY WORDS (Continue on reverse side if necessary and identify by block number)

Silicon Nitride	Hot Pressing
Sialons	Sintering
Nitrogen Ceramics	Phase Diagrams
	Crystal Structures

20. ABSTRACT (Continue on reverse side if necessary and identify by block number)

SEE OVER

DD FORM 1 JAN 73 1473 EDITION OF 1 NOV 65 IS OBSOLETE

78 08 11 021

UNCLASSIFIED
SECURITY CLASSIFICATION OF THIS PAGE (When Data Entered)

The role of additives magnesia, yttria, ceria and zirconia in the densification of silicon nitride and β-sialon is investigated with the objective of improving the high-temperature mechanical and chemical properties of these nitrogen ceramics.

Each of the oxide additions reacts with surface silica and some of the nitride to give an oxynitride liquid that promotes densification by the successive stages of particle rearrangement and solution-precipitation.

The changing contributions of the two stages with the amount and type of oxide, determines the extent of the α-β transformation. The kinetics of both pressureless sintering and hot-pressing are interpreted by a Kingery model.

The liquid phase responsible for desification cools to produce additional crystalline or vitreous phases that can impair the strength, oxidation resistance and creep resistance of the material. Behavior diagrams for each of the systems M-Si-O-N and M-Si-Al-O-N where M is Mg, Y, Ce and Zr are presented and discussed in order to suggest ceramic processing methods that avoid property degradation. So-far, no nitrogen ceramic has been obtained with a combination of properties suitable for engineering applications in an oxidising environment at above 1400°C.

THE ROLE OF ADDITIVES IN THE DENSIFICATION OF NITROGEN CERAMICS

Final Technical Report

by

K.H. JACK

NOVEMBER 1977

EUROPEAN RESEARCH OFFICE
United States Army
London W. 1, England

Grant Number DAERO-76-G-067

University of Newcastle upon Tyne, United Kingdom

ABSTRACT

The role of additives magnesia, yttria, ceria and zirconia in the densification of silicon nitride and β'-sialon is investigated with the objective of improving the high-temperature mechanical and chemical properties of these nitrogen ceramics.

Each of the oxide additions reacts with surface silica and some of the nitride to give an oxynitride liquid that promotes densification by the successive stages of particle rearrangement and solution-precipitation.

The changing contributions of the two stages with the amount and type of oxide determines the extent of the α-β transformation. The kinetics of both pressureless sintering and hot-pressing are interpreted by a Kingery model.

The liquid phase responsible for densification cools to produce additional crystalline or vitreous phases that can impair the strength, oxidation resistance and creep resistance of the material. Behaviour diagrams for each of the systems M-Si-O-N and M-Si-Al-O-N where M is Mg, Y, Ce and Zr are presented and discussed in order to suggest ceramic processing methods that avoid property degradation. So-far, no nitrogen ceramic has been obtained with a combination of properties suitable for engineering applications in an oxidising environment at above 1400°C.

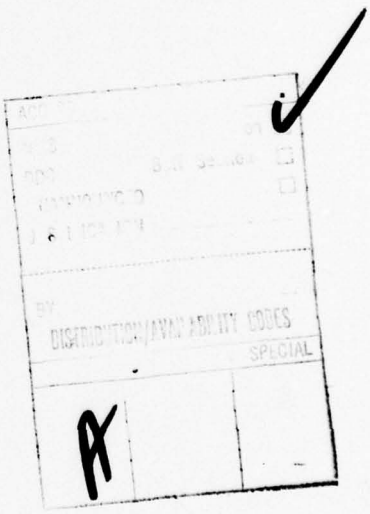

TABLE OF CONTENTS

LIST OF FIGURES

Figure 77 Weight gains for powder samples oxidised for 120h at 1000°C
left: hot-pressed with 5w/o SiO_2 + 5w/o Y_2O_3
middle: hot-pressed with 2w/o MgO
right: hot-pressed with 17.5w/o Y_2O_3

Figure 78 The Si_3N_4 corner of the Y_2O_3-Si_3N_4-SiO_2 system showing 2, 5 and 10w/o surface silica

Figure 79 Si_3N_4 hot-pressed with 5w/o Y_2O_3:5w/o Al_2O_3
upper: after 120h at 1000°C
lower: after 120h at 1400°C

Figure 80 Si_3N:5w/o ZrO_2 oxidised for 120h at 1400°C (S.E.M.)

Figure 81 ZrN" oxidised for 120h at 1400°C (optical micrograph)

I. INTRODUCTION

In fabricating nitrogen ceramics the objective is to produce easily and economically a shaped component with high strength, oxidation resistance, negligible creep and good thermal shock properties all at temperatures above 1400°C. These different requirements are not always compatible and their combination - at least to the extent required by gas turbine applications - has not so far been achieved. Densification of silicon nitride whether by hot-pressing or by pressureless sintering requires an additive, the function of which, as will be shown in the present Report, is to provide conditions for liquid-phase sintering. Magnesium oxide, the first widely used additive, reacts with the silica that is always present as a surface layer on the silicon nitride powder to give what was thought (1) to be a silicate liquid near the $MgSiO_3$-SiO_2 eutectic composition and which on cooling gives a low softening-temperature glass. Impurities, particularly alkali and alkali-earth oxides, lower the glass viscosity still further and so the strength and creep resistance of the high-density, hot-pressed product decrease rapidly above 1000°C. It is now well established (2,3,4) that the liquid phase is an oxynitride. Indeed, bulk samples of nitrogen-glasses in the Mg-Si-O-N and Mg-Si-Al-O-N systems and in the corresponding yttrium systems have been prepared at Newcastle. Densification occurs by the three stages described by Kingery (5), that is, (i) particle rearrangement, (ii) solution-precipitation and (iii) coalescence, and the relative extents to which the first two contribute to densification vary with the additive. There is always some phase transformation of α-Si_3N_4 to β and although Weston & Carruthers (6) considered this to be independent of densification, Brook et al. (7) point out that removal of 30% porosity can be achieved by transport of as little as 15% of solid material so that only partial transformation α-β need accompany complete densification. In the present work it is shown that transformation occurs predominantly by solution of α-Si_3N_4 and precipitation of β. It does not occur during the initial rearrangement stage of the densification process.

With yttria as a hot-pressing additive a Y-Si-O-N liquid also allows liquid-phase densification with α-β transformation, but the improved properties of the product (8) are due to the further reaction of the liquid with silicon nitride to give one or more highly refractory grain-boundary bonding phases. These can accommodate in solid solution the impurities which would otherwise form a low softening-point glass (9). Again, however, one advantage is at the expense of another, and some compositions of the high-strength, creep-resistant silicon nitride hot-pressed with yttria fail catastrophically at 900-1200°C in an oxidising environment. The extensive cracking

that occurs is shown (10,11,12) to be due to the oxidation of the grain-boundary yttrium-silicon oxynitrides to give oxides with a markedly different specific volume to that of the starting material.

The requirements for complete densification by liquid-phase sintering are agreed (5) as (i) an appreciable amount of liquid; (ii) an appreciable solubility of the solid; and (iii) complete wetting. In the case of silicon nitride the rate of material transport occurring by solution of α and precipitation of β will depend upon the difference in solubility of the two forms and hence upon the free energy change, $\Delta G(\alpha-\beta)$. For different additives and the same hot-pressing sequence, the onset of densification should depend mainly on the temperature of liquid formation. The subsequent rate of densification might then be expected to vary with the amount of liquid, the solubility of silicon nitride in the liquid, and the value of $\Delta G(\alpha-\beta)$. With different additives the degree of wetting by the liquid and its viscosity might well be different, and it should also be noted that the liquid characteristics and composition will vary with time and temperature, with the effectiveness of mixing and the initial distribution of the additive, and with the particle size and reactivity of the mixed powders.

For densification, an externally applied pressure increases the extent and rate of particle rearrangement and is additive to the effective pressure derived from capillary forces (13). Thus, the above considerations should apply equally to the pressureless sintering of silicon nitride except, of course, that rates of densification will be correspondingly lower than for hot-pressing under otherwise similar conditions. In the densification of sialons compared with silicon nitride, whether by hot-pressing or by pressureless sintering, the general difference is in the more extensive formation of liquid phases and in the increased free energy change, $\Delta G(\alpha-\beta')$.

The aims of the present work are: (i) to explore the densification and subsequent heat-treatment of silicon nitride with magnesia and yttria additives in order to improve its high-temperature mechanical and chemical properties; (ii) to explore additives other than magnesia and yttria; and (iii) to investigate the role of additives in the densification of β'-sialons. During the current Report period it has been shown that the kinetics of densification with magnesia and yttria, both by hot-pressing and pressureless sintering of silicon nitride and β'-sialon are compatible with a liquid-phase mechanism. Considerable progress has also been made towards understanding the behaviour of ceria and zirconia additives and preliminary work has been carried out with the cooperation of the Lawrence-Livermore Laboratories, University of California, on additions of beryllia and beryllia-magnesia mixtures.

All additives to silicon nitride and sialons react to produce additional crystalline or vitreous phases in the product that can, in some cases, impair properties. The prevention of this material degradation by suitable processing requires a detailed knowledge of the phase limits and phase relationships over a range of temperature for each of the appropriate systems M-Si-O-N and M-Si-Al-O-N where the metal M is Mg, Y, Ce, Zr or Be. The Si-Al-O-N behaviour diagram is basic to the understanding of reactions involving silicon nitride and β'-sialons and so some effort has also been directed towards the investigation of incompletely explored regions of this system. Finally, attempts have been made, so-far without success, to produce "carbon sialons" - phases in the Si-Al-O-N-C system containing all five elements.

Standard methods of powder preparation and mixing are used and the pseudo-isostatic method of hot-pressing with boron nitride as a powder vehicle has previously been described (14). For pressureless sintering and heat-treatment, a cold-pressed cylindrical pellet of the appropriate mix is embedded in boron nitride and heated in pure nitrogen using electrical furnaces with either tungsten, molybdenum or graphite resistance elements. The main techniques used for phase characterization are X-ray diffraction, optical microscopy, scanning and transmission electron microscopy including direct lattice imageing, and electron probe micro-analysis. In addition to following density changes during processing, the main properties examined in the products are oxidation resistance, high-temperature creep and thermal expansion in order to assess potentialities for engineering ceramic applications.

II. THE REPRESENTATION OF Si-Al-O-N and M-Si-Al-O-N SYSTEMS

II.1 The Si-Al-O-N system

The Si-Al-O-N system with four components can be represented by a regular tetrahedron (Figure 1) each of the vertices of which correspond to one atom (or one gram-atom) of the respective elements. A point within the tetrahedron represents one atom of composition

$$Si_{\underline{a}}Al_{\underline{b}}O_{\underline{c}}N_{1-(\underline{a}+\underline{b}+\underline{c})}$$

However, if the elements have fixed valencies Si^{IV}, Al^{III}, O^{II} and N^{III}, one degree of freedom is lost because the sum of the positive valencies must equal that of the negative ones

$$4\underline{a} + 3\underline{b} = 2\underline{c} + 3(1-\underline{a}-\underline{b}-\underline{c}) \qquad .... (1)$$

The composition of any condensed phase is then given by

$$Si_{\underline{a}}Al_{\underline{b}}O_{3-7\underline{a}-6\underline{b}}N_{6\underline{a}+5\underline{b}-2}$$

It is defined by only two variables $\underline{a}$ and $\underline{b}$ and always lies on the irregular quadrilateral plane shown in Figure 2(a) that cuts the edges of the tetrahedron at the compositions $SiO_2/3$, $Al_2O_3/5$, AlN/2 and $Si_3N_4/7$; the system becomes a pseudo-ternary one. The irregular quadrilateral representation has been used recently (15) to illustrate phase relationships but it is inconvenient for plotting compositions and a much simpler representation is obtained by expressing concentrations not in atoms or gram-atoms but in equivalents.

Each corner of the Si-Al-O-N tetrahedron is then one equivalent of an element and, because one equivalent of any element or compound always reacts with one equivalent of any other species, the compositions of the compounds Si_3N_4, AlN, Al_2O_3 and SiO_2 - expressed in equivalents - are located at the mid points of the tetrahedron edges; see Figure 2(b). The square obtained by joining these mid-points is the simplest representation of the Si_3N_4-AlN-Al_2O_3-SiO_2 system; see Figure 3. It is convenient, although not mandatory, to let the bottom, left-hand corner of the square represent one mol of Si_3N_4; the other three corners then represent Al_4N_4, Al_4O_6 and Si_3O_6.

Any point on the square diagrams of Figures 3 and 4 is a combination of 12+ve and 12-ve valencies, i.e. it is convenient to regard compounds in ionic terms even though the interatomic bonding is predominantly covalent. In going from left to right, $3Si^{4+}$ is

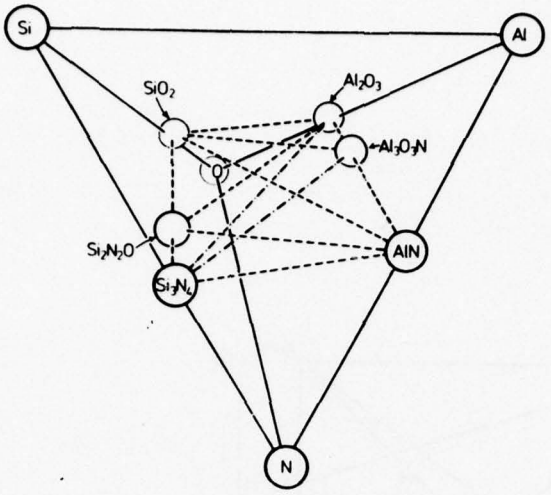

Figure 1. The tetrahedral representation of the Si-Al-O-N system

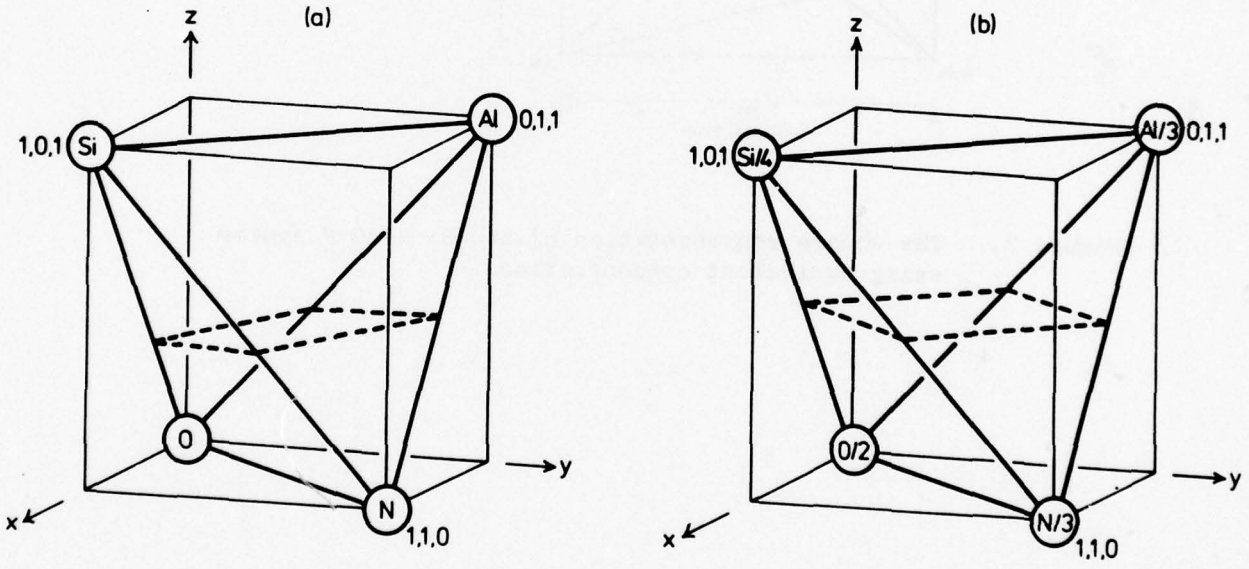

Figure 2. Si-Al-O-N tetrahedra with corners (a) represented in atomic units and (b) equivalent units

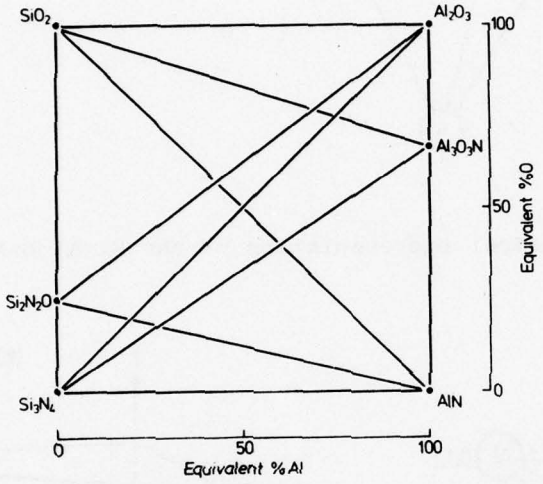

Figure 3. The square representation of the Si-Al-O-N system using equivalent concentrations

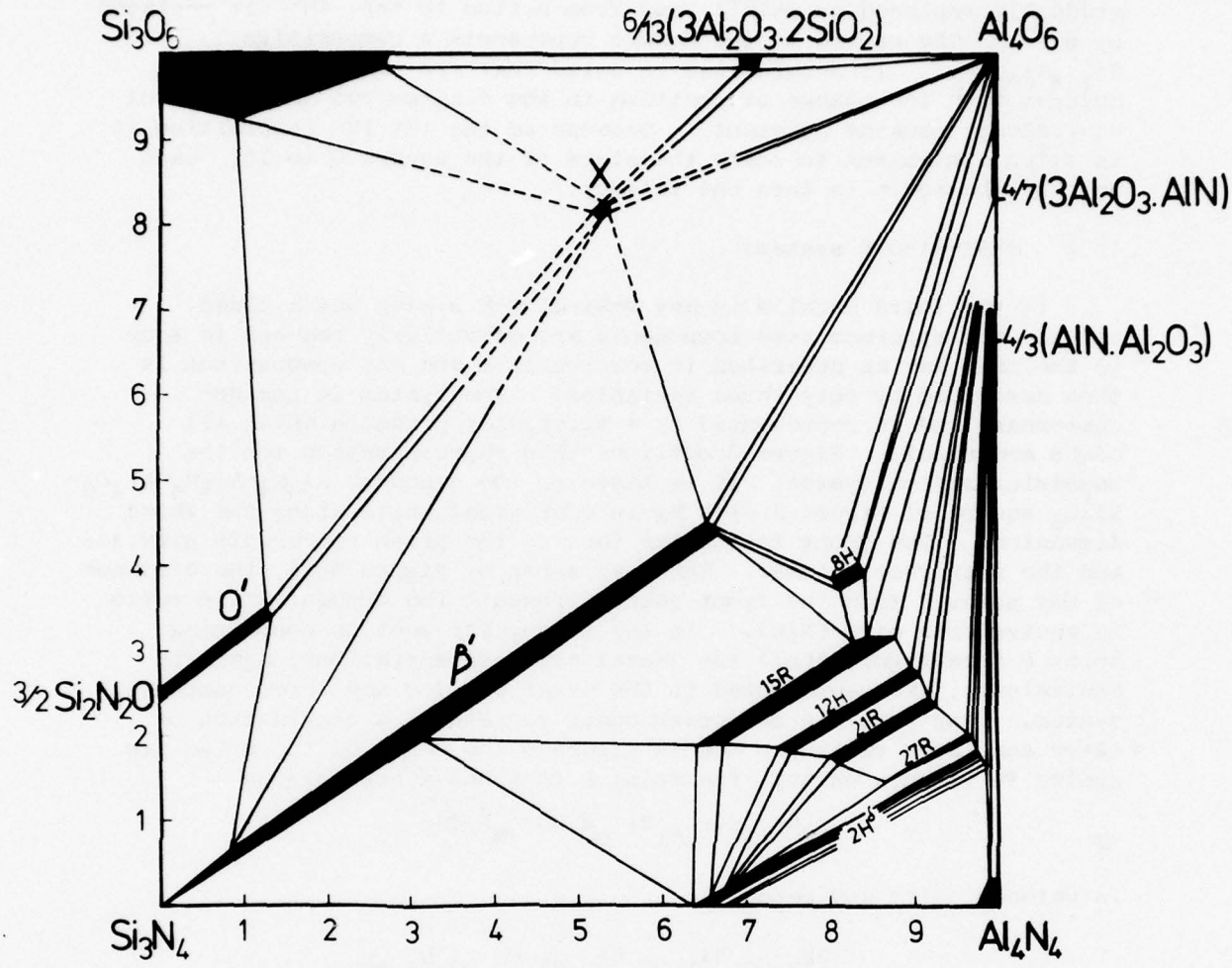

Figure 4. The Si_3N_4-AlN-Al_2O_3-SiO_2 behaviour diagram at 1750°C based on research at Newcastle (December 1976)

gradually replaced by $4Al^{3+}$; and from bottom to top, $4N^{3-}$ is replaced by $6O^{2-}$. The centre of the square represents a composition $Si_{1.5}Al_2O_3N_2$. It should also be noted that the number of atoms changes with the change of position in the diagram but the number of equivalents remains constant. Because of the $12^+:12^-$ composition it is often convenient to scale the sides of the square 0 to 12; each unit of the scale is then one valency.

II.2 M-Si-Al-O-N systems

If the third metal M in any M-Si-Al-O-N system has a fixed valency the apparent five components are effectively reduced to four in the same way as described in section II.1 and any composition is then described by only three variables. The system is pseudo-quaternary and is represented by a triangular prism in which all edges are equal. Figure 5 outlines this representation for the magnesium-sialon system; it is based on the standard Si_3N_4-Al_4N_4-Al_4O_6-Si_3O_6 square of Figure 3 with Mg in equivalent units along the third dimension. The front triangular face of the prism represents nitrides and the rear face oxides. Thus, as shown by Figure 6(a), the distance of any point P from the front face represents the concentration ratio in equivalents of O/(N+O). In the triangular section containing point P (see Figure 6(b)) the metal atom concentrations, again in equivalents, are represented in the usual way for any three-component system. Any point in the prism again represents a combination of 12+ve and 12-ve valencies and in Figure 6 the edges of the prism are scaled in valency units; the point P thus has a composition

$$Mg^{6+}\ Si^{4+}\ Al^{2+}\ O^{6.60-}\ N^{5.40-}$$

in valency units and hence

$$Mg_{3.00}\ Si_{1.00}\ Al_{0.67}\ O_{3.30}\ N_{1.80}$$

in atomic units.

In the Mg-Si-Al-O-N system each of the phases of the basal square plane extends into the prism volume, often along planes of constant M:X value. Such planes cut other triangular planes representing pseudo-ternary sub-systems. Thus in Figure 5 the 3M:4X plane cuts the plane of the Mg_6O_6:Si_3N_4:Al_4O_6 sub-system along a single line joining Si_3N_4 with $3/2(MgAl_2O_4)$.

Other sub-systems (i) Si_3N_4:Y_2O_3:Al_2O_3, (ii) Si_3N_4:Y_2O_3:"Al_3O_3N", (iii) Si_3N_4:Y_2O_3:AlN and the 2M:3X and 3M:4X planes of the Y-Si-Al-O-N system are illustrated by Figure 7. The investigation of a whole

system requires exploration of different sub-systems the representations of which are subsequently integrated to give the complete triangular prism. The sub-systems are therefore depicted by appropriately shaped triangles with compositions shown in equivalent units. Alternatively, any sub-system can be represented by an equilateral triangle with compositions in either mol per cent or weight per cent. To avoid confusion it is essential that the corners of triangles and the diagrams themselves are marked appropriately and, as an example the Y_2O_3-Si_3N_4-Al_2O_3 behaviour diagram showing glass formation after heating to 1900°C is represented in the three different ways by Figures 8(a), (b) and (c).

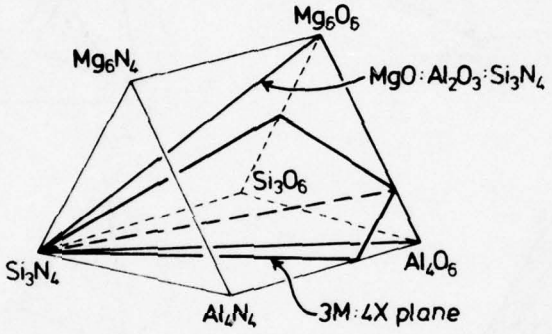

Figure 5. The representation of the Mg-Si-Al-O-N system

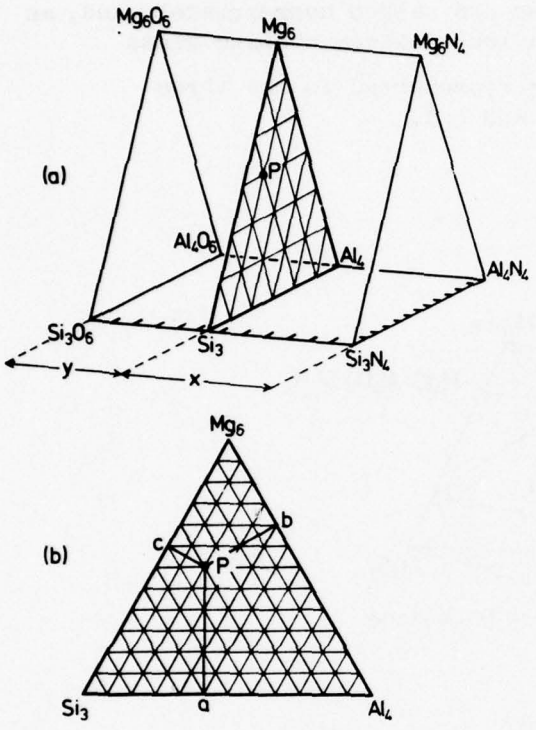

Figure 6. Method of representing a composition by a point within the M-Si-Al-O-N triangular prism. (P represents $Mg_{3.00}Si_{1.00}Al_{0.67}O_{3.30}N_{1.80}$; see text)

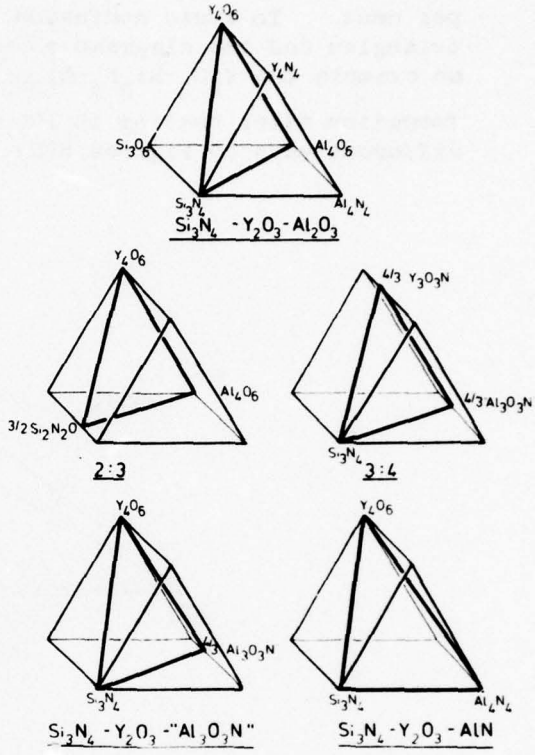

Figure 7. Representative sub-systems and planes of constant M:X value in the Y-Si-Al-O-N system

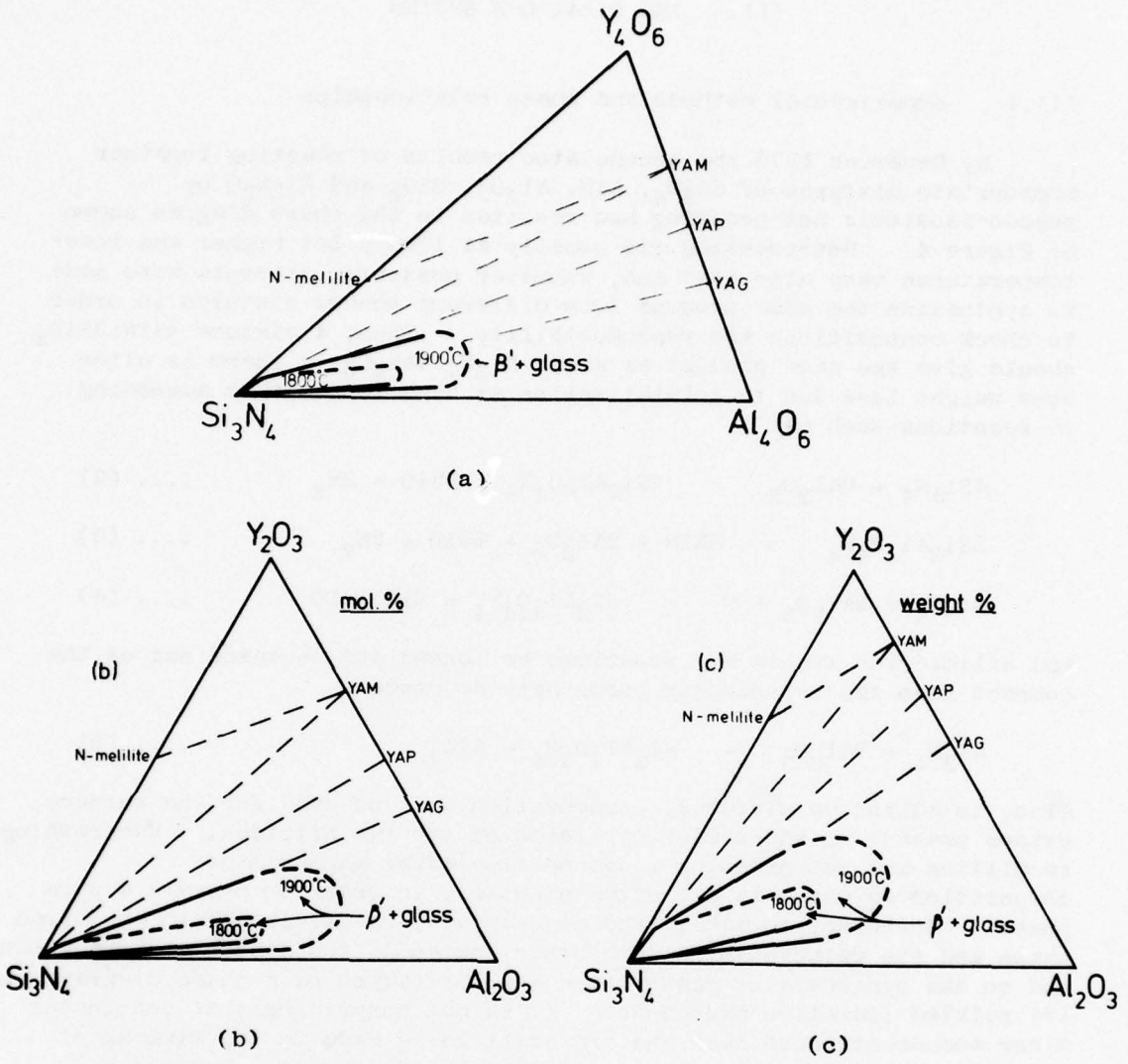

Figure 8. The Y_2O_3-Si_3N_4-Al_2O_3 behaviour diagram showing glass formation after heating to 1900°C

(a) in equivalent concentration units
(b) in mol per cent
(c) in weight per cent

III. THE Si-Al-O-N SYSTEM

III.1 Experimental methods and phase relationships

By December 1976 the accumulated results of reacting together appropriate mixtures of Si_3N_4, AlN, Al_2O_3, SiO_2 and Si_2N_2O by pseudo-isostatic hot-pressing had resulted in the phase diagram shown by Figure 4. Hot-pressing was usually at 1750°C but higher and lower temperatures were also used and, whenever possible, attempts were made to synthesise the same product from different powder mixtures in order to check compositions and reproducibility. Thus, a mixture $4AlN:3SiO_2$ should give the same product as a mix $Si_3N_4:2Al_2O_3$. There is often some weight loss due to volatilisation at high temperature according to reactions such as:

$$4Si_3N_4 + 6Al_2O_3 = 3Si_2Al_4O_4N_4 + 6SiO + 2N_2 \quad .... (2)$$

$$3Si_2Al_4O_4N_4 = 8AlN + 2Al_2O_3 + 6SiO + 2N_2 \quad .... (3)$$

$$Si_3N_4 + 2Al_2O_3 + C = Si_2Al_4O_4N_4 + SiO + CO \quad .... (4)$$

and silica-rich liquid may sometimes be formed and squeezed out of the compact into the surrounding boron nitride powder:

$$Si_3N_4 + 2Al_2O_3 = Si_2Al_4O_4N_4 + SiO_2 \quad .... (5)$$

Also, in making up mixtures, compensation must be made for the surface oxides present on the powder particles of the two nitrides. Re-crushing, re-milling and hot-pressing a second time after making minor composition adjustments are often necessary in order to prepare a pure phase. Moreover, to make these adjustments, the limits of the required phase and its relationships with other phases in the system must be known, and so the synthesis of sialons and the derivation of a phase diagram are related iterative processes. It is not surprising that continuous minor amendments have been and are still being made to the diagram of Figure 4. It should be emphasized that the latter is a behaviour diagram for the particular experimental conditions used at Newcastle and it is not claimed to be an equilibrium diagram in a thermodynamic sense. However, calculations by Torre & Mocellin (16) suggest that it is at least self-consistent and compatible with equilibrium at one atmosphere total pressure.

The most recent revision of the Si-Al-O-N behaviour diagram based on Newcastle data (17) is given by Figure 9. It is essentially the same as Figure 4 except for the locations and limits of sialon-X-phase, sialon-O'-phase and the $2H^{\delta}$-polytype; tie-lines are also modified.

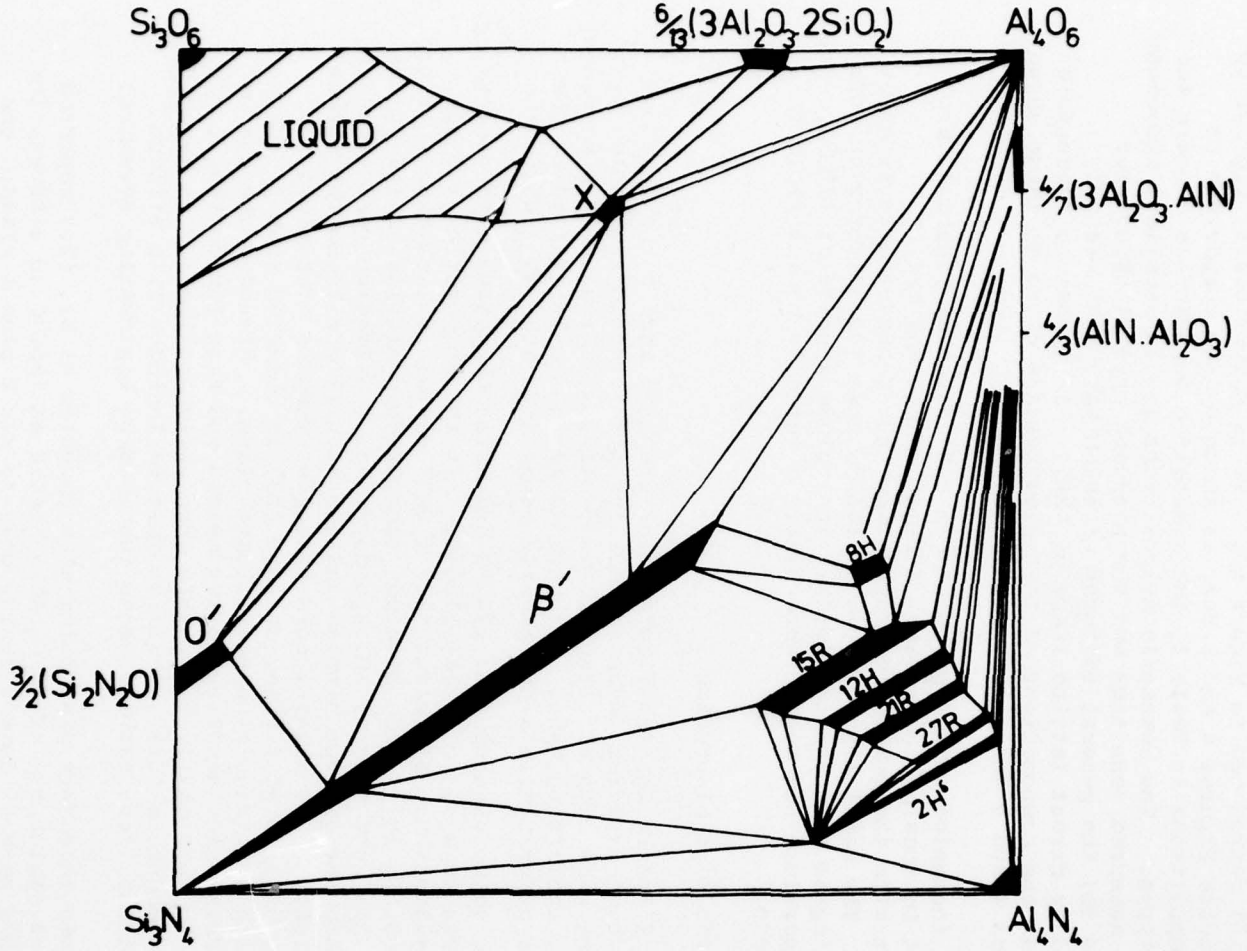

Figure 9. The Si_3N_4-AlN-Al_2O_3-SiO_2 behaviour diagram at 1700°C modified by recent research at Newcastle (September 1977)

The only other reasonably complete diagram is that by Gauckler et al. (18) reproduced as Figure 10. It is superficially similar to the Newcastle Figures 4 and 9 but, as shown by the comparison of phase compositions in Table 1, the greatest discrepancies concern the AlN-polytypes. The Newcastle compositions are in excellent agreement with the measured densities and the proposed crystal structures (19; see 20) the general features of which have been recently confirmed by direct lattice imageing (21). It is beyond reasonable doubt that the compositions of the polytypes are close to those shown by Figures 4 and 9 and not by Figure 10.

The incomplete diagrams by Layden (22) given as Figure 11 are important in showing the extent of liquid phase and are in agreement with the Newcastle observation that X-phase melts at about 1720°C. The small liquid field at 1650°C near the silica-rich corner of the diagram extends considerably to include X-phase at 1750°C. At this temperature and above there exists a large two-phase field of β' plus liquid.

III.2 The β'-sialon phase

The β'-phase was the first sialon prepared and is the only one that has been explored in any detail for its technological potential. It has the same crystal structure as β-silicon nitride with a hexagonal unit cell containing M_6X_8. It extends along the 3M:4X line of the behaviour diagram with a homogeneity range $Si_{6-z}Al_zO_zN_{8-z}$ where the maximum z value exceeds 4 at 1750°C and which decreases with decreasing temperature to about z = 2 at 1450°C. At the composition z=3 the thermal expansion coefficient (2.7×10^{-6} per°C) is less than that of β-Si_3N_4 (3.5×10^{-6}) and, although thermal conductivity is lower, the material has good thermal shock properties. Oxidation resistance is better than for silicon nitride and compatibility with molten metals is excellent. The highest cold strength (modulus of rupture $\simeq$ 190,000 psi) found for any ceramic (23) is observed with β'-sialon bonded with a yttrium alumino-silicate glass. Although the use of such materials for handling molten metals and also for cutting tools is probably more easily realisable than their application to ceramic turbine components (24), β'-sialon must be included with silicon nitride and silicon carbide among the leading engineering ceramics.

It was therefore disturbing when Gauckler et al. (25) reported that a z=4 sialon mix of $2SiO_2$:4AlN heated at 1950°C in nitrogen for two minutes gave β' corresponding only to $z \simeq 2$ plus a glass; the product on subsequent treatment at 1300°C for 8 hours consisted of mullite, alumina, two different AlN-polytypes, an unknown phase, and a greatly reduced amount of β'. This suggested that z=4 β' is highly unstable.

Table 1

Compositions of Si-Al-O-N Phases

Gauckler et al. (1975)		Newcastle research (1976)	
phase designation	M:X ratio	M:X ratio	phase designation
β'	3:4	3:4	β'
-	-	2:3	O'
X_1	8:13	8:13	X
X_4	3:4	4:5	8H
X_2	4:5	5:6	15R
X_5	5:6	6:7	12H
X_6	6:7	7:8	21R
-		9:10	27R
X_7	8:9	> 9:10	2H δ

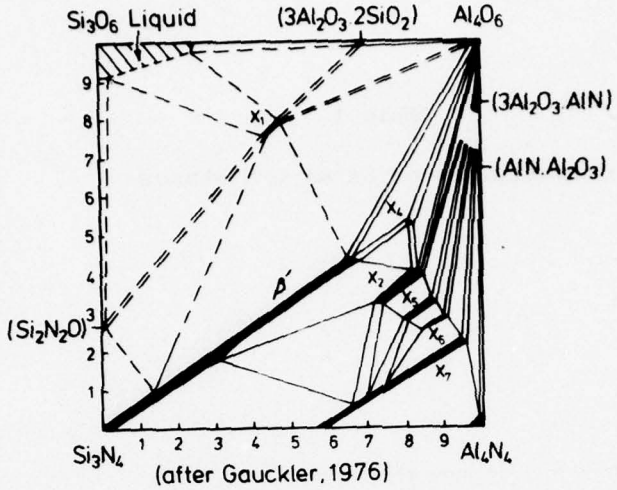

Figure 10. Isothermal section of the Si-Al-O-N system at 1760°C (Gauckler et al., Ref. 18)

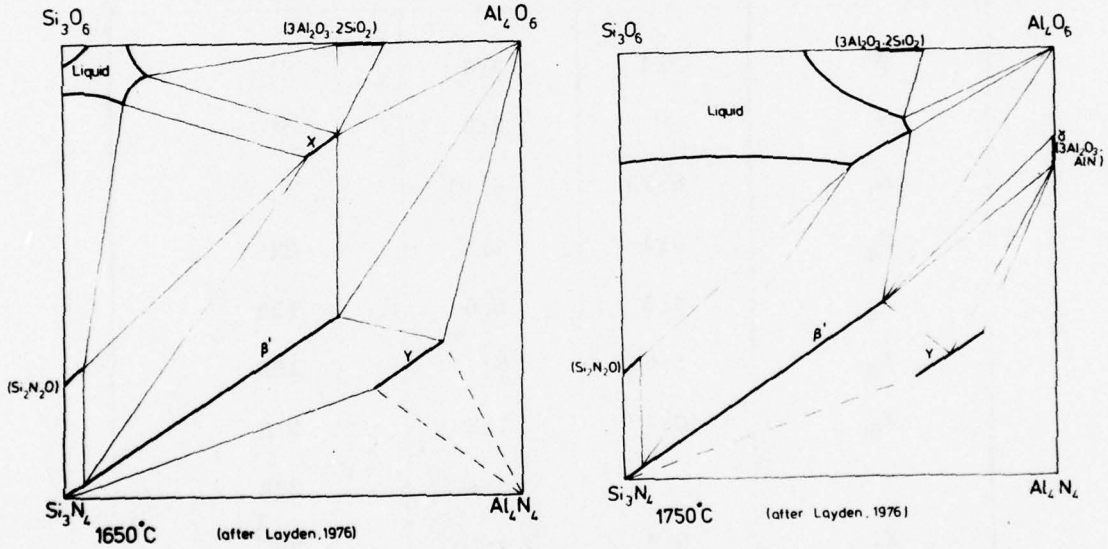

Figure 11. Phase diagram for the Si-Al-O-N system (a) at 1650°C and (b) at 1750°C; (Layden, Ref. 22)

In order to check these observations, hot-pressed blocks of β' (z=3.8) were heated at different temperatures in the range 1900°-2200°C for two minutes in static nitrogen in a graphite resistance furnace. Similar blocks of β-silicon nitride were given identical treatments for comparison. The results of Figure 12 show that β' is stable under the experimental conditions up to 2000°C whereas β is carburized to silicon carbide below 1900°C and then decomposes above this temperature to give silicon and nitrogen.

Products of the decomposition of β' between 2000° and 2200°C are the successive polytypes 15R, 21R, 27R and finally AlN. The results are explained by the volatilisation of silicon monoxide and nitrogen which agrees with observations (26) that these are the major vapour-phase species ($p_{SiO} \simeq 3p_{N_2} \simeq 10^{-2}$atm at 1725°C). The discrepancies between the work at Newcastle and by Gauckler et al. are resolved by an even more recent report (Gauckler, 27) that the apparent thermal decomposition of β' was, in fact, a reaction between finely divided β' powder with major amounts of silica impurity; the formation of a silica-rich glass under these circumstances is exactly what might be expected from the behaviour diagrams of Figures 4 and 9.

III.3 The O'-phase

Figure 9 suggests that the O'-phase with the structure of silicon oxynitride, Si_2N_2O, extends along the 2M:3X line towards Al_2O_3 to an even more limited extent than shown by the earlier Figure 4.

III.4 The X-phase

Sialon X-phase was first reported independently by Oyama & Kamigaito (28) and by Jack & Wilson (29) as a minor phase formed together with β' by reacting together silicon nitride and alumina at 1700°C. As shown in Tables 2 and 3 different compositions and several interpretations of its X-ray diffraction pattern have been proposed.

In the present work, X-phase was prepared pure by reacting together SiO_2, Al_2O_3 and Si_3N_4 in the approximate weight proportions 45:45:10 under controlled conditions at 1600-1800°C. A silica-rich liquid phase forms above 1600°C (see Figures 9 and 11) and complete melting occurs at about 1720°C. Optical micrographs of the products show oriented acicular lamellae when cooled from above the melting temperature ("High-X") and larger, more equiaxed crystals when cooled from below the melting temperature ("Low-X"); see Figure 13. Electron probe analyses of one "High-X" and two "Low-X" samples were

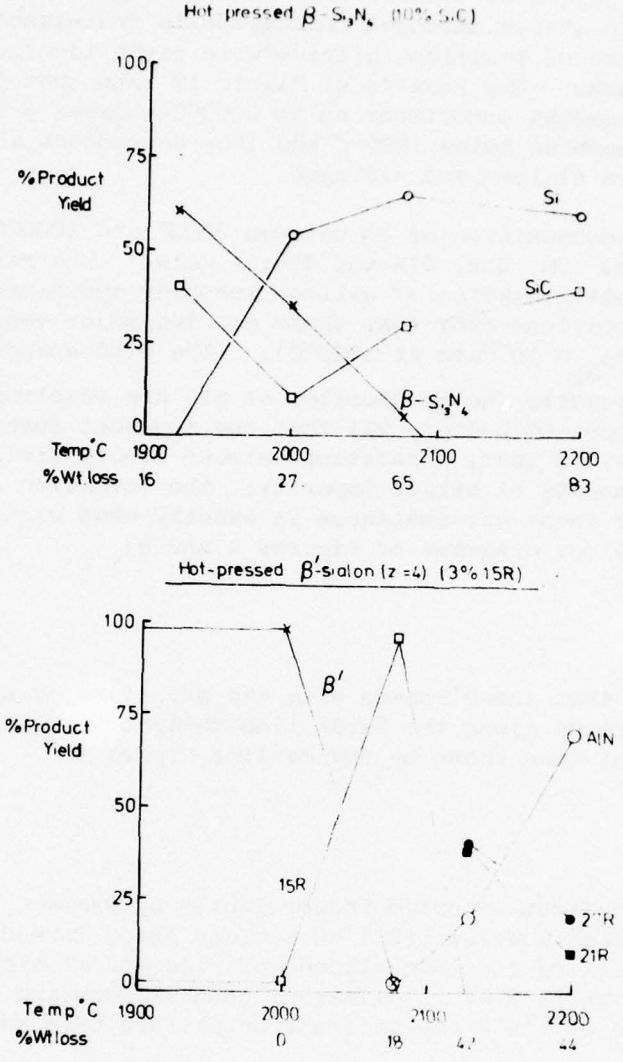

Figure 12. Thermal stabilities of β-Si_3N_4 and β'-sialon (z=3.8)

Table 2

Compositions proposed for sialon X-phase

author	reference	composition	M:X ratio
Oyama & Kamigaito	(28)	$Si_6Al_6O_9N_8$	12:17
Jack	(30)	$SiAlO_2N$	2:3
Gauckler et al.	(18)	$Si_4Al_4O_{11}N_2$	8:13
Layden	(22)	$Si_3Al_6O_{12}N_2$	9:14
present work		$Si_7Al_9O_{23}N_3$	8:13

Table 3

Unit-cell dimensions proposed for sialon X-phase

author	reference	system	unit-cell dimensions					
			Angstroms			degrees		
			a	b	c	α	β	γ
Drew & Lewis	(31)	triclinic	9.9	9.7	9.5	109	95	95
Wild	(32)	orthorhombic	7.92	7.83	9.38	-	-	-
Gugel et al.	(33)	orthorhombic	7.85	9.12	7.965	-	-	-
Thompson & Jack	see (20)	monoclinic	9.728	8.404	9.572	-	109	-
present work	"High"	triclinic	9.658	2.842	11.167	90.0	124.4	98.5
	"Low"	triclinic	9.684	8.561	11.212	90.0	124.5	98.5

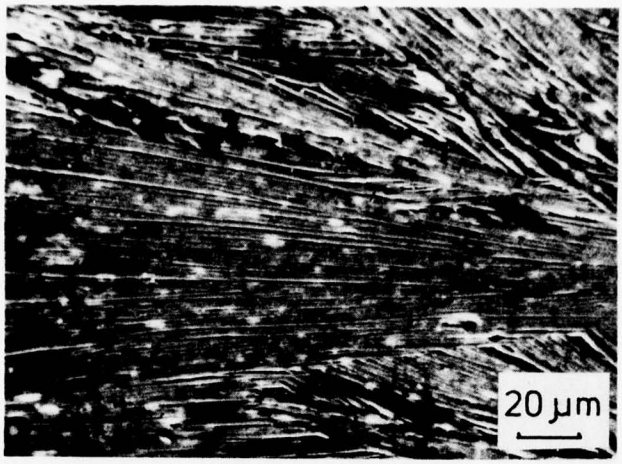

(a)

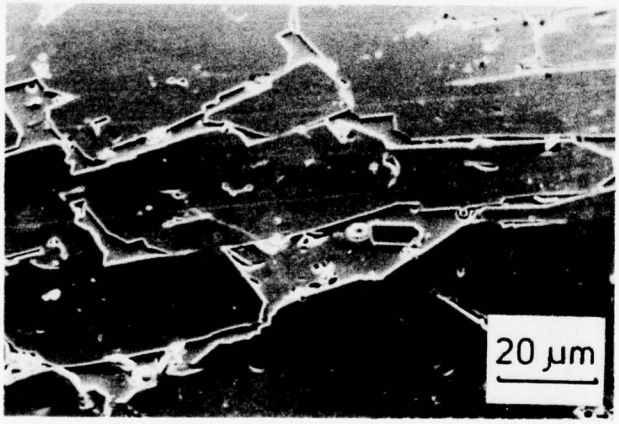

(b)

Figure 13. Scanning electron micrographs of (a) "High" and (b) "Low" X-phases

reasonably close to $Si_7Al_9O_{23}N_3$ but as shown by Figure 14 the considerable spread, particularly in the O:N ratio, makes it impossible to give a precise composition.

Individual lamellae were too small to be examined by single crystal methods but all lamellae in any one grain extinguished together under crossed polars; that is, they showed a high degree of preferred orientation. With the lamellae directions parallel to the rotation axis, "single crystal" rotation, oscillation and Weissenberg X-ray techniques became possible (see Figure 15) from which it was at first concluded that the unit cells were body-centred orthorhombic with dimensions:

	a	b	c
High-X	15.7	2.85	11.2Å
Low-X	47.1	8.55	11.2Å

Because $\underline{a}_L \simeq 3\underline{a}_H$ and $\underline{b}_L \simeq 3\underline{b}_H$, where L and H represent the "Low" and "High" modifications, the cells were obviously simply related. All the diffraction evidence suggested that "Low-X" was a superlattice of "High-X".

Precise powder data obtained by using Hägg-Guinier focussing cameras with monochromatic $CuK\alpha_1$ radiation then showed that the angle between the supposed orthogonal axes $\underline{a}$ and $\underline{c}$ was 91° and not precisely 90°. The more conventional cells corresponding to these body-centred, pseudo-orthorhombic cells are C-centred monoclinic with dimensions:

	a	b	c	β
High-X	19.11	2.842	11.17Å	124.8°
Low-X	57.46	8.560	11.211Å	124.9°

again with $\underline{a}_L \simeq 3\underline{a}_H$, $\underline{b}_L \simeq 3\underline{b}_H$, $\underline{c}_L \simeq \underline{c}_H$ and $\beta_L \simeq \beta_H$

The "High-X" unit cell contains two lattice points (i.e. two units of pattern) and "Low-X" contains eighteen. Finally, it was realised that the systematic absent reflexions for "Low-X", and indeed all the X-ray data, could be simply explained by a related smaller triclinic cell containing three units of pattern. The corresponding "High-X" may then be described by a triclinic sub-cell with the same axial directions as "Low-X" but with one-third of the $\underline{b}$ repeat distance:

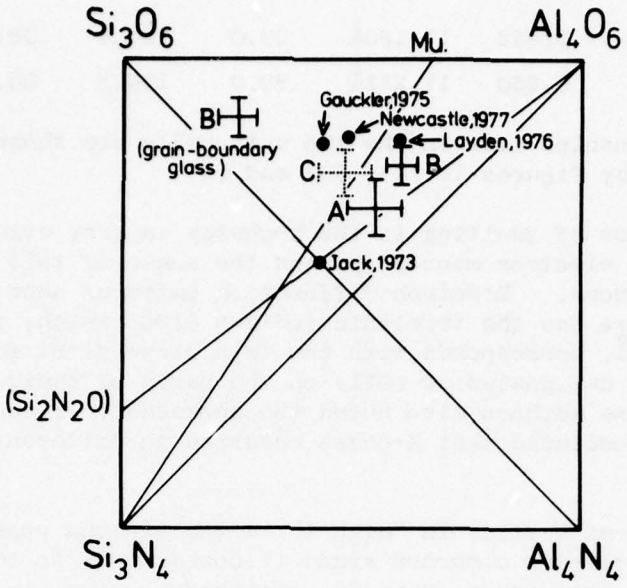

Figure 14. X-phase analyses

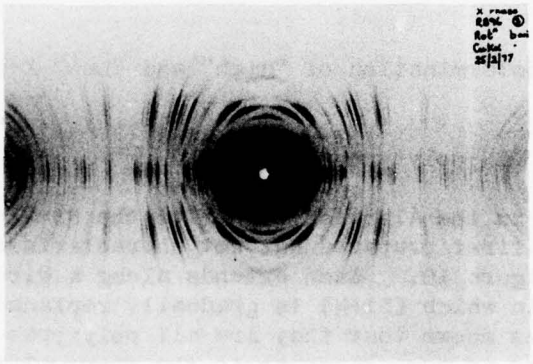

Figure 15. X-ray photograph of "Low" X-phase

	a	b	c	α	β	γ
High-X	9.658	2.842	11.168Å	90.0	124.4	98.5°
Low-X	9.684	8.560	11.211Å	90.0	124.5	98.5°

The relationships between the two unit cells are shown diagramatically by Figures 16 (a), (b) and (c).

The existence of faulting in the X-phases is very evident from both optical and electron microscopy and the scale of this varies from Angstroms to microns. Electron diffraction patterns show that the fault plane always has the triclinic indices (100) which, from its d-spacing of 7.8Å, corresponds with the twin plane first found by Drew & Lewis (31) and designated as (011) on the basis of their incorrect unit cell. These authors also noted the appearance of superlattice reflexions and concluded that X-phase occurred in different structural forms.

The 2.84Å b-axis value in "High-X" is the minimum possible repeat distance in a Si-Al-O-N compound since it corresponds to the edge-length of an MX_6 octahedron or an MX_4 tetrahedron, i.e. to the closest approach of non-metal atoms. Similar repeat distances are found in mullite and in β-Si_3N_4 and this, together with the proximity of the X-composition to that of mullite, suggests that the original description "nitrogen-mullite" (30) might not be inappropriate. The observed density (2.73 g cc^{-1}) corresponds to a mass of 409 for the unit of structure in "High-X" and is in reasonable agreement with the composition M_8X_{13} (425 mass units) considering that the measured density is probably low.

The structure determination of "High" and "Low" X-phases continues.

III.5 Tetrahedral AlN-polytype phases

The six phases in the AlN-rich corner of the Si-Al-O-N system (see Figure 9) were first prepared but not characterized by Gauckler et al. (18); see Figure 10. Each extends along a direction of constant M:X ratio in which (Si+N) is gradually replaced by (Al+O). Work at Newcastle has shown that they are all polytypes of aluminium nitride, AlN, similar in some respects to the many polytypes of silicon carbide, SiC, but differing from the latter in that their structures are directly related to their compositions M_mX_{m+1} where $4 < m < 10$; see Jack (20).

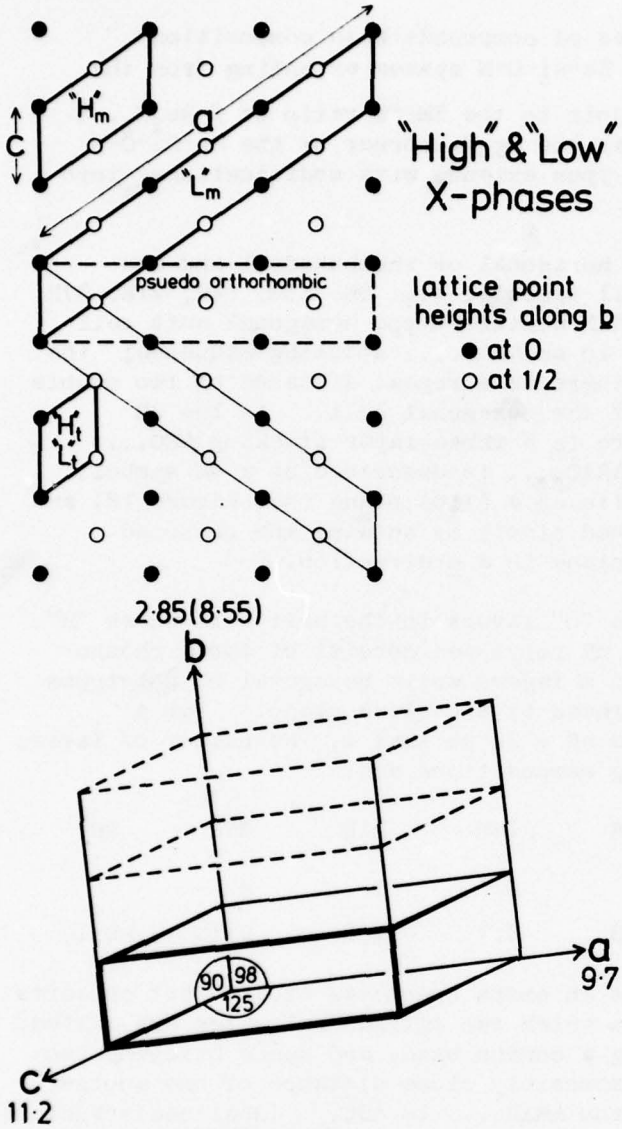

Figure 16. Relationships between "High" and "Low" X-phase unit cells

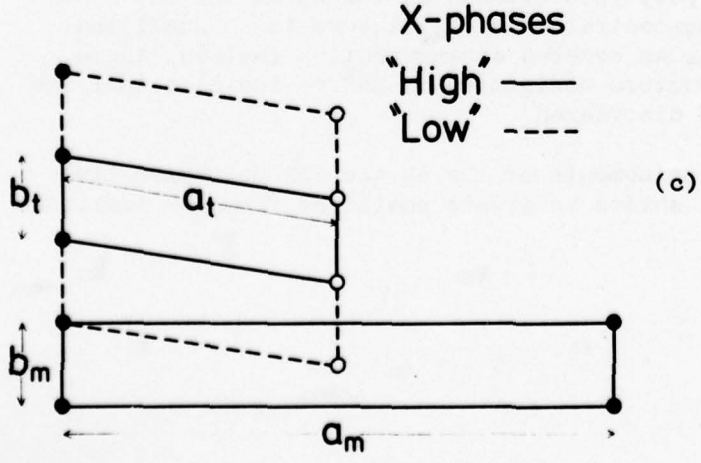

An exactly antitypic series of compounds with compositions $M_{m+1}X_m$ is observed (34) in the Be-Si-O-N system extending from the 1M:1X ratio of the BeO-$BeSiN_2$ join to the 3M:2X ratio of β-Be_3N_2. Similar compounds are found near the Mg_3N_2 corner of the Mg-Si-O-N system and all the sialon polytypes extend, with modifications, into the Mg-Si-Al-O-N system.

The structures are either hexagonal or rhombohedral and are designated by so-called Ramsdell symbols, e.g. 8H, 15R, 12H, 21R, 27R and 2H. Figure 17 shows the AlN wurtzite-type hexagonal unit cell with a succession of MX layers in an ABAB.... stacking sequence; the Ramsdell symbol is 2H because there is a repeat distance of two double layers along the c-direction of the hexagonal cell. In the 3R structure typical of β-SiC there is a three-layer stacking ABC... whereas the stacking sequence ABAC.... is described by a 4H symbol. All the possible atomic sites lie on a (110) plane (see Figure 18) and so the structure can be described simply by showing the occupied positions in sequence on this plane in a c-direction.

For the sialons, there are "n" layers in the unit cell where "n" is the Ramsdell numeral. The nR polytypes consist of three rhombohedrally related blocks each of m layers while hexagonal nH polytypes have two blocks of m layers related by a c-glide plane. For a composition M_mX_{m+1}, nH = 2m and nR = 3m so that m, the number of layers per block and the corresponding compositions are:

	8H	15R	12H	21R	27R	$2H^{\delta}$
m =	4	5	6	7	9	
M:X =	4:5	5:6	6:7	7:8	9:10	>9:10

Each block of m layers contains an extra non-metal atom X that converts one MX layer to an MX_2 layer in which two tetrahedral sites are filled. To avoid two tetrahedra sharing a common base, and hence bringing two non-metal atoms to within an impossibly close distance of one another, the stacking changes locally from ABAB.... to ABC. Idealised structures for the 15R and 12H polytypes are shown by Figure 19.

The range of sialon polytypes extends as far as 9M:10X but nearer the AlN composition the concentration of MX_2 layers is so small that they are too far apart for an ordered arrangement. Instead, there exists an expanded 2H structure designated as $2H^{\delta}$.to indicate that the extra non-metal atoms are disordered.

Detailed structure refinements of the 8H and 15R polytypes (19) show that there are small shifts in atomic positions from the idealised

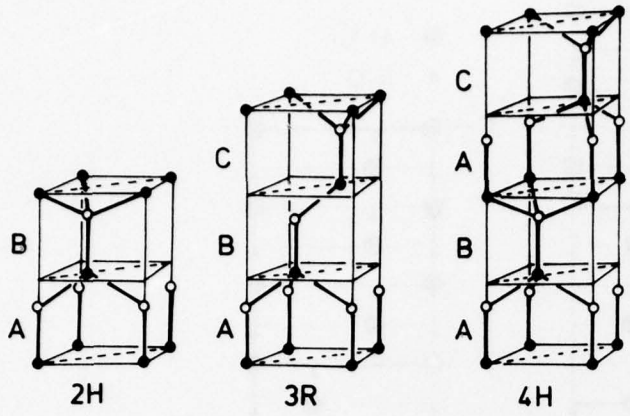

Figure 17. Ramsdell symbols for AlN-polytypes

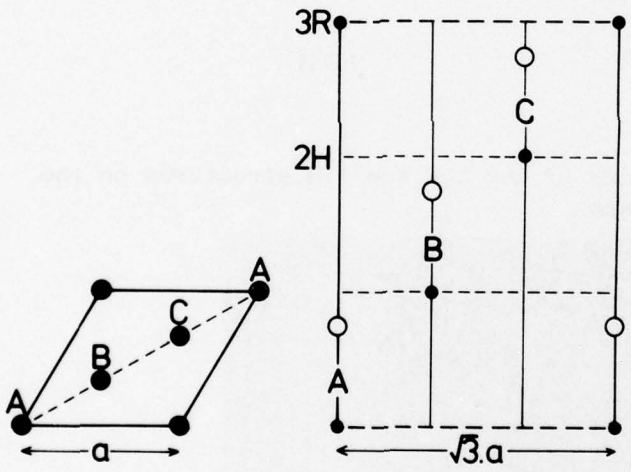

Figure 18. The (110) plane of the AlN-polytype structure

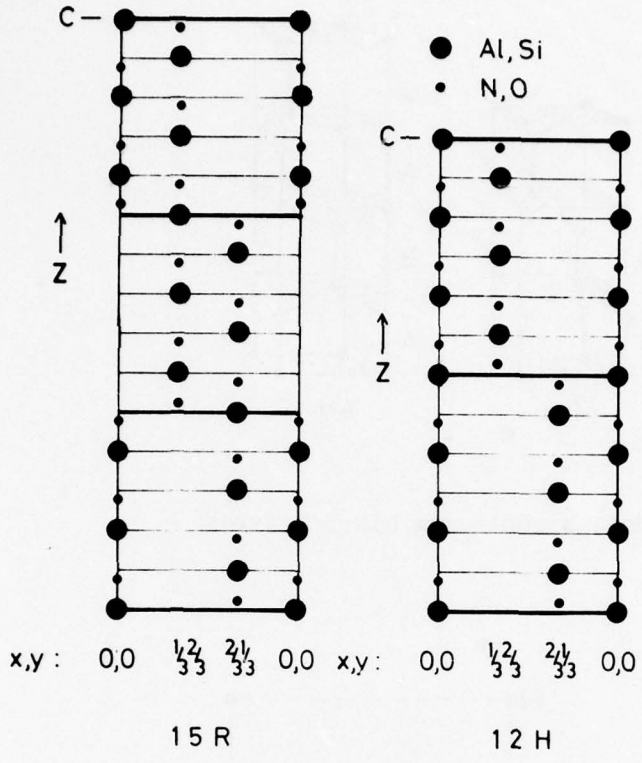

Figure 19. Projections of the 15R and 12H structures on the (110) plane

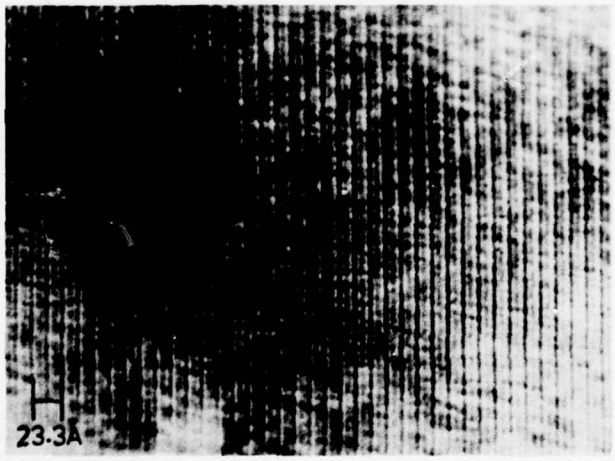

Figure 20. Lattice image of (001) planes of 8H sialon; 23.3Å spacing

models of Figure 19, and the observed interatomic distances suggest that layers of AlO_6 octahedra occur about half-way between successive MX_2 layers. The investigation continues and has recently been supplemented by direct lattice imageing electron microscopy. Figure 20 is an image of the (001) planes of the 8H sialon with a spacing of 23.3Å while Figure 21 resolves the 7M:8X blocks in a 21R sialon. In collaborative work with the Lawrence Berkeley Laboratory, University of California, Department of Materials Science and Engineering, ample evidence (21) has been obtained to confirm the general features of the proposed structures. In Figure 22 individual layer spacings of 2.4Å are resolved for a 6M:5X beryllium-silicon nitride with a 15R structure; blocks of five layers are clearly observed together with occasional faults where some blocks have six and others only four layers.

Thompson (35) has more recently identified a 9R structure of composition M_4X_3 in a Be-Si-O-N specimen prepared at Stüttgart and analagous phases occur in the Al-C-N system with 9R-Al_4C_3, 8H-Al_5C_3N, 15R-$Al_6C_3N_2$ and 12H-$Al_7C_3N_3$.

In all the above systems the kind of polytype depends only upon the metal:non-metal atom ratio. Thus, both M_5X_6 and M_6X_5 have a 15R structure. However, in the Mg-Si-O-N system (see Figure 23) there are compounds that do not have the expected structures. Thus, Mg_4N_2O is 6H with a non-metal stacking sequence ABCACB... and not, as expected, 9R; similarly, Mg_4SiN_4 is 12R and not 8H.

Even more subtle structural variations in polytypes occur in the Mg-Si-Al-O-N system where the lines of constant M:X ratio of the basic Si-Al-O-N system extend into planes. Figures 24(a), (b) and (c) show that different polytypes occur with the same overall M:X ratio depending upon the concentrations of the individual metal atoms. Figure 25 summarises the different polytypes characterized in the present investigation.

It has been suggested by Komeya et al. (36) that the desirable fibrous microstructure responsible for the impact resistance of AlN-SiO_2-Y_2O_3 ceramics is due to an unknown "AlSiON" phase. The latter was identified at Newcastle as a 27R polytype. The most recent information (37) is that the Tokyo Shibaura Electric Company hopes to develop 27R "Alsion" ceramics with controlled microstructures and hence with high strengths combined with improved impact properties.

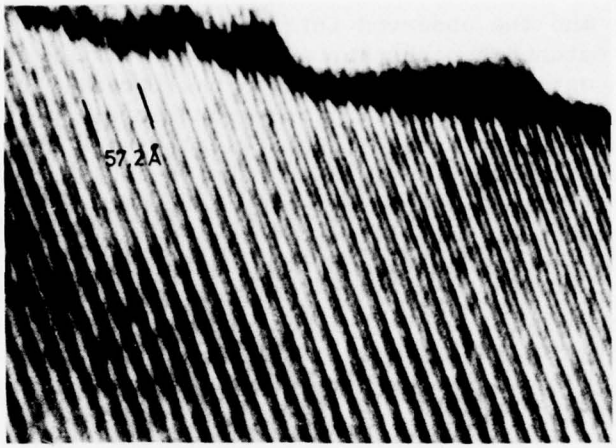

Figure 21. Lattice image of 7M:8X blocks in the 21R sialon

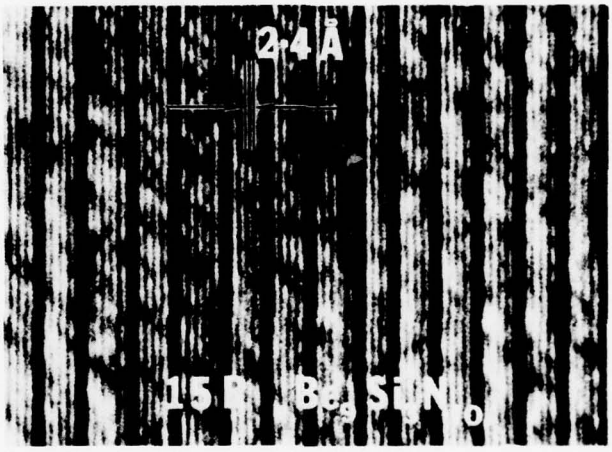

Figure 22. Lattice image of 15R $Be_9Si_3N_{10}$ (6M:5X) showing 2.4Å layer spacing

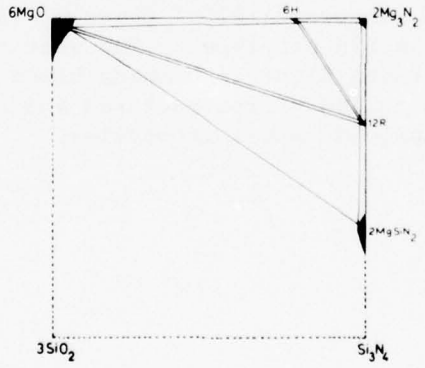

Figure 23. The Mg-Si-O-N system showing 6H and 12R polytypes

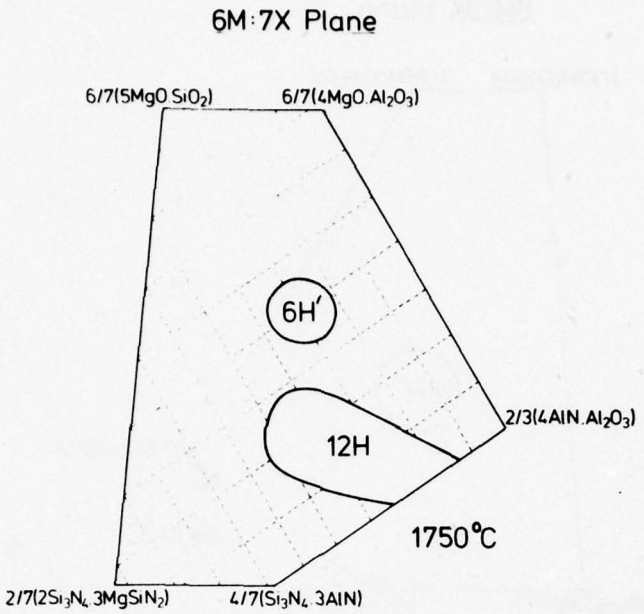

Figure 24(a) The 6M:7X plane of the Mg-Si-Al-O-N system showing two polytype modifications 12H and 6H'

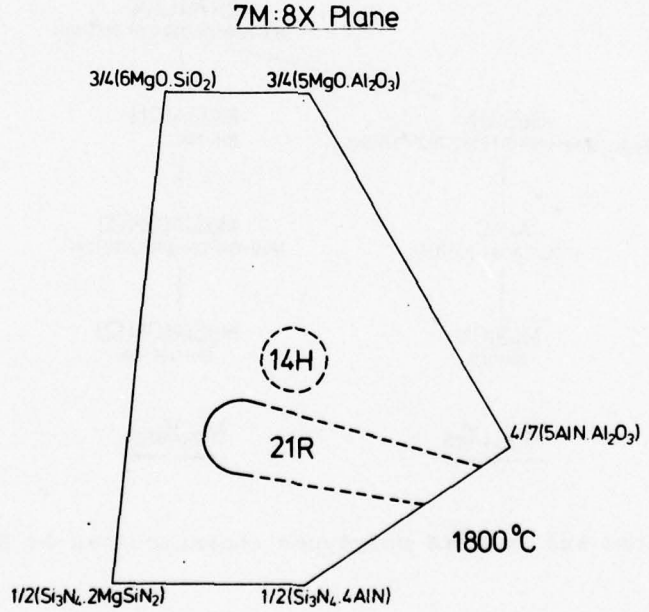

Figure 24(b) The 7M:8X plane of the Mg-Si-Al-O-N system showing two polytype modifications 21R and 14H

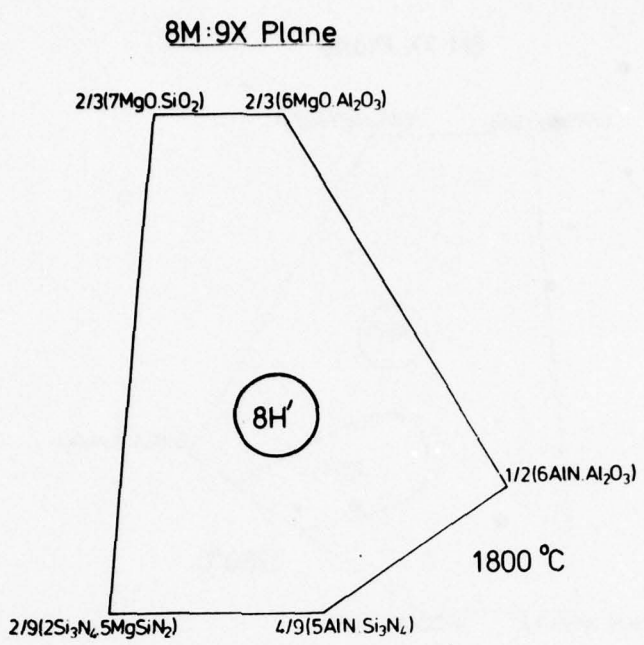

Figure 24(c) 8M:9X plane of the Mg-Si-Al-O-N system showing the polytype modification 8H'

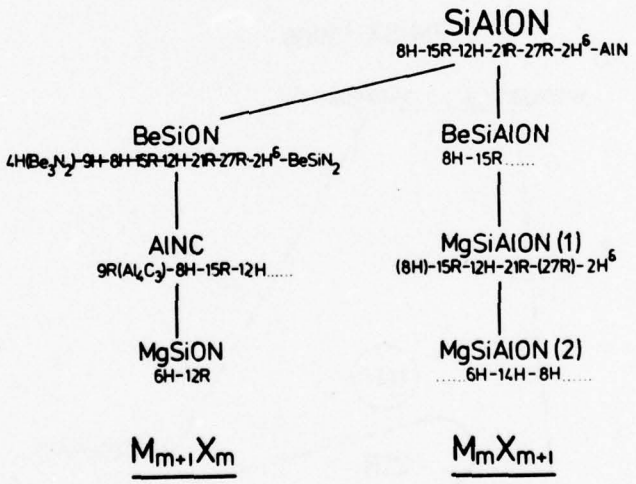

Figure 25. Sialon and related polytypes characterised at Newcastle

IV. MAGNESIUM AND BERYLLIUM SIALONS

IV.1 The Mg-Si-Al-O-N system

Magnesium is tetrahedrally co-ordinated by nitrogen in magnesium nitride and magnesium-silicon nitride whereas it is most frequently co-ordinated octahedrally in oxides and silicates. Magnesium is therefore a "net-work former" in sialons and, as stated in Section II.2, extends all the phases of the basic Si-Al-O-N system from lines of constant M:X ratio into planes of the same ratio in the prism volume; see Figure 5. Early investigations at Newcastle (38) showed that magnesium-aluminium spinel reacted with silicon nitride to give β'-sialons containing magnesium; it also showed the existence of new phases now recognised as 15R and 12H polytypes. Further work at Newcastle has established most of the phase relationships. The MgO-Si_3N_4-Al_2O_3 section shown by Figure 26 cuts across planes of constant M:X ratio and so shows few extended single-phase regions except β'. In general, mixtures of magnesium-containing α', 12H, 15R and nitrogen-spinel are observed. The existence of an α'-phase, a sialon with the structure of an expanded α-silicon nitride, should be noted. The homogeneity range of the nitrogen-spinel is fairly extensive and is shown by the Mg-Al-O-N prism-face of Figure 27. The opposite prism-face, representing the Mg-Si-O-N system, is shown by Figure 28. As discussed later, there is an extensive liquid region at temperatures above about 1500°C which, on cooling, gives a glass. It is clear that silicon nitride with its usual surface silica content (≃ 4w/o) will contain glass after hot-pressing or sintering with added magnesia.

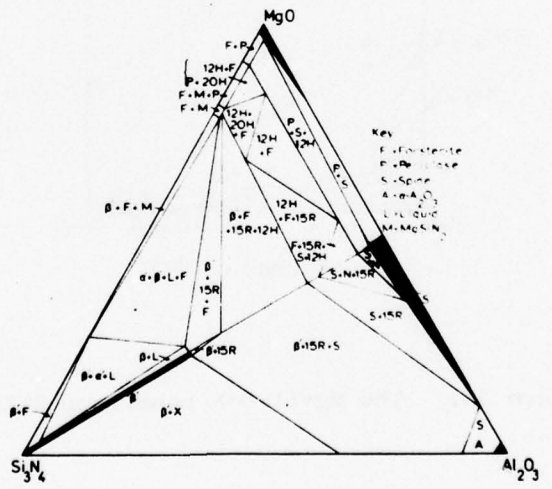

Figure 26. The MgO-Si_3N_4-Al_2O_3 section of the Mg-Si-Al-O-N system at 1800°C

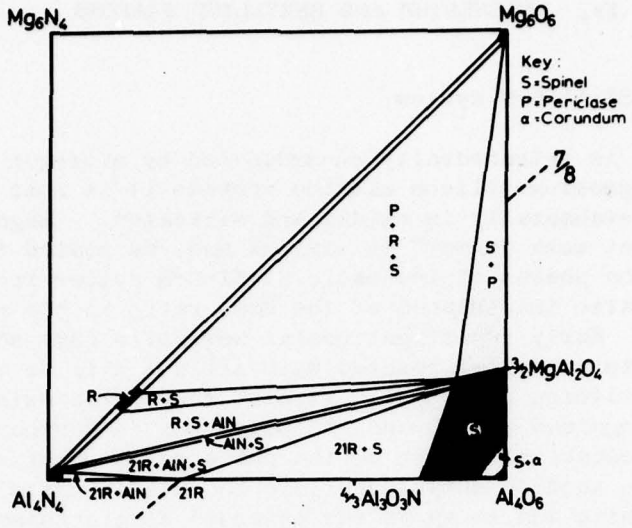

Figure 27. The Mg-Al-O-N prism-face of the Mg-Si-Al-O-N system at 1800°C

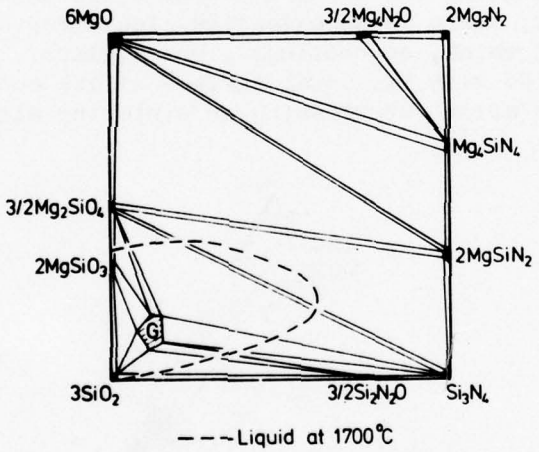

Figure 28. The Mg-Si-O-N behaviour diagram

Liquid and glass-forming regions extend into the Mg-Si-Al-O-N system. Indeed, they probably join up with liquid phases in $MgO-SiO_2-Al_2O_3$ where eutectics occur at temperatures as low as 1355° and 1365°C. The 3M:4X plane of the system shown in Figures 29 and 30 is important because the β'-sialon phase extends along this plane from the $Si_3N_4-Al_3O_3N$ join towards forsterite, $Mg_2SiO_4 \equiv 2MgO.SiO_2$. Starting with any β'-sialon of composition $Si_{6-z}Al_zO_zN_{8-z}$ along the $Si_3N_4-Al_3O_3N$ join, the z-value is maintained constant if each Al is replaced by $Mg_{0.5}Si_{0.5}$ along a direction parallel with the $MgAl_2O_4-Mg_2SiO_4$ join to give a composition

$$Mg_{0.5m}\ Si_{6-z+0.5m}\ Al_{z-m}\ O_z\ N_{8-z}$$

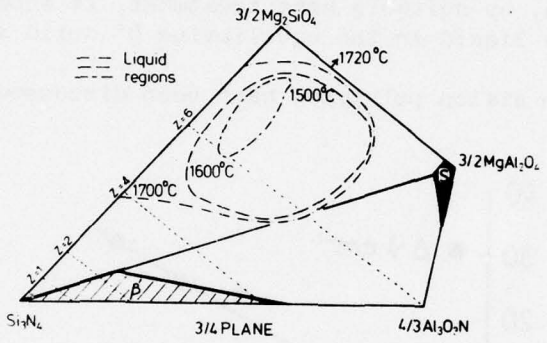

Figure 29. The 3M:4X plane of the Mg-Si-Al-O-N system with liquid regions at 1500-1700°C

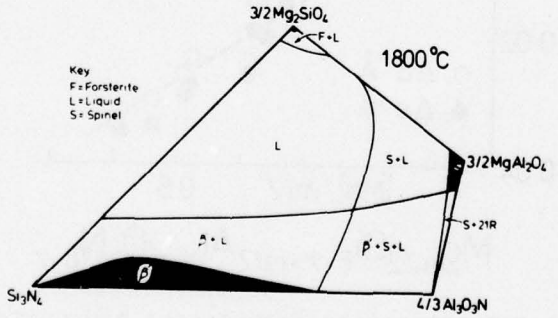

Figure 30. The 3M:4X plane of the Mg-Si-Al-O-N system at 1800°C

Figure 31(b) shows that irrespective of its z-value, the unit-cell dimensions of β'-sialon decrease smoothly as $Mg_{0.5}Si_{0.5}$ replaces Al.

Infra-red absorption measurements made by Wild (39) show that this same replacement is accompanied by an increase in the frequency of a band characteristic of the β'-structure (ν = 580 cm^{-1} for β-Si_3N_4) even though it decreases with increasing z; see Figure 31(a). The phase relationships shown by Figure 29 offer a reasonable and self-consistent explanation for these unit-cell dimensional and infra-red absorption changes. The silica present as a surface layer on silicon nitride prevents the production of a homogeneous, single-phase material by hot-pressing with magnesia. Figures 29 and 30 show that by addition of appropriate amounts of Al_2O_3 and AlN ($\equiv Al_3O_3N$) with just sufficient MgO to react with the surface silica, a homogeneous, single-phase β'-magnesium sialon can be obtained. Moreover, the magnesia and silica react initially with some silicon nitride to produce a Mg-Si-O-N liquid which aids densification by liquid-phase sintering and then, by suitable heat-treatment, it should be possible to incorporate the liquid in the equilibrium β' solid solution.

The magnesium sialon polytypes have been discussed briefly in Section III.5.

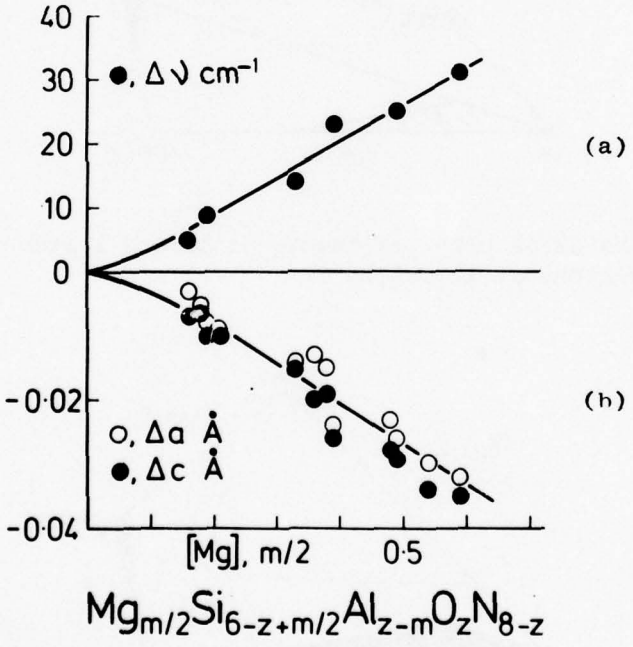

Figure 31. Infra-red absorption frequencies and unit-cell dimensions of β'-magnesium sialons

IV.2 The Be-Si-Al-O-N system

On chemical grounds, beryllia is expected to behave as an additive to silicon nitride and to sialons in a similar way to magnesia. However, because the silicate Be_2SiO_4 (phenacite) has the same atomic arrangement as β-Si_3N_4 it is much more soluble in β and in β'-sialon than forsterite, Mg_2SiO_4 (30,40). Thus, there is a very wide range of homogeneity of β' on the 3M:4X plane of the Be-Si-Al-O-N system; see Figure 32. Oda (41) has reported near-theoretical densities for silicon nitride pressureless sintered at 1760°C with mixed additions of (i) 3w/o BeO:3w/o MgO, and (ii) 1.25w/o BeO:3.75w/o MgO:5w/o CeO_2. The room temperature rupture moduli are also high. Mixtures of BeO and MgO with silicon nitride and with β'-sialon compositions are expected to give lower eutectics than with MgO alone and so at a similar temperature they will extend the liquid regions. Moreover, the greater homogeneity range of β' should allow more compositional flexibility for the subsequent incorporation of all additives and impurities into a single-phase material.

Because of the health hazard in handling finely divided beryllium compounds, facilities for the safe fabrication of beryllium sialons from mixed powders are not available at Newcastle. A collaborative effort with the Lawrence Livermore Laboratory of the University of California was therefore arranged with Dr. R. Landingham. It was agreed to hot-press powder mixes in Livermore, the compositions being specified by Newcastle. Subsequent examination of the products was planned at Newcastle and, if necessary, at the Department of Materials Science and Mineral Engineering of the Lawrence Berkeley Laboratory, University of California.

Seventy-two powder mixes were specified for hot-pressing and their compositions are shown by numbers 1-72 on the Figures 33-43.

The 21 compositions of Figure 33 are intended to cover all the polytypes in the Be-Si-O-N system in order to confirm and refine their crystal structures. In particular, it is hoped to ascertain whether, as previously suggested (34), the structures along the Be_3N_2-BeO join are different to those along the Be_3N_2-$BeSiN_2$ join. If so, then any polytype of composition $M_{m+1}X_m$ would be expected to show a structural discontinuity between nitrogen-rich and nitrogen-poor compositions.

Figure 34 attempts to characterize a quaternary nitride $BeSiAlN_3$ and to discover whether it has a range of homogeneity. The only other known quaternary nitride, $MgSiAlN_3$ (39), is isostructural with $LiSi_2N_3$.

Figure 35 covers the 3M:4X plane of the Be-Si-Al-O-N system, important for the production of homogeneous β'-beryllium sialons, and

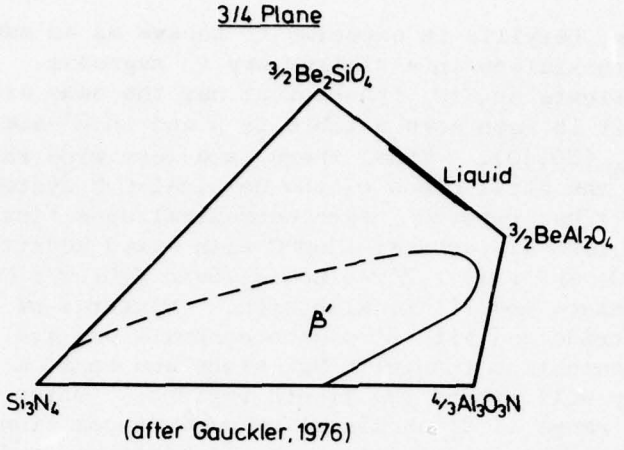

Figure 32. The 3M:4X plane of the Be-Si-Al-O-N system; (Gauckler et al., Ref. 40)

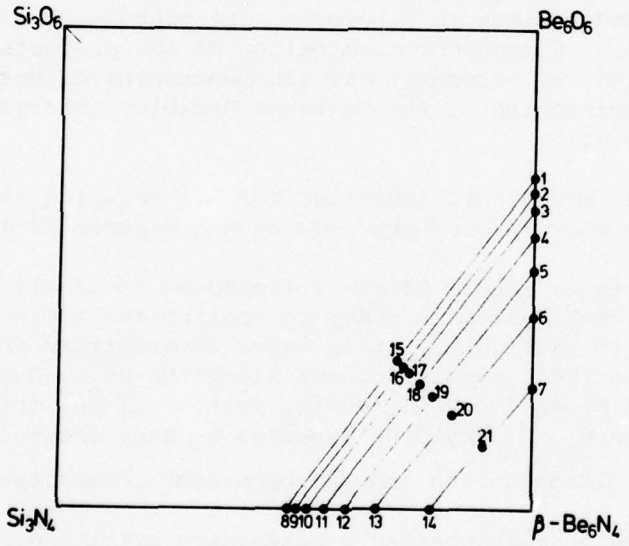

Figure 33. Compositions of beryllium and other sialons etc. specified for preparation at the Lawrence Livermore Laboratory, California.

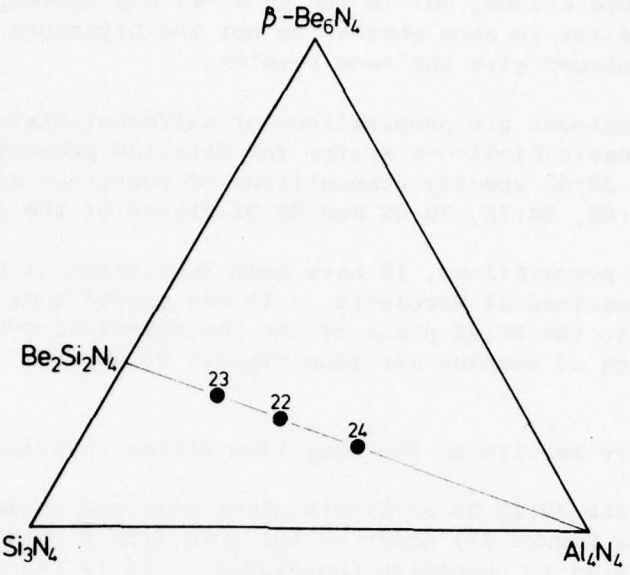

Figure 34

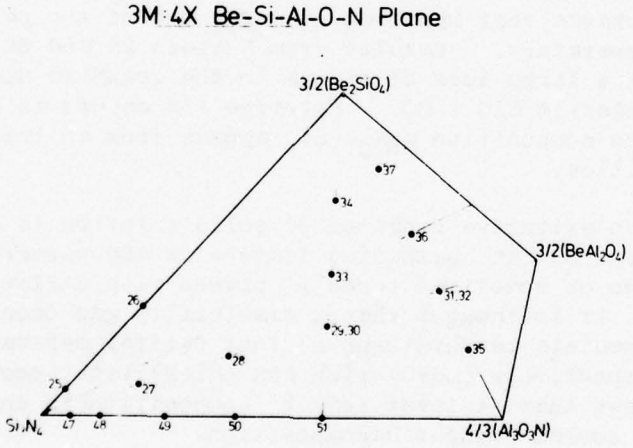

Figure 35

Figure 36 compares similar selected compositions in which half the beryllium is replaced by magnesium . Figure 37 is a repetition of the Figure 36 preparations, but in the Mg-Si-Al-O-N system, and is included as a monitor to show whether or not the Livermore and Newcastle preparative techniques give the same results.

Figure 38 includes six preparations of different mixtures of β' plus 15R in the basic Si-Al-O-N system for detailed property evaluation. Finally, Figures 39-43 specify compositions of beryllium sialon polytypes on the 4M:5X, 5M:6X, 6M:7X, 7M:8X and 8M:9X planes of the system.

Of these 72 preparations, 16 have been fabricated at Livermore and 10 of them examined at Newcastle. It was agreed that priority should be given to the 3M:4X plane of the (Be,Mg)-Si-Al-O-N system and so the first batch of samples are from Figures 35 and 36.

IV.3 Preliminary results of the beryllium sialon investigation

Samples on the 3M:4X Be-Si-Al-O-N plane examined so-far (Numbers 29, 30, 33, 34 of Figure 35) occur on the join from β'-sialon ($Si_2Al_4O_4N_4$; z = 4) to phenacite ($Be_4Si_2O_8$). It is important to prepare the same composition in different ways and so $Be_2Si_3Al_4O_8N_4$ (Numbers 29 and 30) was prepared either with all the aluminium as AlN or with all the silicon as Si_3N_4.

The hot-pressed pellets showed two distinct regions: the inner part was the sialon sample and the outer part was boron nitride containing those phases that had been squeezed out of the pellet as liquid at high temperature. Results from Numbers 29 and 30 are compatible only if a large loss of silica in the graphite die occurred in sample 30 as volatile SiO + CO. Polytype 15R occurs as a secondary product which, with composition M_5X_6, can appear from an initial M_3X_4 only by loss of silica.

In general, an extensive range of β' solid solution is observed at high temperatures but an unexpected feature is the occurrence in any one specimen of two or sometimes three β' phases with different unit-cell dimensions. It is thought that a miscibility gap occurs in the β'-range at intermediate temperatures so that partial separation into two β'-phases, respectively (Be+O)-rich and (Al+N)-rich, occurs. The observations suggest that at least some β' compositions in this system can be melted and cooled without decomposition.

Compositions 38-41 on the 3M:4X (Be,Mg)-Si-Al-O-N plane (Figure 36) show, as expected, that the range of β' is not as extensive as in the Be-Si-Al-O-N system without magnesium. However, samples 38 and 39 give

3M:4X (Be,Mg)-Si-Al-O-N Plane

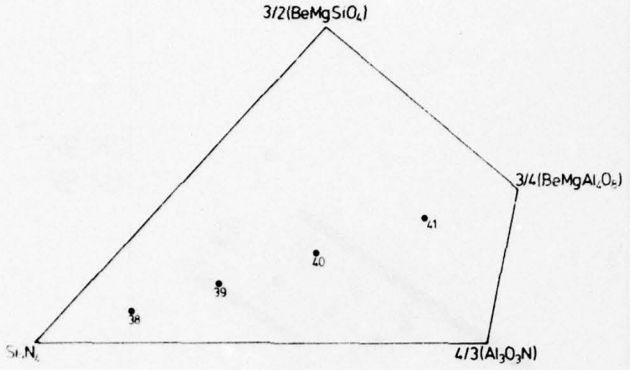

Figure 36

3M:4X Mg-Si-Al-O-N Plane

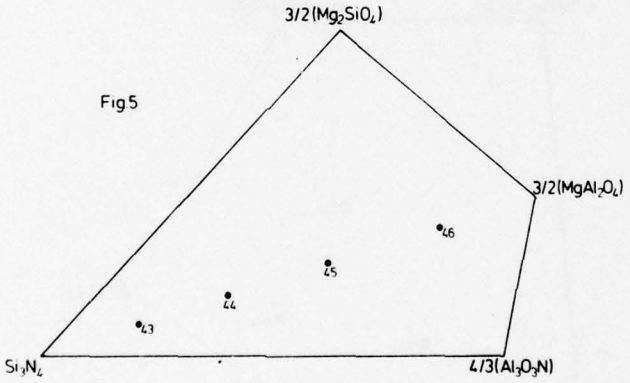

Figure 37

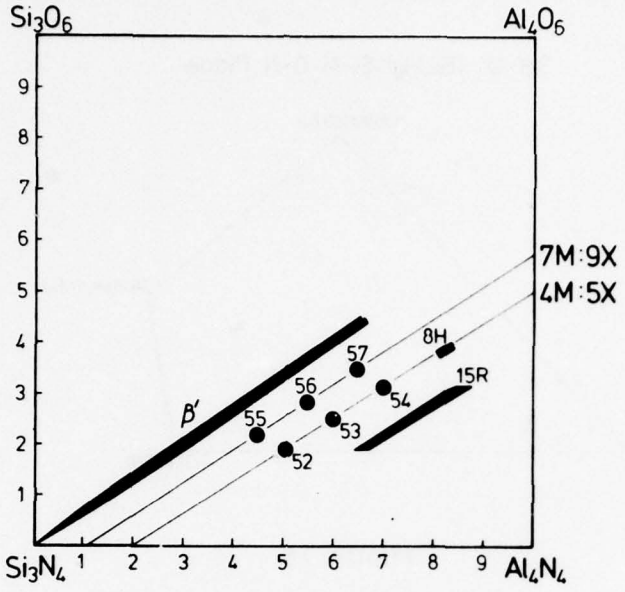

Figure 38

4M:5X Be-Si-Al-O-N Plane

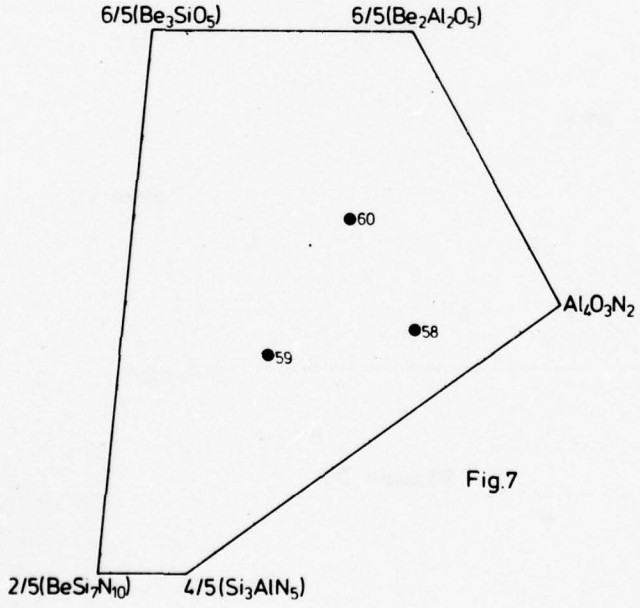

Fig.7

Figure 39

pure β'-sialons, 40 gives β' plus a magnesium-rich sialon glass, and 41 gives glass, 15R and spinel.

Polytype phases, chiefly 15R, are observed in several samples and it is shown that their unit-cell dimensions vary systematically with beryllium substitution. In the beryllium sialon system it is thus confirmed that polytype phases occur on both sides of the 1M:1X plane with compositions M_mX_{m+1} and $M_{m+1}X_m$.

These preliminary results on the Be-Mg-Si-Al-O-N system are most promising and confirm the initial general predictions about the extent of the β'-phase field. If it is also true that β'-compositions can be melted and cooled without decomposition, these materials offer technological advantages which, despite the hazards of beryllium handling, should be pursued.

5M:6X Be-Si-Al-O-N Plane

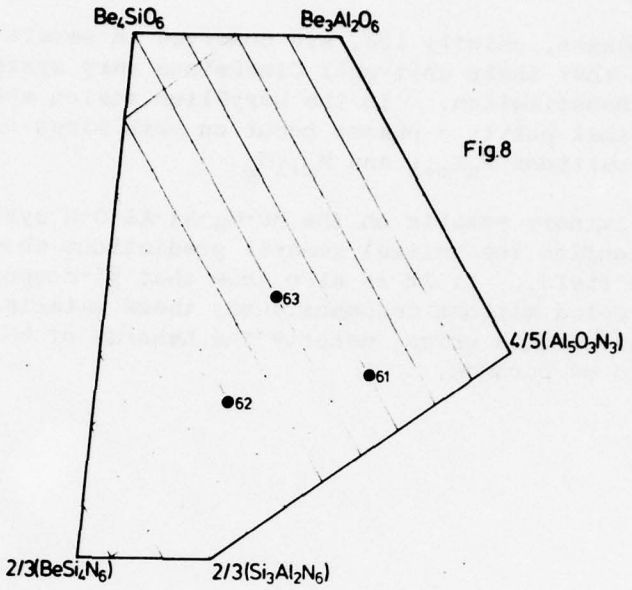

Figure 40

6M:7X Be-Si-Al-O-N Plane

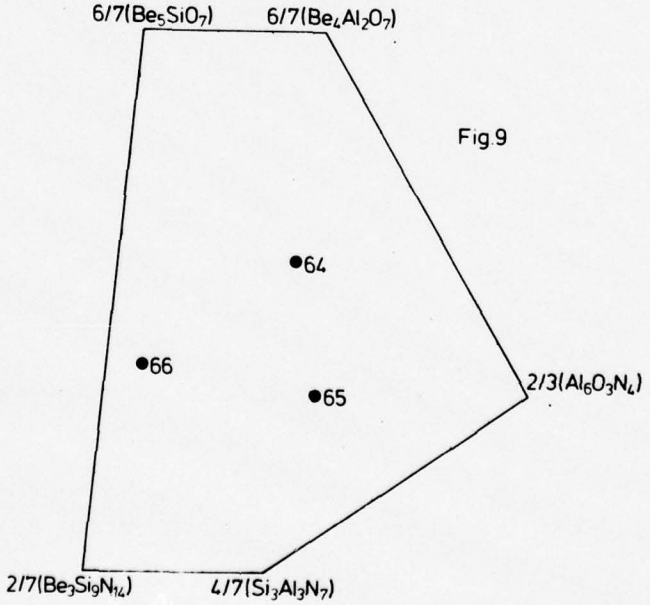

Figure 41

7M:8X Be-Si-Al-O-N Plane

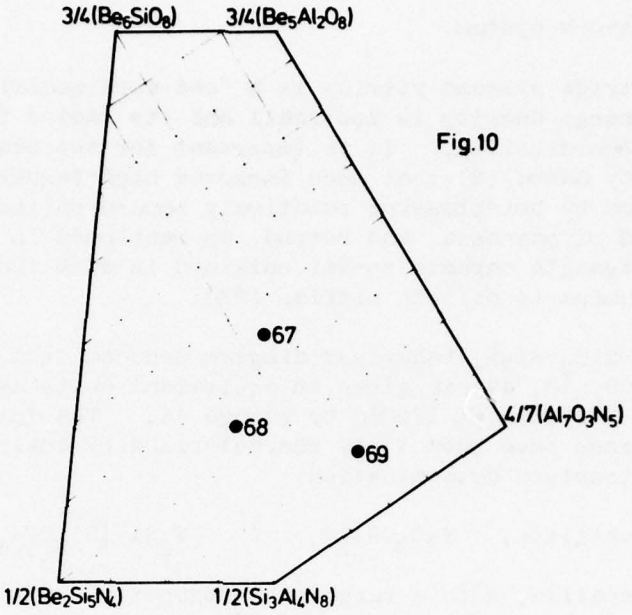

Figure 42

8M:9X Be-Si-Al-O-N Plane

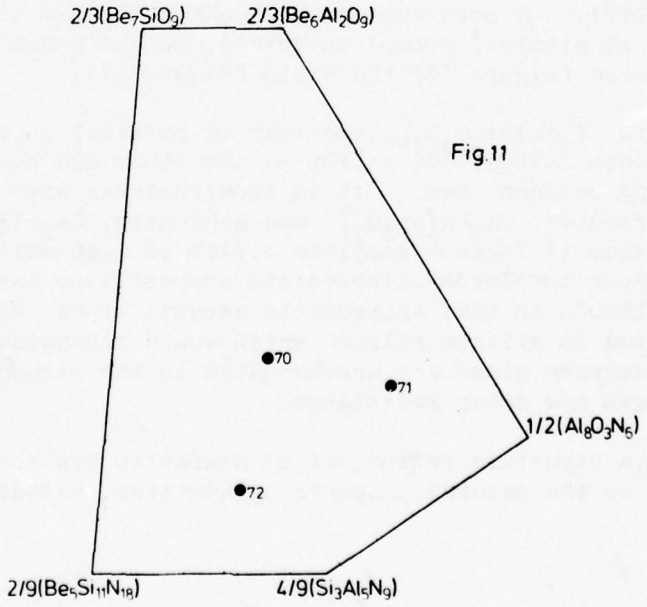

Figure 43

V. YTTRIUM SIALONS

V.1 The Y-Si-O-N system

In oxynitride systems yttrium is a "net-work modifier" presumably because its charge density is too small and its radius too large for tetrahedral co-ordination. It is important for two reasons. First, it was shown by Gazza (8) that much improved high-temperature strengths can be obtained by hot-pressing relatively impure silicon nitride with yttria instead of magnesia, and second, as mentioned in Section III.2, the highest strength ceramic so-far obtained is with the addition of yttria and alumina to silicon nitride (23).

The Y_2O_3-SiO_2-Si_3N_4 behaviour diagram deduced from investigations at Newcastle (9, 12, 42) is given in equivalent units as one face of the Y-Si-Al-O-N system at 1700°C by Figure 44. The following four quaternary phases have been fully characterized by analysis, synthesis and crystal structure determination:

(i) N-melilite, $Y_2O_3.Si_3N_4 \equiv Y_2Si\,[Si_2O_3N_4]$

(ii) N-apatite, with a range of homogeneity

$$(Y,\square)_{10}[Si(O,N)_4]_6(O,N,\square)_2$$

(iii) N-YAM, $2Y_2O_3.Si_2N_2O \equiv Y_4Si_2O_7N_2$ (J-phase)

(iv) N-α-wollastonite, $Y_2O_3.Si_2N_2O \equiv 2YSiO_2N$ (H'-phase)

The existence of (i)-(iii) is confirmed by Lange et al. (10) and Wills et al. (43). A more conventional phase diagram is given by Figure 45 and is similar, except in detail, to the phase diagrams proposed by Lange (Figure 46) and Wills (Figure 47).

N-melilite, $Y_2Si[Si_2O_3N_4]$, consists of parallel sheets of linked Si-O-N tetrahedra stacked one on top of the other and held together by yttrium cations between them. It is isostructural with the melilite silicates akermanite, $Ca_2Mg[Si_2O_7]$, and gehlenite, $Ca_2Al[AlSiO_7]$, and with each of them it forms a complete series of high melting solid solutions. Even the 50:50 intermediate compositions have melting points above 1600°C so that appreciable amounts of Ca, Mg, Al and other impurities in silicon nitride which would otherwise form a low softening-temperature glass are accommodated in the structure without loss of strength and creep resistance.

Although a structure refinement of N-apatite has confirmed that it is similar to the naturally occurring apatites (R-factor, 0.19) it

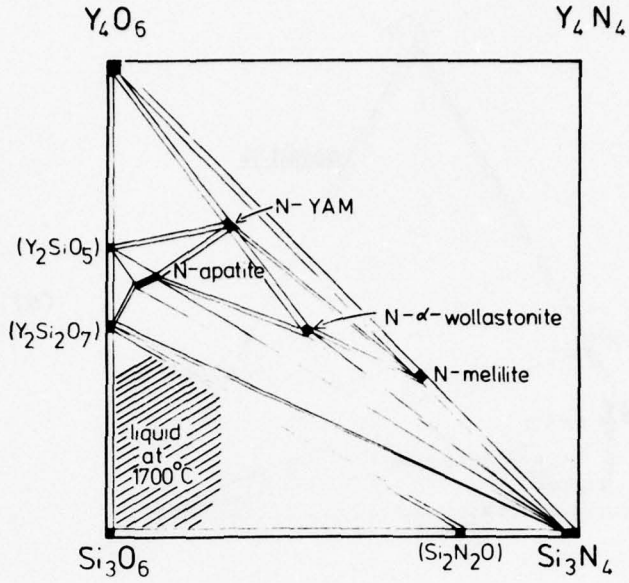

Figure 44. The Y-Si-O-N behaviour diagram at 1700°C

was impossible to determine the exact unit-cell contents. The measured density is in reasonable agreement with a composition close to $Y_{10}(SiO_4)_6N_2$ but variations in unit-cell dimensions show that there must be a homogeneity range. Electron probe analyses suggest that this is between the limits:

$$Y_{10}(SiO_4)_6N_2 \ (\underline{a},\ 9.36;\ \ \underline{c},\ 6.77\text{Å}) \text{ to } Y_{9.7}(SiO_4)_6ON \ (\underline{a},\ 9.37;\ \ \underline{c},\ 6.75\text{Å})$$

N-YAM, originally called J-phase, is isostructural with the yttrium aluminate "YAM", and N-α-wollastonite ("H'-phase") is isostructural with a yttrium aluminate "YAP" the low-temperature modification of which has a similar structure to α-wollastonite ($CaSiO_3$). These two yttrium-silicon oxynitrides lie on the Y_2O_3-Si_2N_2O join of the 2M:3X plane of the Y-Si-Al-O-N system (see Figure 48) and form solid solutions with the corresponding yttrium aluminates.

The complete solid solubility initially proposed (12) between N-YAM ($Y_4Si_2O_7N_2$) and YAM ($Y_4Al_2O_9$) is confirmed by fifteen unit-cell

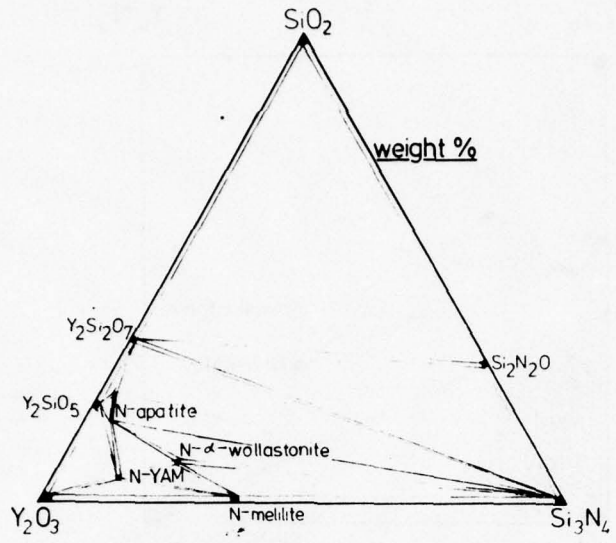

(a)

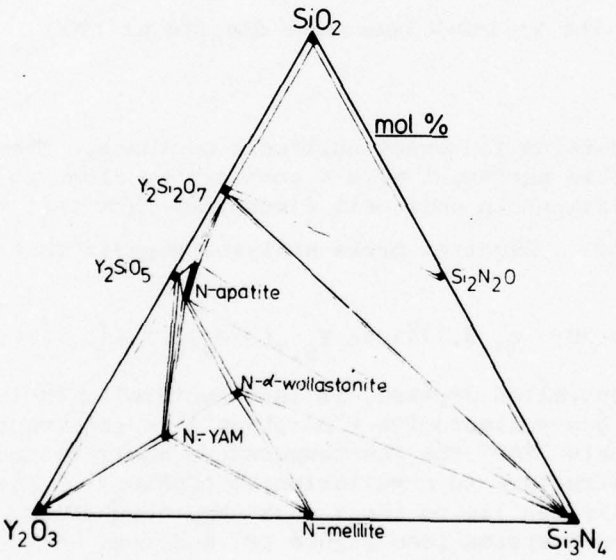

(b)

Figure 45. The Y_2O_3-SiO_2-Si_3N_4 phase diagram at 1700°C from Newcastle data: (a) in weight %; (b) in mol %

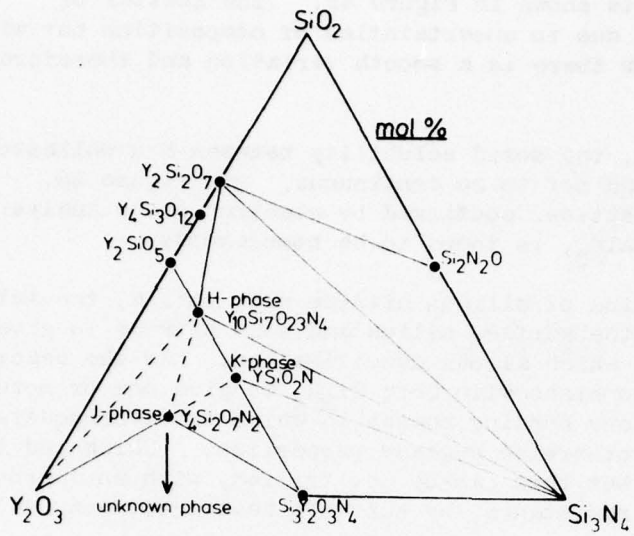

(after Lange et al.,1976)

Figure 46. The Y_2O_3-SiO_2-Si_3N_4 phase diagram at 1700°C; after Lange et al., Ref. 10

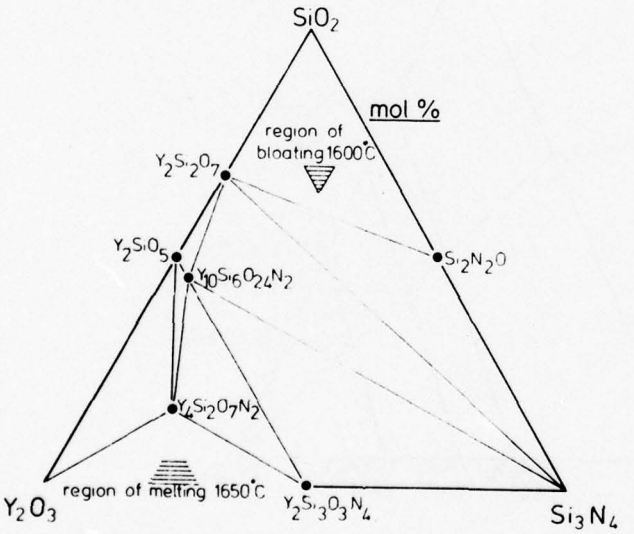

(after Wills et al.,1976)

Figure 47. The Y_2O_3-SiO_2-Si_3N_4 phase diagram at 1700°C after Wills et al., Ref. 44

dimensional measurements shown in Figure 49. The scatter of experimental points is due to uncertainties of composition but within this experimental error there is a smooth variation and therefore complete miscibility.

On the other hand, the solid solubility between N-α-wollastonite and low-YAP is now found not to be continuous; see Figure 50. Only one intermediate composition, confirmed by electron probe analysis as $Y_2SiAlO_5N \equiv YSiO_2N + YAlO_3$, is found to be homogeneous.

In the densification of silicon nitride with yttria, the latter reacts initially with the surface silica and some nitride to give a liquid (see Figure 44) which allows densification. As the reaction proceeds, the liquid combines with more Si_3N_4 to give one or more of the quaternary refractory bonding phases in which are accommodated the impurities that would otherwise degrade properties. Unreacted liquid cools to give a glass but this can be devitrified, with an improvement in strength and creep resistance, by suitable heat-treatment (44).

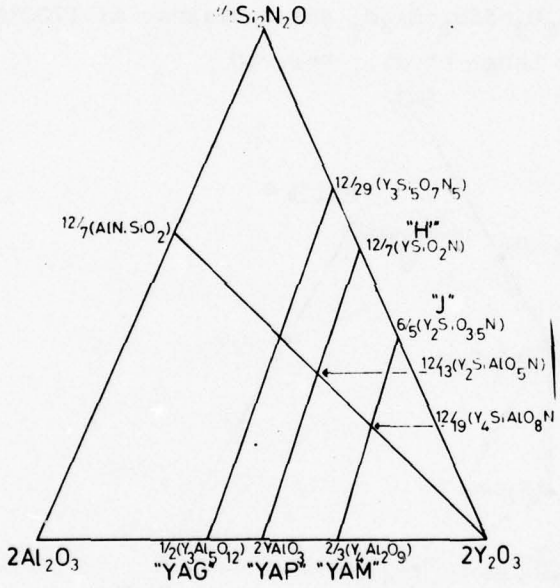

Figure 48. The 2M:3X plane of the Y-Si-Al-O-N system

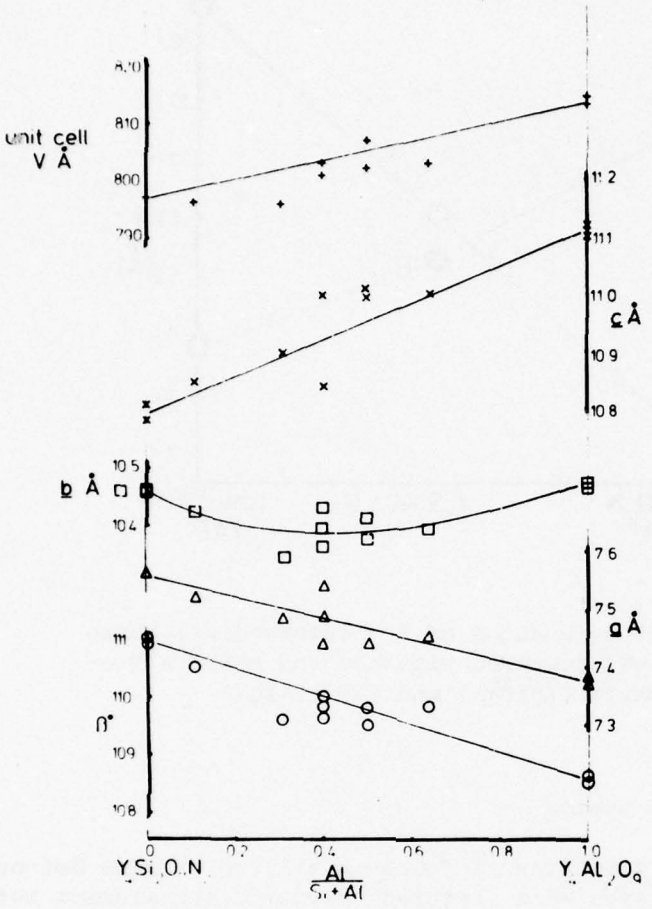

Figure 49. Unit-cell dimensions of solid solutions between N-YAM ($Y_4Si_2O_7N_2$) and YAM ($Y_4Al_2O_9$)

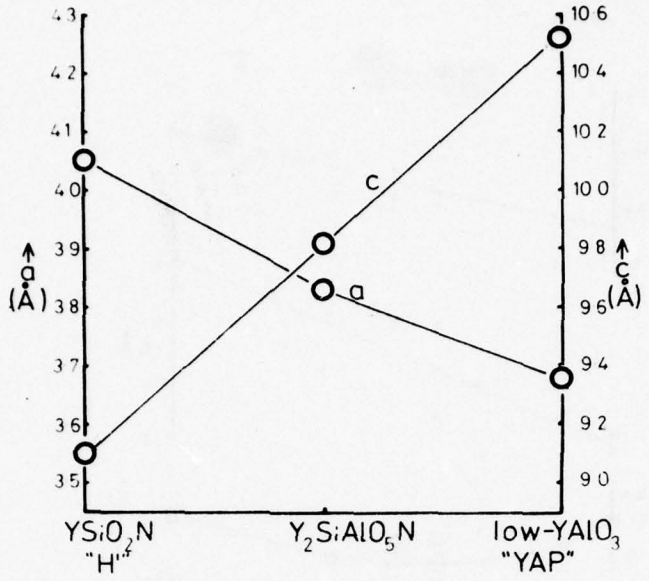

Figure 50. Unit-cell dimensions of the intermediate phase (Y_2SiAlO_5N) compared with the end members N-α-wollastonite ($YSiO_2N$) and YAP ($YAlO_3$)

V.2 The Y-Si-Al-O-N system

Extensive glass formation is found in silicon nitride hot-pressed and pressureless sintered with mixtures of yttria and alumina but no new nitrogen-containing crystalline phases occur in addition to those observed in the Si-Al-O-N and Y-Si-O-N systems.

Figures 51 and 52 show that at 1700°C the tie-lines generally run from the two nitrides AlN and Si_3N_4 to the oxide-rich phases in the system. Hence, nitride-rich compositions will often contain oxide grain-boundary phases rather than yttrium-silicon oxynitrides. Within the Si_3N_4-Y_2O_3-Al_2O_3 triangle (see Figures 8a, b and c) there is a wide compositional range, expanding with increasing temperature, where the products are only β'-sialon and a Y-Si-Al-O-N glass.

It is of interest that "YAP" ($YAlO_3$) has never been observed in preparations that contain silicon although "YAG" ($Y_3Al_5O_{12}$) is often found as a grain-boundary phase with a matrix of β'-sialon.

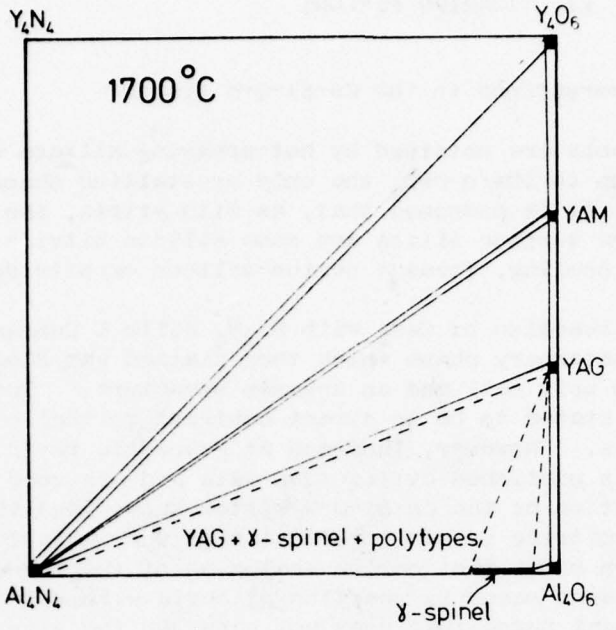

Figure 51. The Y-Al-O-N behaviour diagram at 1700°C

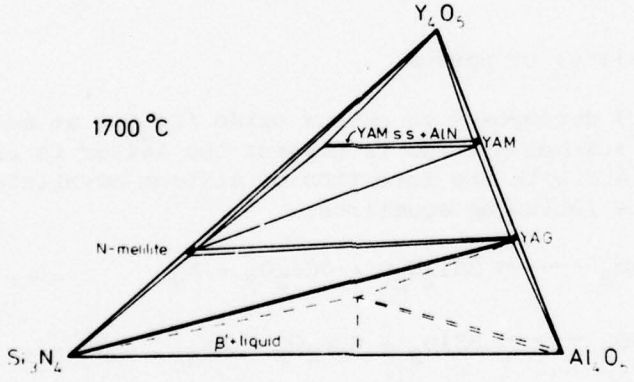

Figure 52. The Y_2O_3-Si_3N_4-Al_2O_3 behaviour diagram at 1700°C

VI. CERIUM SIALONS

VI.1 Preliminary observations in the Ce-Si-O-N system

Fully dense products are obtained by hot-pressing silicon nitride with ceria, and with up to 10w/o CeO_2 the only crystalline phase observed is β-Si_3N_4. It is presumed that, as with yttria, the cerium oxide combines with the surface silica and some silicon nitride to give liquid which, on cooling, forms a cerium-silicon oxynitride glass.

In exploring the reaction of CeO_2 with Si_3N_4 Wills & Cunningham (45) found only one quaternary phase which they claimed was $3Ce_2O_3.2Si_3N_4$ having an orthorhombic unit cell and an unknown structure. The behaviour of CeO_2 was stated to be in direct contrast to that of the other rare earth oxides. However, Thompson at Newcastle re-interpreted Wills' and Cunningham's published diffraction data and his more detailed and continuing examination of the Ce-Si-O-N system shows (46) that the new cerium-silicon oxynitride is similar to yttrium N-α-wollastonite. It has now further been shown that cerium analogues of the three other quaternary Y-Si-O-N phases occur by reaction of ceria with silicon nitride as well as one additional phase that does not occur in the yttrium system.

The properties of silicon nitride containing up to 20w/o CeO_2 and up to 10w/o each of CeO_2 and Al_2O_3 have been investigated and, as an aid to interpreting the results, the phase relationships in the Ce-Al-O-N system have been examined at 1700°C.

VI.2 The variable valency of cerium

Ceric oxide (CeO_2) decomposes to cerous oxide (Ce_2O_3) at above about 1230°C but when silicon nitride is present the latter is oxidised with loss of nitrogen and with the formation of silicon oxynitride or silica according to the following equations:

$$2Si_3N_4 + 6CeO_2 \longrightarrow 3Si_2N_2O + 3Ce_2O_3 + N_2 \qquad .... (6)$$

$$Si_3N_4 + 12CeO_2 \longrightarrow 3SiO_2 + 6Ce_2O_3 + 2N_2 \qquad .... (7)$$

The further reaction of silicon oxynitride with Ce_2O_3 or with Ce_2O_3 plus silica allows the formation of the three quaternary Ce-Si-O-N phases in which cerium is trivalent and that are isostructural with the corresponding yttrium phases (numbered as in Section V.1):

(ii) N-apatite

$$5Ce_2O_3.Si_2N_2O.4SiO_2 \equiv Ce_{10}[(SiO_4)_6]N_2$$
$$5Y_2O_3.Si_2N_2O.4SiO_2$$

(iii) N-YAM

$$2Ce_2O_3.Si_2N_2O \equiv Ce_4Si_2O_7N_2$$
$$2Y_2O_3.Si_2N_2O$$

(iv) N-α-wollastonite

$$Ce_2O_3.Si_2N_2O \equiv 2CeSiO_2N$$

$$Y_2O_3.Si_2N_2O$$

The fourth analogue of the yttrium-silicon oxynitrides

(i) N-melilite

$$Ce_2O_3.Si_3N_4 \equiv Ce_2Si[Si_2O_3N_4]$$

$$Y_2O_3.Si_3N_4$$

is also found in the Ce-Si-O-N system but has not been prepared without the presence of large amounts of the other phases. This is explained by the inability to obtain equimolar mixtures of Ce_2O_3 and Si_3N_4 without the oxynitride Si_2N_2O. If the Ce_2O_3 is formed only by reduction of CeO_2 with simultaneous formation of Si_2N_2O according to equations (6) and (7), the production of other quaternary phases in addition to the N-melilite is inevitable.

An additional quaternary phase found in the Ce-Si-O-N system

(v) $Ce_2O_3.2Si_3N_4 \equiv Ce_2Si_6O_3N_8$

has no yttrium analogue.

VI.3 The Ce-Si-O-N system

Phase relationships in the Ce_2O_3-Si_3N_4-SiO_2 system at 1700°C are shown by the behaviour diagram of Figure 53 with concentrations in equivalents. Except for the additional quaternary phase $Ce_2Si_6O_3N_8$, it is very similar to the Y_2O_3-Si_3N_4-SiO_2 system of Figure 44. The compositions of all the phases have been very satisfactorily confirmed by electron probe microanalysis (see Appendix I).

Cerium-N-apatite has a range of homogeneity but the nitrogen-rich composition is very close to the theoretical $Ce_{10}(SiO_4)_6N_2$ predicted by analogy with the more common phosphate apatites, e.g. $Ca_{10}(PO_4)_6F_2$. By replacing the two 3-planar-coordinated nitrogens in the structure by oxygen, valency requirements are met by cerium sites becoming vacant and the composition becomes $Ce_{9.33}(SiO_4)_6O_2$. The 3-coordinated sites can also become vacant to give a limiting composition $Ce_8(SiO_4)_6$. The

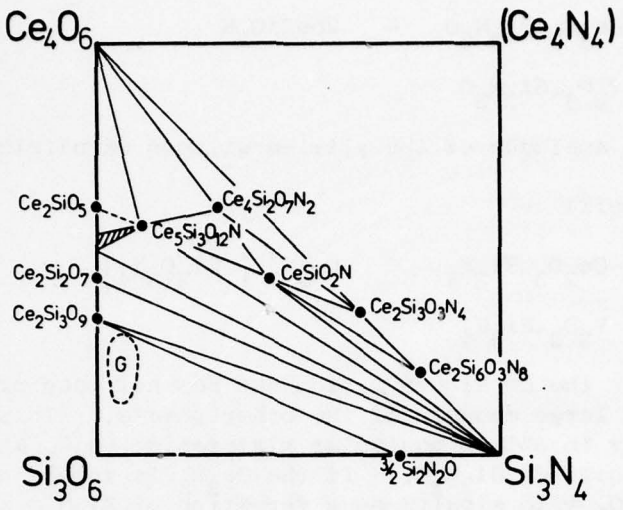

Figure 53. The Ce_2O_3-Si_3N_4-SiO_2 behaviour diagram at 1700°C

three apatites differ slightly in hexagonal unit-cell dimensions:

	a	c
$Ce_8(SiO_4)_6$	9.641	7.124Å
$Ce_{9.3}(SiO_4)_6O_2$	9.520	7.140
$Ce_{10}(SiO_4)_6N_2$	9.644	7.184

and confirm the small triangular phase-field of Figure 53.

The cerium-YAM-type oxynitride $Ce_4Si_2O_7N_2$ was not investigated in the extensive preparative work on YAM phases by Wills et al. (47) but occurs with cell dimensions slightly larger than the comparable yttrium compound.

The cerium-N-α-wollastonite first characterized by Thompson (46) is shown by more recent Newcastle work to be slightly different from the yttrium analogue; see Table 4. Whereas in the monoclinic unit cell of $YSiO_2N$ the c repeat distance consists of approximately two 10Å structural units, there are three in $CeSiO_2N$. Also the a and b edges are interchanged so that the slight monoclinic distortion from an hexagonal or orthorhombic cell is between different corresponding edges. 20Å and 30Å α-wollastonites are well known in silicates and arise because the structure consists of successive layers each made up of three-membered rings of tetrahedra Si_3O_9 or, in the present case, $Si_3O_6N_3$. The layers are held together by sheets of large

cations sandwiched between them and the sandwiches are stacked in either a hexagonal ABAB.... or a cubic ABCABC... close-packing. No detailed study of any α-wollastonite structure has ever been made and although Morgan & Carroll (48) confirm that $YSiO_2N$ and the isostructural $LaSiO_2N$ are of the three-membered-ring type wollastonite, their simplification of using a hexagonal unit cell leaves many details obscured. $YSiO_2N$ is similar to α-$CaSiO_3$ and $CeSiO_2N$ to α-$SrSiO_3$; the difference is probably due to the cation radius (see Table 4).

The cerium melilite, $Ce_2Si[Si_2O_3N_4]$ has not been investigated in detail but its unit-cell dimensions, as with the other cerium-silicon oxynitrides, are slightly larger than the corresponding yttrium phases. Although the new phase $Ce_2Si_6O_3N_8$ has not yet been characterized it appears to have an analogue in the La-Si-O-N system; see Wills et al. (47).

A characteristic feature of the Y-Si-O-N system is the complexity of the Y_2O_3-SiO_2 join. There exist two silicates of composition Y_2SiO_5 and no fewer than six modifications of $Y_2Si_2O_7$, and the nature of these silicate phases is important when considering the oxidation of silicon nitride containing small additions of yttria. In the CeO_2-Ce_2O_3-SiO_2 system further preparation and characterization is required but there is evidence so-far of one Ce_2SiO_5 phase, two $Ce_2Si_2O_7$ phases and one $Ce_2Si_3O_9$. In addition, the cerium-apatite extends along the oxide join. The unit cells of Ce_2SiO_5 and $Ce_2Si_2O_7$ are unknown but $Ce_2Si_3O_9$ is tetragonal with $\underline{a}$ = 6.798 and $\underline{c}$ = 24.726Å. None of the silicates bear any resemblance to those in the yttrium system.

The region marked "G" in Figure 53 is liquid at high temperature and cools to give a glass. This is similar to the behaviour observed in the Y-Si-O-N system.

VI.4 The Ce-Al-O-N system

Figure 54 is the Ce-Al-O-N behaviour diagram at 1700°C. There are two phases along the Ce_2O_3-Al_2O_3 join: (i) the perovskite-type $CeAlO_3$ which is tetragonal with $\underline{a}$ = 3.762 and $\underline{c}$ = 3.794Å and not rhombohedral as reported by Mizuno et al. (49); (ii) the β-alumina type $Ce_2O_3.11Al_2O_3$ with hexagonal unit-cell dimensions $\underline{a}$ = 5.555 and $\underline{c}$ = 22.009Å in good agreement with previous work (49, 50). The only oxynitride has the approximate composition $Ce_2O_3.3AlN$ and is yet uncharacterized; it has no analogue in either the yttrium or lanthanum systems.

It should be noted that cerium in its silicates, aluminates, aluminosilicates and oxynitrides is trivalent but under conditions of

Table 4

Unit-cell dimensions of α-wollastonites

	Angstroms			degrees	cation
	a	b	c	β	radius, Å
$YSiO_2N$	7.012	12.168	18.202	90.8	0.93
α-$CaSiO_3$	6.90	11.78	19.65	90.8	0.99
$CeSiO_2N$	12.545	7.269	28.396	90.4	1.02
α-$SrSiO_3$	12.40	7.16	30.36	90.0	1.13

Table 5

Unit-cell dimensions of aluminium carbides

	a,A	c,A	V,A^3	poly-type	stacking sequence
Al_4C_3	3.332	24.96	240.0	9R	ABCBCACABABC...
δ-Al_4C_3	3.408	15.92	160.1	6H	ABCACBABC...

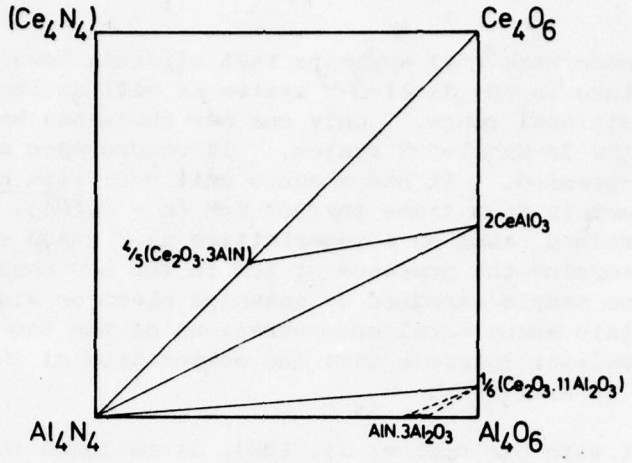

Figure 54. The behaviour diagram of the Ce-Al-O-N system at 1700°C

high oxygen potential it becomes tetravalent and the compounds decompose to give ceric oxide, CeO_2, when heated in air to about 1400°C.

VII. ZIRCONIUM SIALONS

Recent Japanese work (51) suggests that zirconia lowers the liquidus temperature in the Si-Al-O-N system as well as increasing the liquid compositional range. Only one new phase has been found at Newcastle in the Zr-Si-Al-O-N system. It occurs when a mixture $ZrO_2.2AlN$ is hot-pressed. It has a cubic unit cell with $\underline{a}$ = 18.32Å, that is, approximately four times that of ZrN ($\underline{a}$ = 4.56Å). The structure is therefore based on a superlattice of ZrN and so it is impossible to determine the presence of ZrN in the new phase by X-ray diffraction. One sample examined by scanning electron microscopy was found to contain about equal concentrations of the two phases and microprobe analysis suggests that the composition of the superlattice material is $ZrAl_5O_5N_3$.

In agreement with Claussen et al. (52), it is found that nitrogen stabilises cubic ZrO_2. The latter is observed on cooling compositions where monoclinic zirconia with additional nitride or oxynitride phases might have been expected.

From the Zr-Si-O-N behaviour diagram at 1700°C (see Figure 55) a small amount of liquid which dissolves silicon nitride will be formed locally at the silica-rich grain boundaries when silicon nitride is hot-pressed with 5w/o ZrO_2; this is adequate to provide conditions for liquid-phase densification.

It has been reported (53) that reaction of ZrO_2 with silicon nitride can lead to the formation of zirconium nitride. Given an initial composition within the Si_3N_4-Si_2N_2O-ZrO_2 triangle of Figure 55, loss of the volatile silicon monoxide and nitrogen ($3SiO + N_2$ corresponds to the mid-point of the $3SiO_2$-Si_3N_4 join) will certainly move the composition of the remaining condensed material into the three-phase field Si_3N_4-ZrN-ZrO_2. In other words, the reaction given by equation

$$2Si_3N_4 + 2SiO_2 + 2ZrO_2 \longrightarrow 2ZrN + 8SiO + 3N_2 \qquad \ldots\ (8)$$

is thermodynamically possible if silicon monoxide and nitrogen are removed by volatilisation.

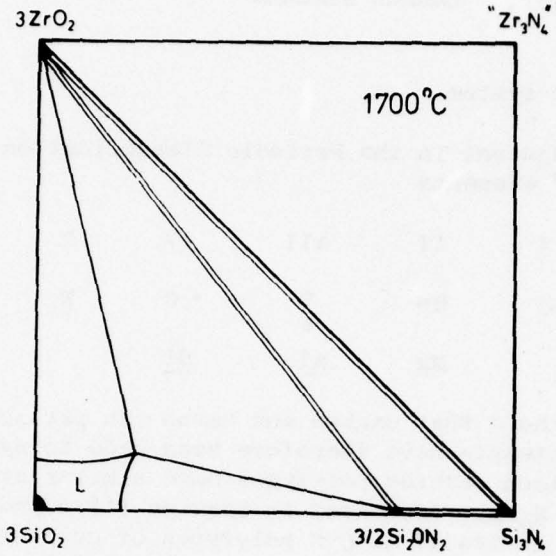

Figure 55. The Zr-Si-O-N behaviour diagram at 1700°C

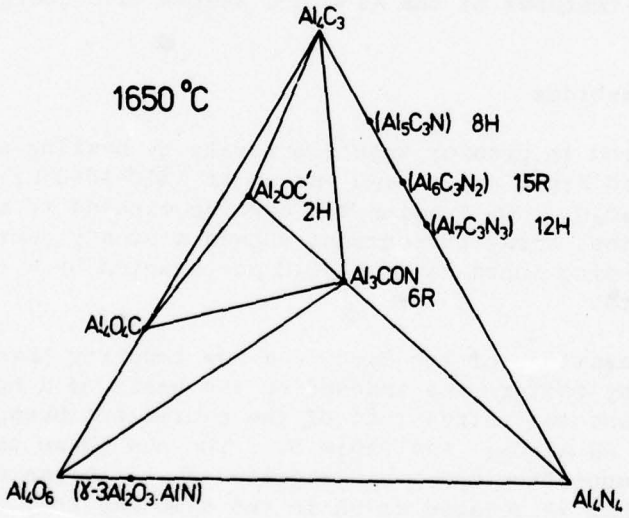

Figure 56. The Al_4C_3-Al_4O_6-Al_4N_4 behaviour diagram at 1650°C

VIII. CARBON SIALONS

VIII.1 The Si-Al-O-N-C system

Because they are adjacent in the Periodic Classification to the sialon "net-work former" elements

periodic group	I	II	III	IV	V	VI
	Li	Be	B	C	N	O
		Mg	Al	Si		

there seems every likelihood that carbon and boron can participate in "ceramic alloying". Attempts have therefore been made to synthesise "carbon sialons". Silicon carbide polytypes have similar structures to the sialon-polytypes M_mX_{m+1} discussed in Section III.5 and there exists (54, 55) a whole series of Al-C-N polytypes of composition $M_{m+1}X_m$ similar to the new Be-Si-O-N polytypes. Thus, although silicon nitride and silicon carbide are immiscible, it was thought that the sialon polytypes and the aluminium carbonitrides might react to give Si-Al-O-N-C compounds. No phase that contains all five elements has so-far been prepared in the present or in any other work but in efforts to do so new features of the Al-O-N-C system have emerged.

VIII.2 Aluminium carbides

Al_4C_3 was prepared in greater than 95% purity by heating aluminium and carbon in purified argon or in high vacuum at 1200-1650°C; the major impurity is Al_4O_4C. On leaving the carbide exposed to air over a period of four months, X-ray photographs showed a steady decrease of Al_4C_3 and a corresponding increase of Al_4O_4C accompanied by a colour change yellow to white.

In several preparations of the carbide a new impurity phase appeared and its X-ray pattern was indexed on the basis of a hexagonal unit cell with a volume two-thirds that of the equivalent hexagonal cell of rhombohedral 9R Al_4C_3; see Table 5. The new phase occurs at or near the Al_4C_3 composition and was designated δ. It has a 6H polytype structure that is related to 9R in the same way that wurtzite is related to zinc blende.

VIII.3 The Al-O-N-C system

The Al_4C_3-Al_4O_6-Al_4N_4 behaviour diagram at 1650°C is shown by Figure 56. One new phase is observed, namely Al_3ONC, lying on the line between Al_2OC and AlN. No trace of the aluminium carbonitrides 8H-Al_5C_3N, 15R-$Al_6C_3N_2$ and 12H-$Al_7C_3N_3$, known to exist at 1800°C (56), was found at 1650°C.

Henry et al. (56) reported an extensive range of solid solution, including the composition Al_3ONC, between Al_2OC and AlN but no such range is observed at 1650°C in the present work and only a small range for the oxycarbonitride is found at 1700°C. Al_3ONC is rhombohedral with equivalent hexagonal unit-cell dimensions

$$\sqrt{3}\underline{a} \simeq \underline{a}' = 5.453; \qquad \sqrt{3}\underline{c} \simeq \underline{c}' = 14.935\text{Å}$$

where $\underline{a}$ and $\underline{c}$ are the dimensions of the AlN unit cell. The structure is a superlattice of the AlN wurtzite-type with ordering of the three different non-metal atoms and probably small shifts of all the atoms from their ideal positions.

Along the Al_4C_3-Al_2O_3 join two aluminium oxycarbides are reported (56). As mentioned above, the room temperature oxidation of Al_4C_3 gives Al_4O_4C and none of the intermediate oxycarbide Al_2OC is found up to 1650°C. However, small amounts of nitrogen stabilise this phase and so Al_2OC' with a 2H structure is located on the behaviour diagram of Figure 56 inside the Al_4C_3-Al_4O_6 join.

No properties of the oxycarbonitrides have yet been measured and the difficulty of preparing these and the other phases of the Al-O-N-C system pure and homogeneous seems likely to be a barrier to any technological development.

IX. LIQUIDS AND GLASSES

IX.1 Vitreous phases containing nitrogen

Glasses occur in all the sialon systems so-far examined and it is perhaps not surprising that nitrogen can replace some of the oxygen in molten and vitreous silicates considering that it readily does so in the crystalline ones. Even in the first investigation of the role of magnesia in hot-pressed silicon nitride (1) the glass formed on cooling the "magnesium silicate" liquid gave silicon oxynitride as one of its devitrification products and so, quite clearly, must have contained nitrogen. These glasses are important because the mechanical properties of nitrogen ceramics, particularly their high-temperature strength and creep resistance, depend markedly on the amount and characteristics of the grain-boundary glass.

Nitrogen glasses are also of interest as materials in their own right. Even small concentrations of nitrogen not exceeding 1a/o in oxide glasses are reported (57) to increase the softening temperature, viscosity and resistance to devitrification. Glasses with 10a/o N or more might be expected to have more unusual properties because if the nitrogen in the tetrahedral net-work is co-ordinated by three ligands the structure should be more rigid and have a higher viscosity than the silicate glasses. The ease of shaping glasses, and also the possibility of producing glass-ceramics in which the crystalline phases are refractory nitrides and oxynitrides, suggest that nitrogen-containing glasses are well worth scientific and technological exploration. It extends still further the field of nitrogen materials and emphasizes the need for investigation over a wide enough temperature range to include liquids as well as solids.

IX.2 Mg-Si-O-N and Mg-Si-Al-O-N glasses

Glass formation in these magnesium systems is remarkably easy as shown by the series of X-ray photographs of Figure 57. When mixtures of 20w/o MgO:80w/o SiO_2 are pressed at 1700°C without Si_3N_4 the product, as expected, consists of crystalline protoenstatite and cristobalite. Addition of 10w/o Si_3N_4 to this same mix gives, after the same treatment, a completely vitreous product that devitrifies at 1500°C to cristobalite, clino enstatite and silicon oxynitride. Corresponding optical micrographs are shown by Figure 58.

Additions of Al_2O_3 to Mg-Si-O-N compositions extend the vitreous region and mixtures of MgO, SiO_2 and AlN cold-compacted, heated to 1650°C for 30 minutes and then cooled, give glasses containing up to 10a/o N; this glass forming region is shown by the shaded area of

Figure 59 in which the highest nitrogen corresponds with a glass composition $Mg_9Si_{21}Al_{10}O_{50}N_{10}$.

IX.3 Yttrium-sialon glasses

Figure 60 shows the glass forming region of the Y_2O_3-SiO_2-AlN system. The first bulk sample of glass in this system was obtained by melting a mixture of molar composition

$$14Y_2O_3:59SiO_2:27AlN \text{ (i.e. } Y_9Si_{20}Al_9O_{53}N_9)$$

in a graphite crucible lined with boron nitride at 1650°C under nitrogen and then cooling to room temperature. Electron probe microanalysis showed that the glass was homogeneous with a composition close to that of the starting mix. In thin sections it was transparent with a refractive index 1.76. Devitrification at 1200°C for 16 hours gave a mixture of crystalline products β-$Y_2Si_2O_7$, $Y_3Al_5O_{12}$ (yttrium-aluminium garnet) and Si_2N_2O.

Grain-boundary glasses in silicon nitride hot-pressed with relatively small additions of yttria and alumina have recently all been found by electron probe analysis to have similar compositions, for example

$$Y_9Si_{14}Al_{15}O_{58}N_4,\ Y_{10}Si_{12}Al_{17}O_{57}N_5 \text{ and } Y_{11}Si_{13}Al_{14}O_{57}N_5$$

A glass with the composition $Y_{10}Si_{12}Al_{16}O_{57}N_4$ has been prepared pure by melting Y_2O_3, SiO_2, Al_2O_3 and Si_3N_4 in the hot press at 1800°C for 30 minutes and future work will include an investigation of the oxidation, devitrification and creep properties of the glass in order to predict the properties of yttrium-sialons containing a grain-boundary glass of this composition.

Figure 61 shows the X-ray photograph of the product made by heating 27w/o Y_2O_3:18w/o Al_2O_3:45w/o SiO_2:10w/o Si_3N_4 at 1600°C; it is completely vitreous. Devitrification to β-$Y_2Si_2O_7$, Al_2O_3 and Si_2N_2O takes about ten days at 1360°C; photomicrographs showing these transformations are given in Figure 62.

IX.4 Other vitreous phases

Calcium-sialon glasses have also been prepared containing nearly 10a/o nitrogen; a typical microprobe analysis is $Ca_{11}Si_{18}Al_{11}O_{51}N_9$.

Even in the Si-Al-O-N system nitrogen-containing glasses can be produced by rapid cooling of melts near the X-phase composition. For example, Figure 63 shows the X-ray photograph of a mixture of silica, alumina and aluminium nitride quenched after heating for 30 minutes at 1700°C; the composition $Si_{27}Al_9O_{57}N_7$ is completely vitreous but the same treatment followed by slow cooling gives X-phase, mullite and silicon oxynitride.

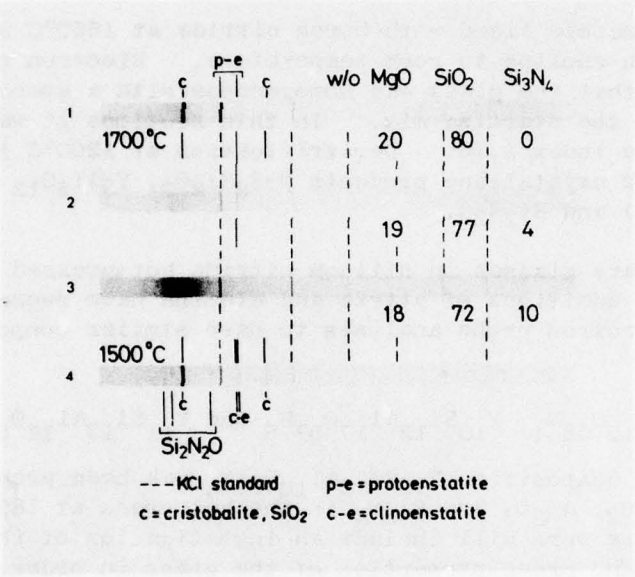

Figure 57. X-ray photographs showing Mg-Si-O-N glass formation and devitrification

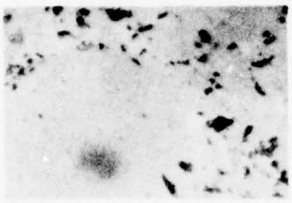

19MgO:77SiO_2:4Si_3N_4(wt%)
Partially vitrified

18MgO:72SiO_2:10Si_3N_4(wt%)
Glass

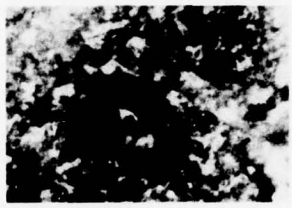

Above glass
devitrified

Figure 58. Optical micrographs showing Mg-Si-O-N glass formation and devitrification (x 150)

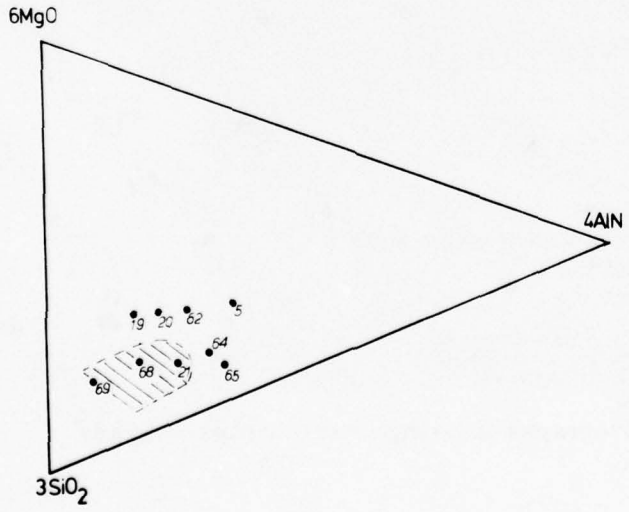

Figure 59. The glass forming region of the MgO-SiO_2-AlN system

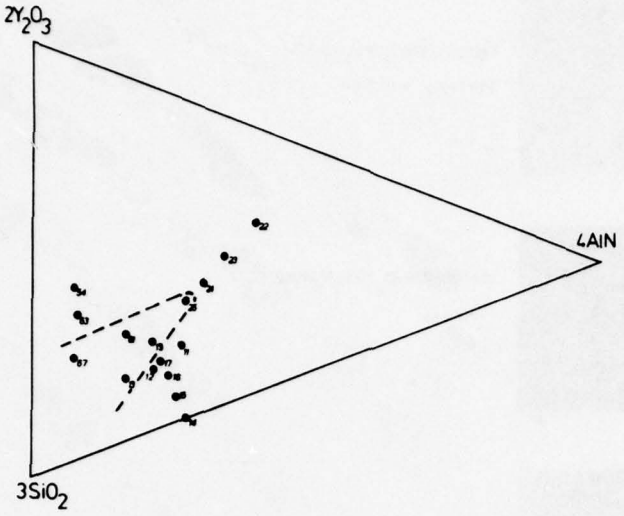

Figure 60. The glass forming region of the Y_2O_3-SiO_2-AlN system

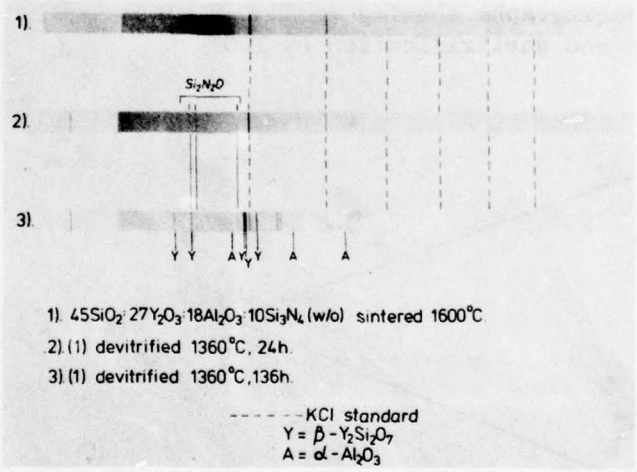

Figure 61. X-ray photographs showing yttrium-sialon glass formation

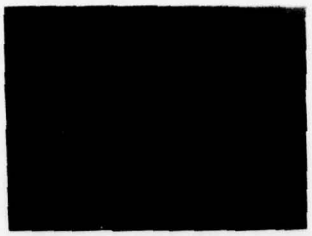

$45SiO_2\ 27Y_2O_3\ 18Al_2O_3\ 10Si_3N_4$ (w/o)
Glass

Above devitrified 1360°C, 24h

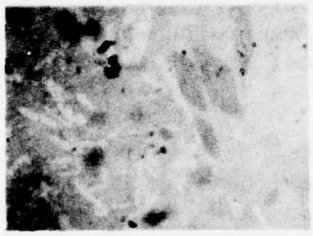

Devitrified 1360°C, 136h

Figure 62. Optical micrograph showing yttrium-sialon glass formation (x 150)

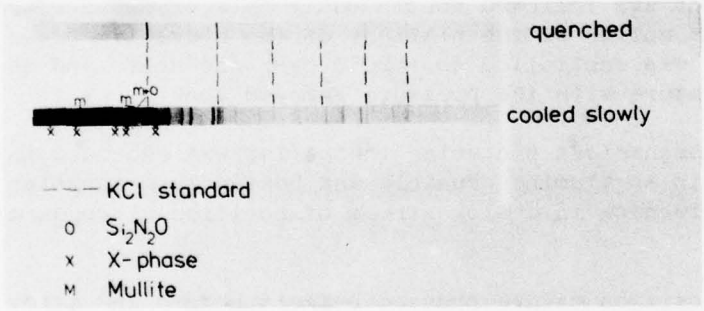

Figure 63. X-ray photographs of the composition $Si_{27}Al_9O_{57}N_7$:
(a) after quenching from 1700°C (completely vitreous);
(b) after slow cooling from 1700°C (mixture of X-phase, mullite and silicon oxynitride)

X. THE DENSIFICATION OF SILICON NITRIDE AND SIALONS WITH OXIDE ADDITIVES

X.1 Experimental

In order to compare the densifying characteristics of different additives, 20g of the appropriate powder mix was milled for 18h in a polypropylene jar with tungsten carbide balls (12 mm diameter; 130g) and butan-1-ol (100 ml). After evaporating the milling medium the powder was vacuum dried at 110°C and then remixed dry. Samples were cold-compacted in a steel die to approximately 60% theoretical density and the pellet so-produced trimmed to a cylinder 22 mm diameter x 25 mm high for hot-pressing or 10 mm diameter x 10 mm high for pressureless sintering.

For the initial appraisal of hot-pressing behaviour, the pellet was placed between graphite plungers inside a graphite die with all surfaces protected by a deposited boron nitride layer and with the pellet embedded in boron nitride powder. A pressure of $31.7 MNm^{-2}$ (4600 psi) was applied from cold and maintained constant during each run. Heating to 1800°C required about 30 minutes with an almost linear rise in temperature.

In the subsequent measurements of hot-pressing kinetics, the pressure of 4600 psi was applied before heating to compress the pellet and its surrounding boron nitride, and then the pressure was reduced to less than 100 psi during heating in order to minimise densification before the required hot-pressing temperature was reached. At the temperature to be investigated, the full pressure of 4600 psi was applied instantaneously and the shrinkage during isothermal densification was followed continuously by a transducer that monitors the relative motion of the plattens of the hydraulic press. The temperature was controlled to $\pm$ 20°C over one hour, and then cooling to room temperature with the pressure removed took about two hours.

For pressureless sintering the pellet was embedded in boron nitride powder within an alumina crucible and heated in a tungsten element resistance furnace in a slow stream of purified nitrogen at one atmosphere pressure.

The densities of die-pressed pellets before and after heat-treatment were measured by mercury displacement and the open porosity by a standard boiling water penetration method.

The α-β ratio of each hot-pressed and sintered product was obtained by micro-densitometry of Hägg-Guinier X-ray powder photographs of the crushed sample using the Newcastle calibration curves (58). A

correction for the amount of α-β transformation before reaching the desired temperature was obtained by determining the extent of transformation after heating to that temperature and cooling it immediately.

X.2 Hot-pressing silicon nitride

Figure 64 compares the relative shrinkages for 5w/o of each of the additives MgO, Y_2O_3, ZrO_2 and CeO_2 during the 30 minutes required to reach 1800°C. With all four additives full density is reached after a further 30 minutes at not less than 1800°C but the rate of densification and the density on first reaching the maximum temperature are roughly related to the appearance of liquid in the system. Although the solidus in the MgO-SiO_2 system is at 1547°C, impurities in the silicon nitride and also reaction with silicon nitride to give a nitrogen containing eutectic account for observations of liquid at 1450-1500°C (59, 60). The solidus in Y_2O_3-SiO_2 is at 1660°C but liquid formation occurs, again probably due to Si_3N_4 solubility, at least 60°C below this. With yttria, densification is slower than with magnesia because of the smaller amount of liquid formed and because of its higher viscosity.

It is impossible to account for the behaviour of ZrO_2 and CeO_2 in terms of large volume liquid-phase formation at the low temperatures at which slow densification is observed. The rates seem characteristic of a particle rearrangement process involving only small amounts of liquid.

Without additives, densification of silicon nitride is negligible below 1700°C and although the surface silica becomes vitreous at higher temperatures, it reacts with silicon nitride to give oxynitride before its viscosity becomes low enough to aid sintering.

X.3 Pressureless sintering of silicon nitride

Terwilliger & Lange (61) showed that silicon nitride powder (90α:10β) could be pressureless sintered with addition of 5w/o MgO by heating in the range 1500-1750°C either for long periods at the lower temperatures or for short periods at the higher ones. In the present work, almost full densification (i.e. less than 5% closed porosity) is achieved with 5w/o MgO at temperatures as low as 1450°C. Above 1700°C, decomposition with weight losses prevents complete sintering. Table 6 shows that at 1350°C, below the α-β thermodynamic transformation temperature (62, 63), no transformation is in fact observed and there

Table 6

Pressureless sintering of silicon nitride for 3h

at 1350° and 1450°C ($-\Delta V/V_o$ for zero porosity ~40%)

starting powder α:β	additive w/o	% change at 1350°C $-\Delta V/V_o$	1350°C β	1450°C $-\Delta V/V_o$	1450°C β
90:10	none	0	0	1	+5
	5MgO	3	0	37	+40
	7 Y_2O_3	2	0	13	+80
30:70	none	0	0	1	0
	5 MgO	3	0	2	+15

is negligible densification. Also, under conditions which give almost complete densification and appreciable transformation (40% transformation with 5w/o MgO at 1450°C) with high α-powder, there is no densification with high β-powder and, of course, little transformation. With yttria instead of magnesia there is much more transformation but much less densification. As will be shown, there is less liquid with yttria than with magnesia.

X.4 Hot-pressing β'-sialon compositions

As shown by Figures 9 and 11 the small silica-rich liquid field at 1650°C in the Si-Al-O-N system extends as the temperature rises and includes X-phase at about 1720°C. There then exists a considerable two-phase field, β' + liquid. Mixtures of Si_3N_4, Al_2O_3 and AlN or other appropriate starting powders can be hot-pressed to give a pure, theoretical density β'-sialon provided that compensation is made for the surface oxides that are always present on the nitrides. Chemical reaction starts at about 1450°C and the densification that also starts at this temperature is probably due to particle rearrangement accompanying the chemical reaction. The densification is complete at 1750°C but completion of the α-β' transformation requires about one hour at this temperature and, if the composition is perfectly balanced, all liquid phase should disappear just when the reaction is finished.

Densification and transformation are facilitated by using an additive because, in general, liquid metal-alumino-silicates containing nitrogen are formed and so allow rearrangement as well as the solution-precipitation transport of material. Also, the driving force for the transformation to β' is much greater than that for α-β. Thus, if the chemical activity of "β-silicon nitride" is reduced to 0.1 of its value by its reaction to give a β' solid solution then, as shown by Figure 65, the transformation temperature is reduced by 200°C.

X.5 Pressureless sintering of β'-sialon compositions

Table 7 shows that the additives MgO, Y_2O_3, ZrO_2, CaO and B_2O_3 promote β' formation during the pressureless sintering of a z=3 β'-sialon composition and all, except B_2O_3, give considerable densification at 1600°C and 1650°C. 5w/o MgO is the most effective at 1650°C for 30 minutes but 4w/o Y_2O_3 and 3w/o ZrO_2 also give theoretical density if maintained long enough at 1650°C or if the temperature is raised to 1700°C. Above 1700°C loss of silica occurs by volatilisation or oxidation or both, and the remaining composition moves towards the AlN corner of the system to produce polytype phases.

Table 7

Pressureless sintering β'-sialon compositions (z=3)

for 30 minutes at 1500-1650°C ($-\Delta V/V_o$ for zero porosity ~ 32%)

w/o additive to z=3 mix	% change					
	1500°C		1600°C		1650°C	
	$-\Delta V/V_o$	β	$-\Delta V/V_o$	β	$-\Delta V/V_o$	β
0	-	-	-	-	6	75
3MgO	4	20	23	90	25	90
5MgO	7	15	29	80	31	85
7MgO	2	20	22	90	25	90
$4Y_2O_3$	7	50	29	90	30	90
$3ZrO_2$	8	60	24	90	29	90
4CaO	4	20	25	90	26	90
$3B_2O_3$	3	40	9	90	13	90

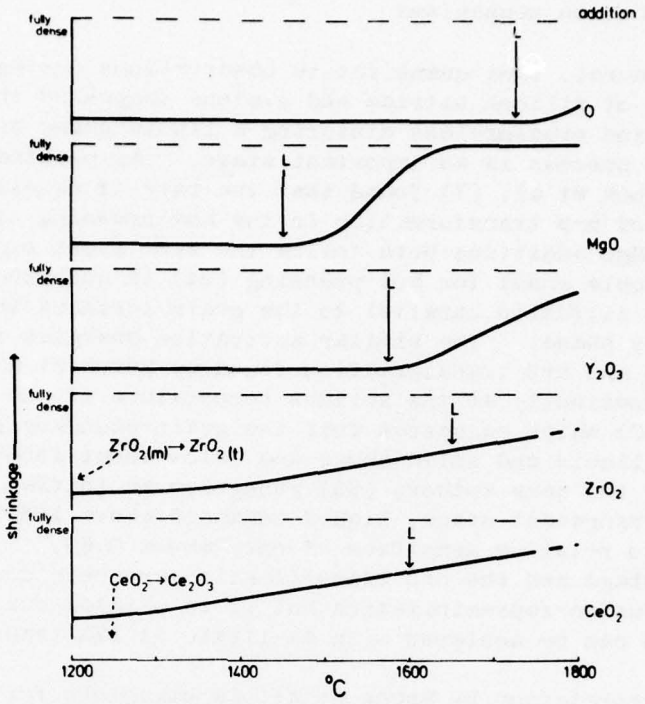

Figure 64. Shrinkage v. temperature for 5w/o additives in hot-pressed Si_3N_4

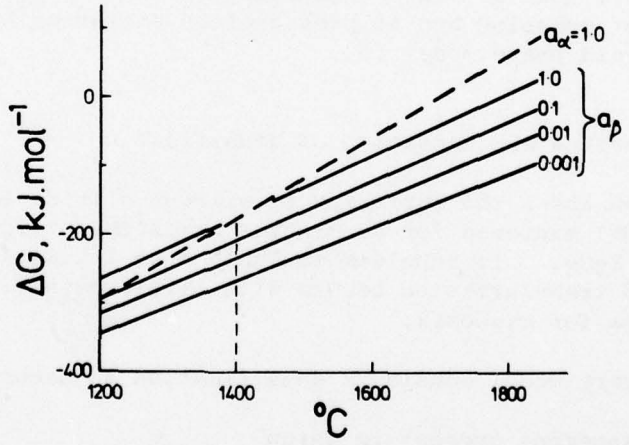

Figure 65. Change in α-β transformation temperature with reduction of the "β-Si_3N_4" activity

X.6 Densification mechanisms

These general, semi-quantitative observations during the densification of silicon nitride and sialons suggested that in both hot-pressing and pressureless sintering a liquid-phase solution-precipitation process is an important stage. As pointed out in Section I, Brook et al. (7) found that the rate of densification and the rate of α-β transformation in the hot-pressing of silicon nitride with MgO additions both follow the same first order kinetics and, if the Coble model for hot-pressing (64) is accepted, are controlled by diffusion parallel to the grain surfaces through the grain-boundary phase. The similar activation energies for densification and α-β transformation found by Brook et al. both show the same discontinuity at the solidus temperature of the MgO-SiO_2 system (1543°C) which suggested that the grain-boundary phase is respectively liquid and solid above and below about 1550°C. In a further paper the same authors (65) recognise an initial very rapid particle rearrangement stage, liquid enhanced above 1550°C, that operates up to relative densities of only about 0.65. The second, much slower stage and the α-β transformation are both controlled by solution-diffusion-reprecipitation but it is pointed out that complete densification can be achieved with as little as 12% transformation.

The interpretation by Brook et al. is plausible for hot-pressing with MgO additive but it ignores the quite different characteristics of densification with other oxides, for example Y_2O_3. Moreover, it seemed from the present work and following Terwilliger & Lange (66) and Mitomo (67) that similar mechanisms of densification might be applied to hot-pressing and to pressureless sintering by using Kingery's liquid-phase model (5).

X.7 The kinetics and mechanism of densification

Figure 66 shows the shrinkage of silicon nitride ($\Delta V/V_o$ for zero porosity 40%) sintered for 30 minutes at different temperatures with MgO and with Y_2O_3. It supplements Table 6 in illustrating that extensive α-β transformation occurs with little densification for yttria and vice versa for magnesia.

The Kingery model considers densification to occur in three stages:

(i) a rearrangement process in which

$$\Delta V/V_o \propto t^{1+y}$$

where the exponent 1+y is not much larger than unity;

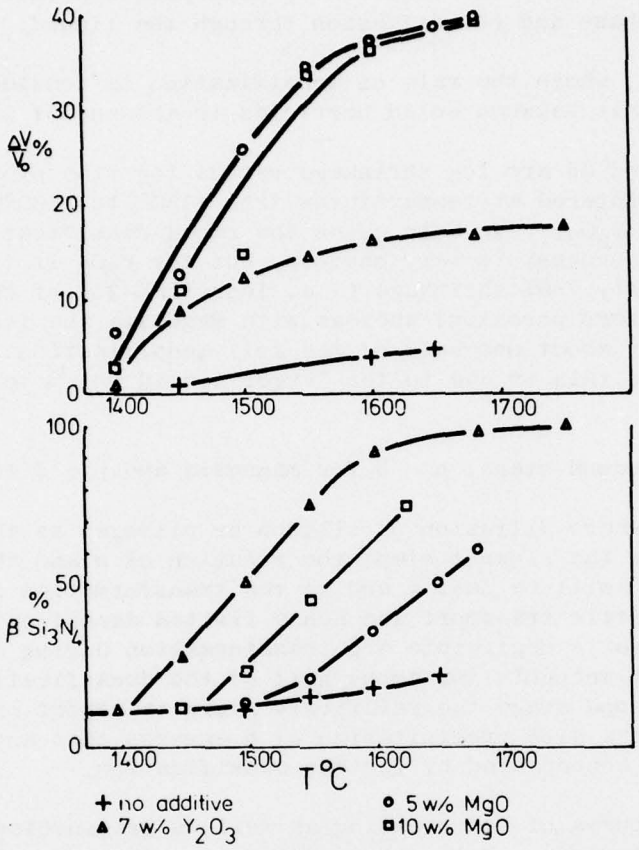

Figure 66. Shrinkage and α-β transformation for Si_3N_4 sintered for 30 minutes at different temperatures with MgO and Y_2O_3 additives

(ii) solution-precipitation in which

$$\Delta V/V_o \propto t^{1/n}$$

and where n = 3 or 5 depending on whether the rate controlling step is respectively (a) solution or precipitation into or from the liquid phase and (b) diffusion through the liquid;

(iii) coalescence, where the rate of densification is considerably reduced to that between solid particles in absence of liquid.

Figures 67 and 68 are log shrinkage versus log time plots for silicon nitride sintered at temperatures from 1450° to 1600°C with 5w/o MgO and 7w/o Y_2O_3. In both cases the rapid densification of the rearrangement process is very obvious, but for Y_2O_3 it is responsible for only 7-9% shrinkage (i.e. less than 25% of the total densification to zero porosity) whereas with magnesia the first stage is responsible for about one-half of the full densification. As might be expected, this is due to the larger liquid volume obtained with magnesia.

During the second stage, n = 3 for magnesia and n = 5 for Y_2O_3.

For yttria, where diffusion of silicon or nitrogen is the rate-limiting and hence the slowest step, the solution of α and the precipitation of β will be faster and so the transformation α-β can occur with only little transport and hence limited densification. With magnesia there is negligible α-β transformation during the initial rearrangement that accounts for about half of the densification, and then during the second stage the relatively rapid transport of material by diffusion and the slow precipitation of β ensures that any α-β transformation is accompanied by further densification.

The main features of hot-pressing as well as pressureless sintering are explained. Full densification never occurs without some transformation because the second stage of the process involves solution of α and precipitation of β. On the other hand, solution of α and precipitation of β can occur without major transport of material and so some transformation takes place without densification. The amount of densification without transformation during the first stage depends on the quantity of liquid formed and hence on the amount of additive, on the kind of additive, and on the amount of surface silica present on the nitride. The amount of transformation without densification during the second stage depends on whether solution or diffusion is rate-controlling and hence upon the characteristics of the liquid, i.e. again upon the specific additive used. No densification during this stage can occur without some α-β transformation but, as pointed out by Brook et al. (7), the amount required for the removal of (say) 25% porosity need only be 12%.

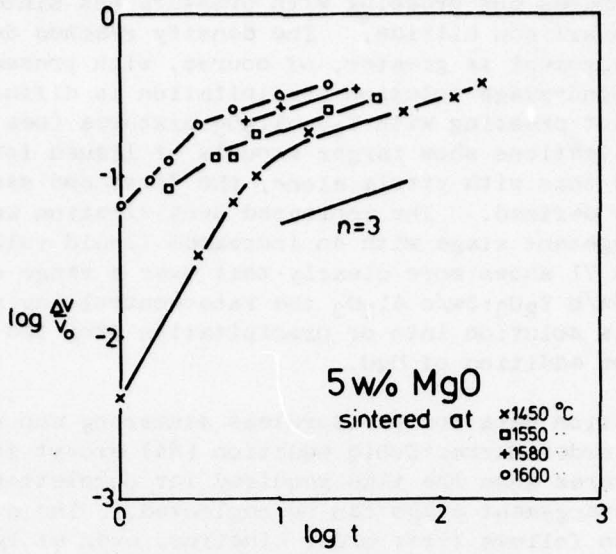

Figure 67. Log shrinkage ($\Delta V/V_o$) versus log time (t, minutes) for Si_3N_4 sintered with 5w/o MgO at 1450-1600°C

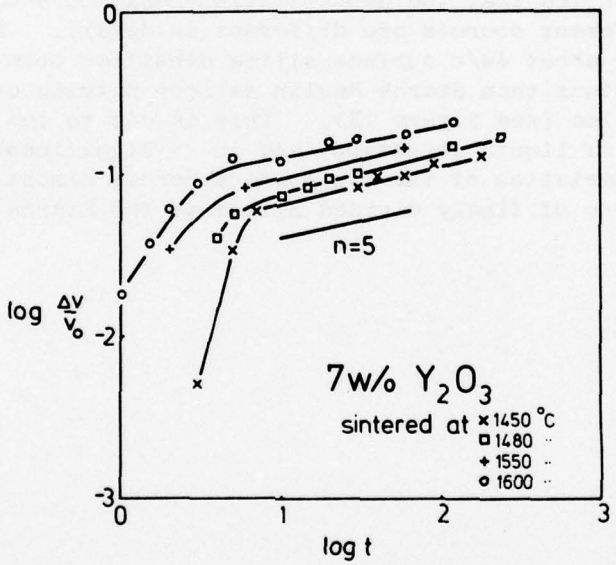

Figure 68. Log shrinkage ($\Delta V/V_o$) versus log time (t, minutes) for Si_3N_4 sintered with 7w/o Y_2O_3 at 1450-1600°C

Figure 69 compares hot-pressing with pressureless sintering for 7w/o Y_2O_3 added to silicon nitride. The density reached during the first-stage rearrangement is greater, of course, with pressure but in both cases the second-stage solution-precipitation is diffusion controlled. In hot-pressing with Y_2O_3-Al_2O_3 mixtures (see Figure 70) where phase investigations show larger amounts of liquid formation at lower temperatures than with yttria alone, the first and second stages are not so clearly defined. The increased densification achieved during the rearrangement stage with an increased liquid volume is expected. Figure 71 shows more clearly that over a range of temperature with 5w/o Y_2O_3: 5w/o Al_2O_3 the rate-controlling step during the second stage is solution into or precipitation from the liquid in the same way as for addition of MgO.

The densification data for pressureless sintering can not be fitted to a first order Murray-Coble equation (64) except fortuitously at higher temperatures when the time required for completion of the rapid initial rearrangement stage can be neglected. The α-β transformation also follows first order kinetics, even at lower temperatures, once the rearrangement stage is complete. This is expected if transformation occurs only by second stage solution-precipitation.

It should be noted that the densification behaviours of silicon nitrides from different sources are different in detail. Lucas silicon nitride containing about 4w/o surface silica densifies more readily under given conditions than Starck Berlin silicon nitride containing less than 3w/o silica (see Figure 72). This is due to the different volumes and rates of liquid formation, and it is significant that the densifying characteristics of the two powders become almost identical by adding about 1w/o of finely divided silica to the Starck Berlin silicon nitride.

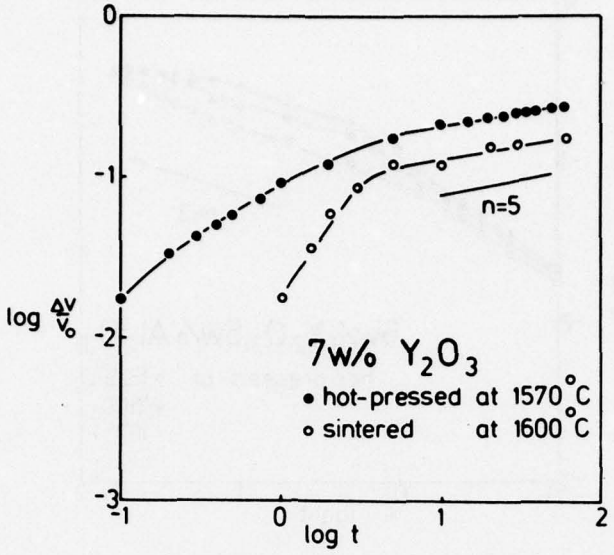

Figure 69. Comparison of hot-pressing Si_3N_4 with 7w/o Y_2O_3 at 1570°C with sintering at 1600°C

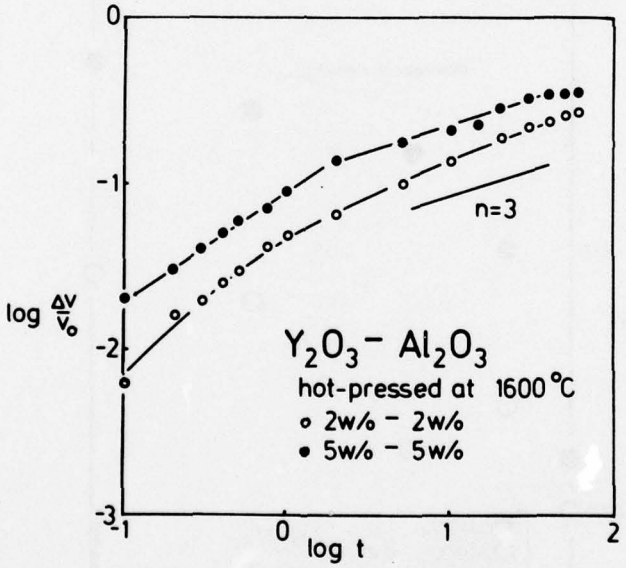

Figure 70. Hot-pressing Si_3N_4 with Y_2O_3:Al_2O_3 at 1600°C

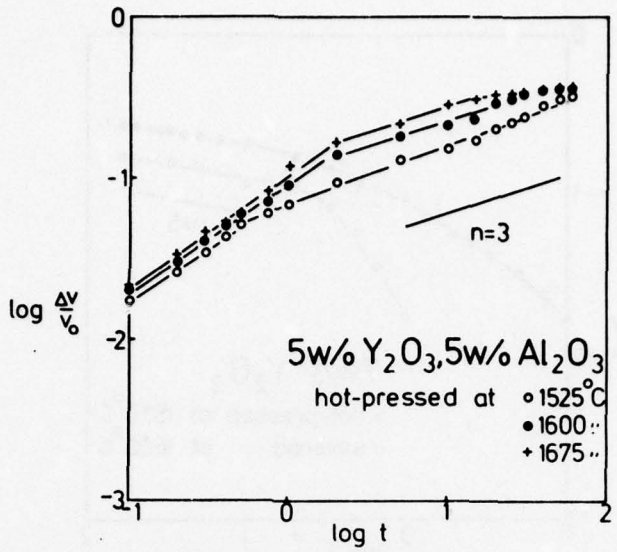

Figure 71. Hot-pressing Si_3N_4 with 5w/o Y_2O_3: 5w/o Al_2O_3 at 1525-1675°C

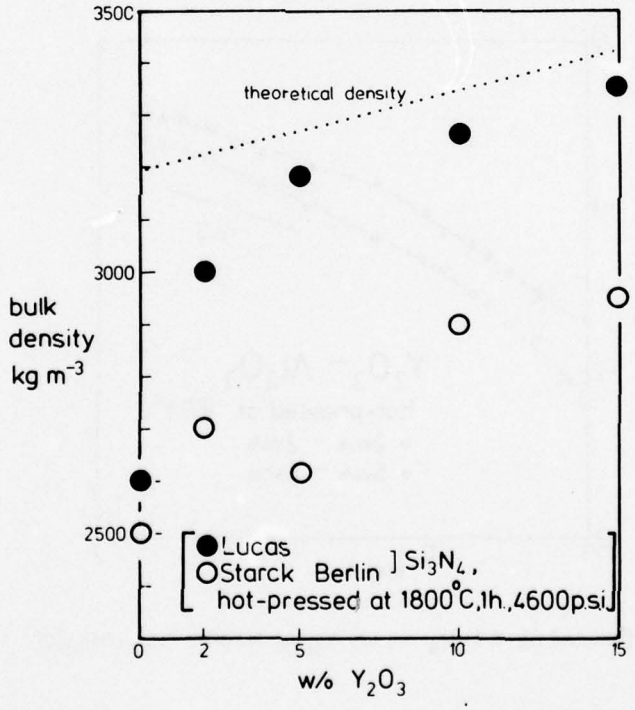

Figure 72. Densities of Starck Berlin and Lucas silicon nitrides hot-pressed for 1h at 1800°C with 2-15w/o Y_2O_3

XI. THE EFFECTS OF ADDITIVES ON PROPERTIES

XI.1 Magnesia

The oxidation of MgO-Si_3N_4 materials follows parabolic kinetics indicating that diffusion is rate controlling. Between 750° and 1000°C an amorphous protective layer of silica is formed on the surface but at higher temperatures crystalline oxidation products, principally cristobalite (SiO_2) and enstatite ($MgSiO_3$) are formed. Above 1400°C there is a rapid increase in the rate of oxidation which is explained by partial melting of the oxide scale with a resultant increase in the mobility of the diffusing species. Impurities such as Ca and Fe concentrate in the oxidised layer, reducing its melting temperature and so further lowering the oxidation resistance. As shown by Figure 73, the surface oxide coating on a sample of HS-110 hot-pressed silicon nitride oxidised at 1400°C for 120h has obviously been fluid at temperature. The presence of bubbles in the surface layer may be explained by the evolution of nitrogen on cooling due to its reduced solubility in the Mg-Si-O-N liquid, or by the reaction of silicon nitride with oxygen

$$Si_3N_4 + 3O_2 \longrightarrow 3SiO_2 + 2N_2 \qquad \ldots\ (9)$$

The cracks visible in the oxidised layer are typical of cooling cracks formed by mis-match of the thermal expansion with that of the underlying silicon nitride. *These cracks expose fresh nitride surfaces for* oxidation and so will reduce the oxidation resistance during thermal cycling.

Lange (68) states that the maximum strength and oxidation resistance at 1400°C occur with MgO-SiO_2 ratios that approach either zero or infinity, that is along the tie-lines Si_3N_4-Si_2N_2O or Si_3N_4-MgO. Strength is a *minimum* along the Si_3N_4-Mg_2SiO_4 join. It is clear from the glass composition region given in Figure 28 that silicon nitride with its usual surface silica content ($\simeq$4w/o) will contain glass after hot-pressing or sintering with added magnesia. Only when the MgO content is low enough to bring the overall composition within or near the Si_3N_4-Si_2N_2O two-phase region ($MgO:SiO_2$ ratio $\simeq 0$) or is high enough to bring it into the three phase triangle Si_3N_4-$MgSiN_2$-Mg_2SiO_4 ($MgO:SiO_2$ ratio $\simeq \infty$) will glass be avoided.

Formation of liquid is necessary for densification by liquid-phase sintering but subsequent formation of glass on cooling the liquid will reduce the hot-strength, oxidation resistance and creep resistance of the material.

AD-A058 807 NEWCASTLE-UPON-TYNE UNIV (ENGLAND) F/G 11/2
THE ROLE OF ADDITIVES IN THE DENSIFICATION OF NITROGEN CERAMICS--ETC(U)
NOV 77 K H JACK DA-ERO-76-G-067

UNCLASSIFIED NL

2 OF 2

AD A058 807

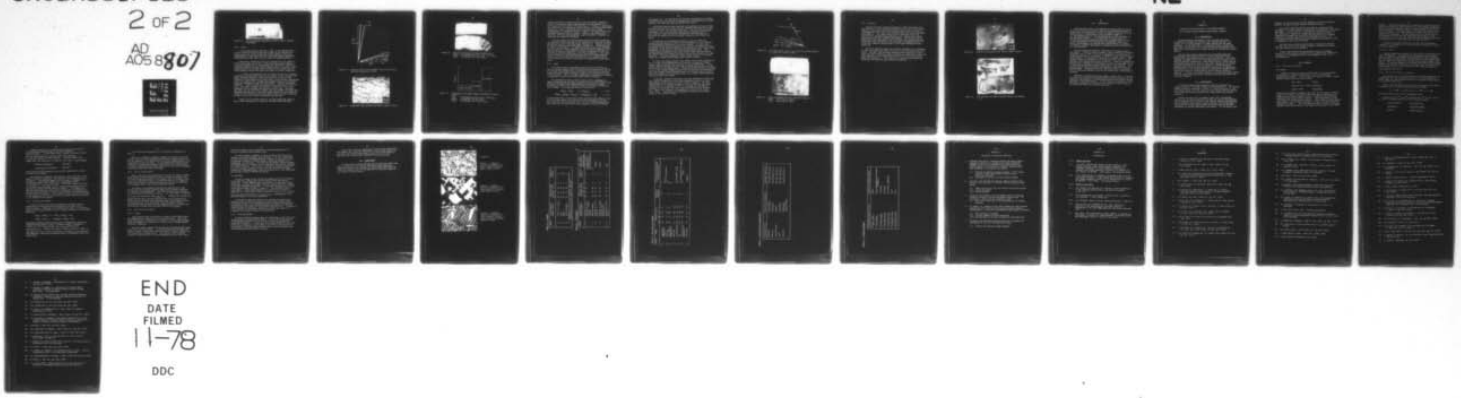

END
DATE FILMED
11-78
DDC

Figure 73. HS-110 Si_3N_4-MgO oxidised for 120h at 1400°C (optical micrograph)

XI.2 Yttria

It has been stated in Section V.1 that in the densification of silicon nitride with yttria the first-formed liquid combines with Si_3N_4 to give one or more refractory bonding phases in which are accommodated the impurities that would otherwise degrade properties. Yttria would at first seem to be the ideal hot-pressing additive.

The product containing 15w/o Y_2O_3 oxidises only very slowly at 1400°C (see Figures 74 and 75) to give cristobalite and γ-$Y_2Si_2O_7$ in a protective glaze but at lower temperatures, 900-1100°C, there is extensive cracking and this exposes fresh surfaces for further attack. Large quantities of y-$Y_2Si_2O_7$ and cristobalite are produced and the volume change initiates the cracks that make the process progressive.

It is only the quaternary Y-Si-O-N phases (N-melilite, N-apatite, N-YAM and N-α-wollastonite) that oxidise readily to give products with widely different specific volumes and Lange (10) points out that materials in which these do not occur, that is with overall compositions within the compatibility triangle Si_3N_4-Si_2N_2O-$Y_2Si_2O_7$, show excellent oxidation resistance at both 1000° and 1400°C. This has been amply confirmed. Figure 76 shows two specimens both oxidised at 1000°C for 120h. The upper, straight bar showing no change from its initial appearance was hot-pressed with additions of 5w/o SiO_2 + 5w/o Y_2O_3; the lower one, bent and widely cracked, was hot-pressed with 15w/o Y_2O_3. Comparative weight gains on oxidised powder samples are illustrated by Figure 77 which shows that the best yttria-silicon nitride is superior at 1000°C to silicon nitride hot-pressed with 2w/o MgO.

Figure 78 is the Si_3N_4-corner of the Y_2O_3-Si_3N_4-SiO_2 system on which lines representing 2, 5 and 10w/o surface silica are drawn.

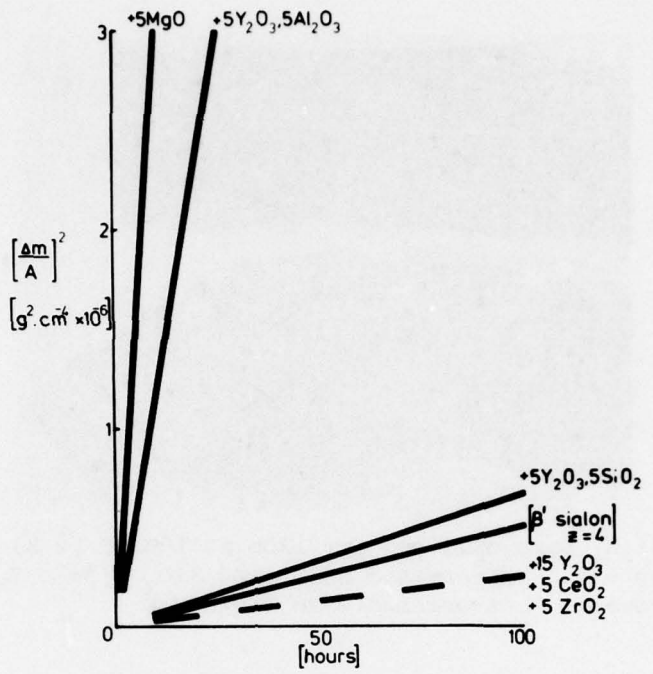

Figure 74. Oxidation rates of hot-pressed silicon nitride with different additives at 1400°C

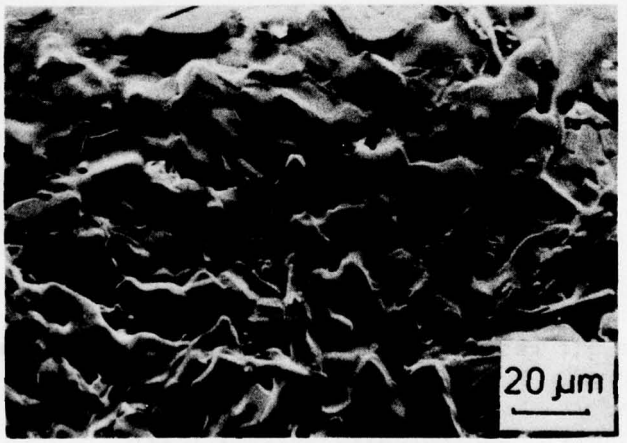

Figure 75. Si_3N_4:15w/o Y_2O_3 oxidised for 120h at 1400°C (S.E.M.)

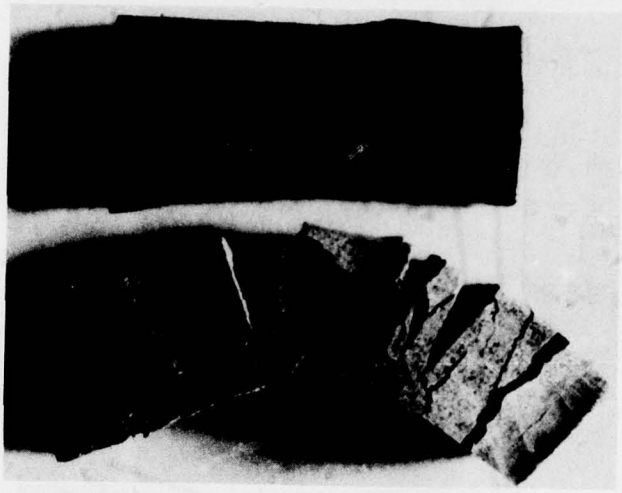

Figure 76. Si_3N_4 bars oxidised for 120h at 1000°C (x 2)
upper: hot-pressed with 5w/o SiO_2 + 5w/o Y_2O_3
lower: hot-pressed with 15w/o Y_2O_3

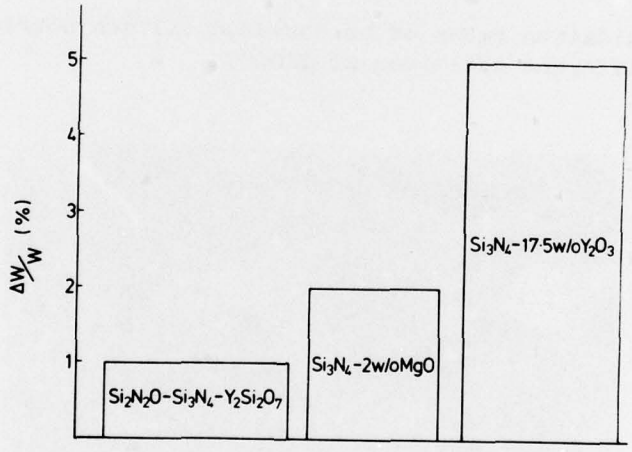

Figure 77. Weight gains for powder samples oxidised for 120h at 1000°C
left: hot-pressed with 5w/o SiO_2 + 5w/o Y_2O_3
middle: hot-pressed with 2w/o MgO
right: hot-pressed with 17.5w/o Y_2O_3

Clearly the amount of added yttria to bring the overall composition within the favourable Si_3N_4-Si_2N_2O-$Y_2Si_2O_7$ triangle depends very critically upon this amount of surface silica. However, in preventing the formation of the quaternary oxynitrides and so avoiding catastrophic oxidation at 1000°C, impurities such as calcium are no longer accommodated in a refractory phase but remain in the glass formed when the grain-boundary liquid is cooled. There is the possibility, therefore, that the high-temperature creep resistance is impaired by improving the oxidation resistance.

Both hot-pressed and pressureless-sintered materials containing 5w/o Y_2O_3: 5w/o Al_2O_3 show none of the break-down on oxidation at 1000°C experienced by some of the Y_2O_3-Si_3N_4 compositions. Samples oxidised for 120h at 1000° and 1400°C are shown in Figure 79. The weight gain at 1000°C is negligible. At 1400°C the surface glaze which contains some cristobalite is not completely protective and the parabolic rate constant of about $10^{-1}mg^2cm^{-4}h^{-1}$ is nearly 10^3 greater than that of the best hot-pressed Y_2O_3-Si_3N_4 at the same temperature. The lowest liquid formation in the Y_2O_3-SiO_2-Al_2O_3 system is at approximately 1350°C and so at temperatures much above this the oxidation of any yttrium-sialon will involve liquid and will consequently become more rapid.

XI.3 Ceria

The almost exact correspondence between the Ce-Si-O-N and the Y-Si-O-N systems suggests that the behaviour and properties of silicon nitride and sialons densified by addition of ceria will be similar to those using yttria after allowance is made for the reduction of ceric to cerous oxide. Thus, to prevent catastrophic oxidation the formation of quaternary cerium-silicon oxynitrides should be avoided.

The advantage of ceria is that it has a built-in safeguard to assist in maintaining the overall composition within what should be the oxidation-resistant Si_3N_4-Si_2N_2O-$Ce_2Si_2O_7$ compatibility triangle. According to equation (7), one mol of SiO_2 is produced for every two mols of Ce_2O_3. By comparing equations (10 and (11):

$$18SiO_2 + 9Y_2O_3 \longrightarrow 9Y_2Si_2O_7 \quad \ldots\ (10)$$

$$18SiO_2 + 24CeO_2 + 2Si_3N_4 \longrightarrow 12Ce_2Si_2O_7 + 4N_2 \quad \ldots\ (11)$$

it can be seen that for the same initial surface silica content on the silicon nitride nearly three times the molar concentration of CeO_2 (i.e. more than twice the weight per cent) can be added compared with Y_2O_3 before any nitrogen-apatite phase appears in the final product

(see Figure 78). On this basis, for the same concentrations by weight of additives, silicon nitride hot-pressed with ceria should be much more oxidation resistant than when hot-pressed with yttria.

Theoretical densities are obtained by hot-pressing silicon nitride with 2w/o CeO_2 for 1h at 1750°C and with somewhat more than 2w/o of each of CeO_2 and Al_2O_3 under the same conditions. Bars of silicon nitride containing 0, 2, 5, 10 and 20w/o CeO_2 have been oxidised for 120h at both 1000° and 1400°C and similar examinations have been made on specimens hot-pressed with 5w/o CeO_2:5w/o Al_2O_3 and 10w/o CeO_2:10w/o Al_2O_3.

As expected, the catastrophic oxidation found at 1000°C for compositions exceeding a critical yttria concentration is not observed at corresponding compositions in the ceria system. All the ceria-containing silicon nitrides showed little oxidation at 1000°C and X-ray photographs of the surface identified cristobalite and ceric oxide formed, presumably, by oxidation of the intergranular glassy phase. Both alumina-containing materials gave more surface oxide than the alumina-free specimens with a net-work of cracks and sub-micron holes due to gas evolution. With 10w/o Y_2O_3:10w/o Al_2O_3, layers of scale 1-2 um thick flaked off to expose fresh surfaces for further oxidation.

At 1400°C the Si_3N_4 with 2w/o CeO_2 showed little surface degradation but the higher ceria samples were all seriously corroded and showed clearly that the surface layer had been liquid at temperature. X-ray surface examination gave only cristobalite suggesting that the ceria was still present in the glassy phase. Extensive surface cracking on cooling is due to the thermal mismatch between this glassy phase and cristobalite. Again the alumina-containing samples were less oxidation resistant with micron-size grains of cristobalite growing in a surface glaze containing large gas bubbles and cracks.

In general, oxidation resistance with ceria additions is worse than with yttria, probably due to the lower temperature at which a liquid phase appears in the Ce-Si-O-N and Ce-Si-Al-O-N systems. The main disadvantage of the variable valency of cerium is that at high oxygen potentials Ce^{III} is oxidised to Ce^{IV} but, because the oxynitrides, silicates and aluminates all exist only with cerium in the trivalent Ce^{III} state, this oxidation is accompanied by conversion to CeO_2 at about 1400°C. Oxynitrides are decomposed with gas evolution which breaks up the oxidised surface.

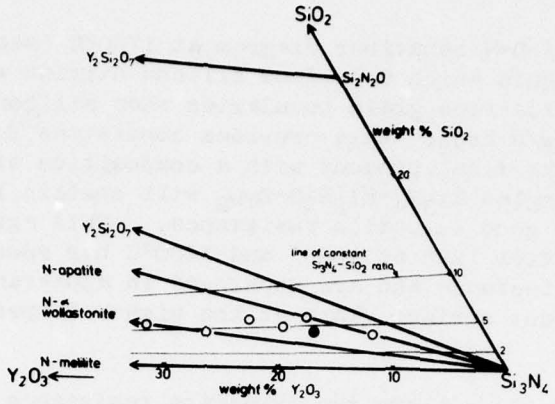

Figure 78. The Si_3N_4 corner of the Y_2O_3-Si_3N_4-SiO_2 system showing 2, 5 and 10w/o surface silica

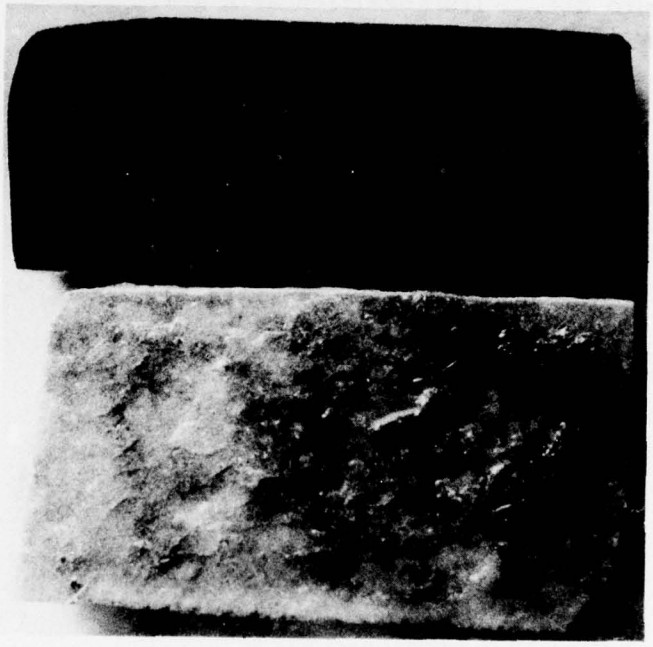

Figure 79. Si_3N_4 hot-pressed with 5w/o Y_2O_3:5w/o Al_2O_3 (x 5)
upper: after 120h at 1000°C
lower: after 120h at 1400°C

XI.4 Zirconia

From the Zr-Si-O-N behaviour diagram at 1700°C (see Figure 55) a small amount of liquid which dissolves silicon nitride will be formed locally at the silica-rich grain boundaries when silicon nitride is hot-pressed with 5w/o ZrO_2; this provides conditions for liquid-phase densification. The final product with a composition within the compatibility triangles Si_3N_4-Si_2N_2O-ZrO_2 will contain little glass and so should show good oxidation resistance. This agrees with the observation that after 120h at 1000° and 1400°C bar specimens show no detectable weight increase and are unchanged in appearance except for a very thin, coherent surface glaze at the higher temperature (see Figure 80).

With 5w/o ZrO_2:5w/o Al_2O_3 the oxidation resistance is no different at 1000° and 1400°C from that of silicon nitride hot-pressed with ZrO_2 alone. The ZrN''-type zirconium-aluminium oxynitride has not been found with small additions of ZrO_2 and Al_2O_3 but compositions containing large amounts of it disintegrate at 1000°C in air with large weight gains (see Figure 81). Its formation as a grain-boundary phase must therefore be avoided for good oxidation resistance.

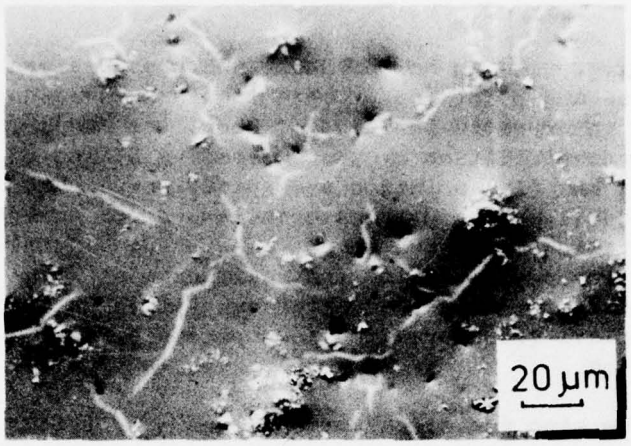

Figure 80. Si_3N:5w/o ZrO_2 oxidised for 120h at 1400°C (S.E.M.)

Figure 81. ZrN" oxidised for 120h at 1400°C (optical micrograph) (x 5)

XII. CONCLUSIONS

Oxide additives used in hot-pressing and pressureless sintering of silicon nitride and β'-sialon promote liquid-phase densification. Kinetic data are interpreted in terms of Kingery's model in which the contributions to densification by the successive stages of (i) rearrangement and (ii) solution-precipitation vary according to the particular additive. α-β transformation occurs during the solution-precipitation stage and where, as with MgO additions, much of the densification occurs during the rearrangement stage, only partial transformation is observed after densification is complete. In contrast, complete transformation accompanies partial densification with Y_2O_3 additions.

All additives give additional crystalline or vitreous phases in the product. These can impair strength, creep resistance or oxidation resistance, and in order to avoid this degradation of properties by suitable processing it is necessary to establish phase limits and phase relationships in the appropriate quaternary or quinary system. More research effort is required in this direction before some of the outstanding technological problems can be solved. So-far, an engineering ceramic with a combination of properties suitable for prolonged use in an oxidising environment at above 1400°C has not been obtained. With silicon nitride each of the additives magnesia, yttria and ceria has disadvantages. Zirconia has not yet been sufficiently investigated and it is uncertain whether it can be used effectively in pressureless sintering.

Additions of alumina with other oxides, notably yttria, to produce low z-value β'-sialons give promising materials and the possibility of obtaining single-phase β' by pressureless sintering with MgO or MgO-BeO additions is worth exploration. In both cases, post-preparative heat-treatment is necessary to devitrify grain-boundary vitreous phases or to incorporate them into the sialon structure.

Appendix I

Electron Probe Micro-analysis of Nitrogen Ceramics at the Atomic Energy Research Establishment, Harwell

I. Introduction

Nitrogen ceramics as-prepared in the hot-press are almost invariably multi-phase and therefore bulk chemical analysis is of limited use in the determination of phase compositions and phase relations. As the grain-size in hot-pressed silicon nitride-based materials is typically $\simeq$ 10um, an electron microprobe analyser is an ideal tool for the analysis of single crystals in polished hot-pressed samples.

Only the more recent microprobes have wavelength-dispersive spectrometers sufficiently sensitive to give quantitative X-ray analysis for light elements such as oxygen and nitrogen; the Cameca "Camebax" at Harwell has two of these spectrometers in addition to an energy-dispersive analyser and a computerised control system enabling simultaneous analysis for three or more heavy elements on the energy-dispersive analyser with two light elements on the spectrometers. Standardisation using internal standards, corrections for background and comparison of the energy-dispersive spectrum with standard element spectra are carried out automatically and the results printed by teletype. A typical five-element analysis, including two light elements, takes no longer than 120 seconds including counting, computations and printing of results.

II. Experimental

Hot-pressed samples were mounted in resin and polished to a 0.25μm finish by a "Logitech" automatic polishing machine. The polished samples, mounted as cylinders 1 cm dia. x 1 cm or 2.5 cm dia. x 1 cm, were carbon coated to reduce charging by the electron beam and earthed to the specimen holder by painting the contact area with colloidal graphite.

During the first visit to Harwell (April 1977) simultaneous operation of the energy dispersive analyser and the two spectrometers was not possible due to a fault in the computer software and therefore areas analysed by the energy-dispersive analyser were photographed to aid return to the same crystals after the beam conditions had been readjusted for optimum spectrometer performance. By the second visit,

however, the control system had been upgraded to allow simultaneous analysis of light and heavy elements as described above.

ZAF (atomic number-absorption-fluorescence) corrections were performed on the heavy elements assuming that the remainder of the sample was oxygen. As yet there is no satisfactory theoretical basis for ZAF correction of oxygen and nitrogen and thus corrections were by comparison with materials of similar known composition, for example N-melilite, $Y_2O_3Si_3N_4$, was used as the standard for N and O in investigation of the Y-Si-Al-O-N system, whereas AlN and MgO were used as standards in the Si-Al-O-N system.

The only other correction applied was to balance the analyses for the (total metals) and (total non-metals) concentrations using the known valencies of the elements.

Errors, where quoted, are calculated as twice the standard deviation of the analyses obtained and thus represent the statistical uncertainty in the analyses but not the systematic errors in the ZAF corrections.

III. Results

III.1 The Si-Al-O-N system

(a) X-phase

X-phase is found as a grain-boundary phase in the hot-pressing and sintering of Si_3N_4 with Al_2O_3 and is thus of considerable technological interest. Since it was first reported, however, several possible compositions have been proposed:

Jack (1973)	$SiAlO_2N$
Gauckler et al. (1975)	$Si_8Al_8O_{22}N_4$
Layden (1976)	$Si_3Al_6O_{12}N_2$

Recent work at Newcastle suggests that there are two forms of X-phase; "High-X" is formed by cooling from above the melting temperature and forms acicular crystals whereas "Low-X" is formed below the melting temperature and forms equiaxed crystals. Both are prepared in high yields near the composition $Si_7Al_9O_{23}N_3$. Three etched polished samples were analysed, one of "High-X" and two of "Low-X", and the results are summarised in Table 1. All the samples are deeply etched in the grain-boundary region and analysis of this region was possible in the "Low-X"

samples. This grain-boundary phase, deduced to be glassy due to the absence of crystalline second phases on the X-ray powder photographs, has a silica-rich composition and its presence agrees well with the previous evidence of vitreous phases in the low-melting region of the Si-Al-O-N system. The three analyses of X-phase lie close to the composition $Si_7Al_9O_{23}N_3$; the main variation is in the O/N ratio of the analyses, which is the most unreliable determination in the microprobe due to the low count rates observed for these elements and the unavailability of ZAF corrections for light elements.

Although these analyses agree fairly well with the proposed composition of X-phase they are not sufficiently accurate to pinpoint a precise composition.

(b) "8H" + "15R"

A sample containing a mixture of the Si-Al-O-N polytypes "8H" and "15R" was examined. The material was inhomogeneous and contained areas of Al_2O_3 and AlN (identified unambiguously by probe analysis) but the contrast difference and the grain sizes of the polytype phases were too small to be resolved in the reflected-electron image of the sample. Twenty-five random point analyses were taken and the average composition, neglecting areas rich in AlN and Al_2O_3, was found to be $Si_8Al_{37}O_{20}N_{34}$, close to the theoretical "15R" polytype composition $Si_8Al_{32}O_{16}N_{32}$ ($4AlN.SiO_2$).

III.2 The Y-Si-O-N system; N-apatite

The yttrium-silicon oxynitride N-apatite, isostructural with the mineral apatites, was originally reported to have the composition $Y_{10}(SiO_4)_6N_2$, but later preparations at this composition have failed to produce the phase pure.

X-ray powder photographs of N-apatite are indexed on the basis of a hexagonal unit cell, with dimensions varying between

$$\underline{a},\ 9.36\text{Å};\ \underline{c},\ 6.77\text{Å} \quad \text{and} \quad \underline{a},\ 9.37\text{Å};\ \underline{c},\ 6.75\text{Å}$$

The phase therefore has a small homogeneity range.

Substitution of Y^{3+} for Ca^{2+} together with Si^{4+} for P^{5+} and O^{2-} for $(OH)^{1-}$ in hydroxy-apatite gives the following series:

hydroxy-apatite	$Ca_{10}(PO_4)_6(OH)_2$
abukumalite	$Ca_4Y_6(SiO_4)_6(OH)_2$
spencite	$Ca_2Y_8(SiO_4)_6(O)_2$

Complete substitution of other trivalent cations such as La^{3+} gives an apatite with both cation and anion vacancies $La_8\square_2(SiO_4)_6\square_2$. In the present study, neither a yttrium silicate with the above composition nor with that quoted by Wills, $Y_{9.33}\square_{0.67}(SiO_4)_6O_2$, has been produced. Although density data suggest that the composition of N-apatite lies close to $Y_{10}(SiO_4)_6N_2$:

N-apatite (measured),	4430 kgm^{-3}
$Y_{10}(SiO_4)_6N_2$ (calculated),	4504 kgm^{-3}

compositional evidence suggests that the real composition is richer in silicon and nitrogen.

Four samples of N-apatite were analysed, two at each end of the range of unit cell dimensions; the results of the analyses are given in Table 2. The analyses suggest that the range of homogeneity of the N-apatite phase lies between the two approximate limits $Y_{10}(SiO_4)_6N_2$ and $Y_{9.67}\square_{0.33}(SiO_4)_6NO$. Subsidiary phases identified in the sample are consistent with the accepted phase diagram with the exception of a grain boundary phase in sample A. This phase lies near the lowest eutectic in the Y-Si-O-N system and its presence as a glass has been confirmed by etching with HF samples of N-apatite which are pure by X-ray analysis. It is suggested that previous difficulties in the preparation of pure N-apatite at its actual composition were due to the presence of this glass.

III.3 The Ce-Si-O-N system

Work on the Ce-Si-O-N system at Newcastle indicates that the phases found in this system are isostructural with those in the Y-Si-O-N system. When CeO_2 is hot-pressed with Si_3N_4 it is reduced to Ce_2O_3 and the Si_3N_4 oxidised to SiO_2 or Si_2N_2O according to the following equations:

$$Si_3N_4 + 12CeO_2 \longrightarrow 3SiO_2 + 6Ce_2O_3 + 2N_2$$

$$4Si_3N_4 + 6CeO_2 \longrightarrow 6Si_2N_2O + 3Ce_2O_3 + 2N_2$$

The phases formed by further reaction are N-wollastonite, N-YAM, and N-apatite which appears to have a triangular range of homogeneity between the limits $Ce_{10}(SiO_4)_6N_2$, $Ce_{9.33}\square_{0.67}(SiO_4)_6O_2$ and $Ce_8\square_2(SiO_4)_6\square_2$. Addition of carbon to reduce the silica content of the samples by loss of CO and SiO allows the formation of a N-melilite-type phase and a previously unobserved phase of approximate composition $Ce_2O_3.2Si_3N_4$.

Five samples were analysed and the results are summarised in Table 3.

There is an excellent agreement between the analyses of the oxynitride phases and their proposed compositions, as shown in Table 4. The only unknown in the system which is not fully characterized is the oxide apatite solubility range. In the samples there exists a fine dispersion of Ce_2O_3 among the apatite grains and so it was difficult to identify and analyse individual grains due to the very low contrast difference between the apatite and Ce_2O_3.

III.4 The Zr-Al-O-N system

When 1 mol ZrO_2 is hot-pressed with 2 mols AlN a phase is formed which appears to be structurally related to zirconium nitride, ZrN. The X-ray diffraction pattern of this phase, ZrN", is related to that of ZrN by a superlattice and it is therefore difficult to judge the relative proportions of nitride and oxynitride due to the overlap of the strongest lines in the X-ray diffraction pattern.

One sample of hot-pressed $ZrO_2.2AlN$ was examined and it was obvious from the reflected electron image that the sample contained two phases in equal quantities. One phase contained only zirconium and nitrogen and was analysed as $ZrN_{0.5}$. The other phase, containing aluminium, was analysed as $ZrAl_{4.6}O_{6.1}N_{0.7}$. Although the nitrogen and oxygen analyses may be fairly inaccurate due to the difficulty of correcting for zirconium, which absorbs oxygen and nitrogen strongly, the Zr:Al ratio of 1:4.6 and the fact that the sample contains approximately 50% zirconium nitride, suggests that ZrN" contains less zirconium and nitrogen than originally proposed ($ZrAl_2O_2N_2$).

III.5 The Y-Si-Al-O-N system

(a) β' + glass

There exists within the Y-Si-Al-O-N system a large region where hot-pressed samples contain only β'-sialon and glass. The aim of these analyses was to determine the composition of the grain-boundary phase and compare its composition with that of pure nitrogen glasses prepared at Newcastle.

The first sample examined was prepared by hot-pressing 20w/o Y_2O_3, 40w/o Al_2O_3, and 40w/o Si_3N_4. In the reflected-electron image (see Figure 1) there is excellent contrast between the dark β' crystals and the lighter grain-boundary glass. The z-value of the β'-sialon obtained by analysis (2.4) is in good agreement with the X-ray value

(2.6) and the glass, with a composition of $Y_9Si_{14}Al_{15}O_{58}N_4$ (a/o) is within the expected glass-forming region.

The second sample, prepared in the 2:3 plane of the Y-Si-Al-O-N system by hot-pressing Si_2N_2O, Y_2O_3 and Al_2O_3 in the molar proportions 15:8:20, had shown a considerable weight loss and in this case the BN surrounding the sample in the hot-press is dense and appears to be impregnated with the glass. The electron micrograph (Figure 2) shows well-shaped grains of β'-sialon with a hexagonal cross section contained in a matrix of glass. The z value of the sialon crystals, determined as 2.4 by analysis, agrees well with the X-ray value, and the glass composition, $Y_{10}Si_{12}Al_{17}O_{57}N_5$, both as free glass and in the impregnated BN is close to that of the previous sample.

(b) Y_2SiAlO_5N

In the 2:3 plane of the Y-Si-Al-O-N diagram there are two phases, N-α-wollastonite ($YSiO_2N$) and low-YAP ($YAlO_3$) which have similar structures. Midway between these compositions, at Y_2SiAlO_5N, lies a phase which is produced at temperatures near 1650°C and can be indexed on the same hexagonal pseudo-cell. An electron micrograph of a sample containing the phase is shown in Figure 3. The specimen contains three phases: a dark phase analysed as β'-sialon with z-value 3.3; dendrites of a light-coloured phase, analysed as $Y_{2.0}Si_{1.0}Al_{0.9}O_{5.4}N_{0.7}$; and a grey matrix analysed as $Y_{11}Si_{13}Al_{14}O_{57}N_5$, corresponding to the glasses analysed in the previous samples.

This analysis shows the power of the electron microprobe as an analytical tool in that the contrast in the electron imaging system allows three phases to be distinguished easily although one phase only is apparent on the X-ray diffraction pattern and there is no contrast whatsoever when the sample is viewed under reflected light. Furthermore, a full analysis of each phase identified β'-sialon and glass and confirmed the proposed composition for Y_2SiAlO_5N.

III.6 Nitrogen glasses

Nitrogen-containing glasses have been identified in the Y-Si-Al-O-N system and also the Ca-Si-Al-O-N system. These results and analyses of the amorphous phases in the Y-Si-O-N and Si-Al-O-N systems are summarised in Table 5. In each case the nitrogen content is less than 10a/o with the exception of the glass in the Y-Si-O-N system but this is explained by the fact that the glass areas in this case were small and contained acicular crystals of Si_3N_4.

The Y-Si-Al-O-N glass compositions lie very close together and they suggest that under the conditions of slow cooling within the hot press, the glass-forming region in the Y-Si-Al-O-N system is small and has the approximate composition $Y_{10}Si_{13}Al_{15}O_{57}N_5$.

IV. Conclusions

Although electron probe analyses must be used with caution and only in conjunction with results obtained by other analytical techniques such as X-ray diffraction, these results show that the probe is a powerful tool for the analysis of individual phases in multi-phase nitrogen ceramics.

Appendix I

Figure 1. Scanning electron micrograph of β'-sialon (dark) and YSiAlON glass (light) (x 2000)

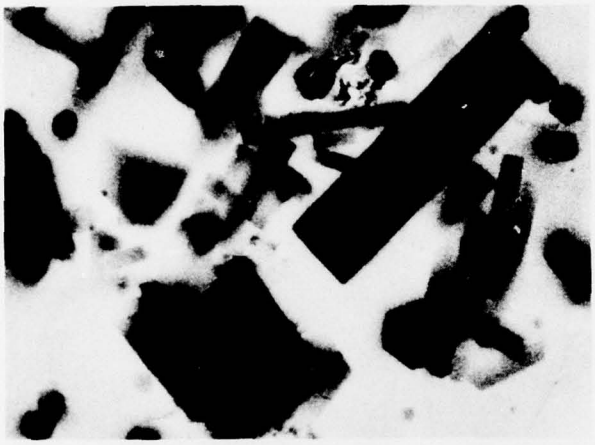

Figure 2. Scanning electron micrograph of β'-sialon grains in a YSiAlON glass matrix (x 3000)

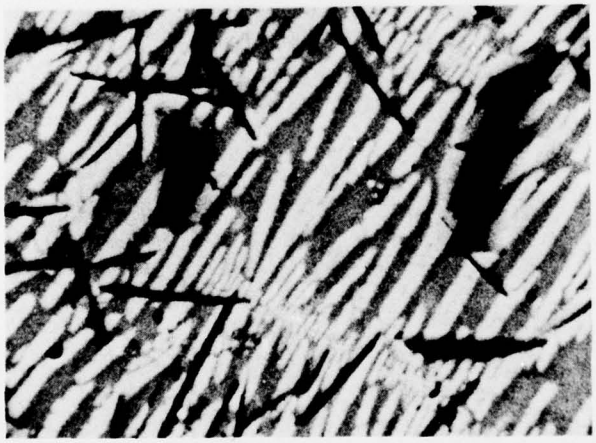

Figure 3. Scanning electron micrograph of β'-sialon (black), YSiAlON glass (grey) and Y_2SiAlO_5N (white) (x 2000)

Table 1. X-phase

sample	X-ray analysis phases present	electron probe analysis (w/o) Si	Al	O	N	number of analyses
A	Low X, β', Al_2O_3	26	31	34	9	6
B	Low X	22	33	38	6	5
C	High X	29	27	37	7	4*
B	Grain boundary	41	13	42	3	2

* analyses on first visit to Harwell when simultaneous determination of Si,Al,O,N was not possible

Table 2. Y-N-Apatite

sample	X-ray analysis phases present	electron probe analysis (w/o) Y	Si	O	N	number of analyses	other phases identified by electron probe
A	Apatite, a, 9.37; c, 6.75; Si_3N_4, $Y_2Si_2O_7$	61	11	27	1	3	Si_3N_4 (mainly dispersed in grain-boundaries)
A	Grain-boundary	41	25	28	7	2	
B	Apatite, a, 9.37; c, 6.75	62	11	21	1	4	$Y_2Si_2O_7$
C	Apatite, a, 9.36; c, 6.77; N-α-wollastonite	63	10	26	2	5	N-YAM
D	Apatite, a, 9.36, c, 6.77	63	10	25	2	3	Y_2O_3

Table 3. The Ce-Si-O-N system

sample	phase	analysis (a/o)				number of analyses	other phases identified by electron probe
		Ce	Si	O	N		
A	$Ce_8(SiO_4)_6$ (apatite)	21	16	63	0	3	B-N-C inclusions
A	$Ce_2Si_2O_7$	20	17	63	0	2	
B	$Ce_{9.3}(SiO_4)_6$ (apatite)	27	11	63	0	4	
C	Melilite	17	25	23	35	3	New phase, Si_3N_4
C	α-wollastonite	20	20	40	20	4	
D	YAM	28	13	45	15	2	Wollastonite, new phase, Ce_2O_3
D	$Ce_{10}(SiO_4)_6N_2$ (apatite)	23	15	56	6	3	
E	New phase	11	31	16	42	3	Apatite

Table 4. Cerium-silicon oxynitrides

structural type	theoretical composition	analysed composition
Apatite	$Ce_{10}Si_6O_{24}N_2$	$Ce_{10.0}Si_{6.4}O_{23.8}N_{2.6}$
Melilite	$Ce_2Si_3O_3N_4$	$Ce_{2.0}Si_{3.0}O_{2.7}N_{4.2}$
α-Wollastonite	$CeSiO_2N$	$Ce_{1.0}Si_{1.0}O_{2.0}N_{1.0}$
"YAM"	$Ce_4Si_2O_7N_2$	$Ce_{4.0}Si_{1.8}O_{6.5}N_{2.2}$
New type	$Ce_2Si_6O_3N_8$ ($Ce_2O_3.2Si_3N_4$)	$Ce_{2.0}Si_{5.7}O_{2.9}N_{7.7}$

Table 5. Nitrogen glasses

microprobe analysis (a/o)	crystalline phases present
$Si_{25}Al_{11}O_{58}N_5$	Low-X
$Y_{13}Si_{25}O_{48}N_{14}$	Si_3N_4 dispersed within glass; N-apatite
$Y_9Si_{14}Al_{15}O_{58}N_4$	β'-sialon
$Y_{10}Si_{12}Al_{17}O_{57}N_5$	β'-sialon
$Y_{11}Si_{13}Al_{14}O_{57}N_5$	β'-sialon, Y_2SiAlO_5N
$Ca_{10}Si_{18}Al_{11}O_{57}N_4$	none
$Ca_{11}Si_{18}Al_{11}O_{51}N_9$	none

Appendix II

Attendance at Scientific Meetings

1. Professor Jack and Dr. Thompson attended the meeting "High-temperature chemistry of inorganic and ceramic materials" arranged jointly by the Chemical Society and the British Ceramic Society at the University of Keele, September 1976. They presented, by invitation, two papers:

   (i) "Sialons and related nitrogen ceramics: their crystal chemistry, phase relationships, properties and industrial potential"
   (ii) "Polytypes in the Si-Al-O-N and related systems"

2. Professor Jack attended the American Ceramic Society's Fall Meeting in San Francisco in November 1976 and presented three papers:

   (i) "Phase relations in the Y-Si-O-N and Y-Si-Al-O-N systems"
   (ii) "Sialon polytypes"
   (iii) "Sialon glasses"

3. Professor Jack attended the Fifth AMMRC Materials Technology Conference "Ceramics for High-Performance Applications - II" at Newport in March 1977 and presented a paper:
   (i) "The role of additives in the densification of nitrogen ceramics"

4. Dr. Hendry, Dr. Thompson and Dr. Rae attended the "3eme Journees d'Etudes dur les Nitrures" at the Ecole des Mines de Paris, Fontainebleau, in June 1977 and presented three papers (in French):

   (i) "The structure of X-phase"
   (ii) "Lattice imageing of sialon polytypes"
   (iii) "The oxidation of silicon nitride with oxide additions"

5. Professor Jack attended a meeting "Corrosion of ceramics" at Leatherhead in June 1977 and presented a paper:

   (i) "Sialons and related nitrogen ceramics"

Appendix III

Publications

III.1 Papers published

(i) K.H. Jack, "Sialons and related nitrogen ceramics: their crystal chemistry, phase relationships, properties and industrial potential" in "High Temperature Chemistry of Inorganic and Ceramic Materials" edited by F.P. Glasser and P.E. Potter, pp 204-221. 1977 London: The Chemical Society

(ii) P.H.A. Roebuck and D.P. Thompson, "Polytypes in the Si-Al-O-N and related systems" in "High Temperature Chemistry of Inorganic and Ceramic Materials" edited by F.P. Glasser and P.E. Potter, pp 222-228. 1977 London: The Chemical Society

III.2 Papers in the press

(i) D.R. Clarke, T.M. Shaw and D.P. Thompson, "Direct observation of the polytype periodicities in the Be-Si-O-N system", J. Mat. Sci.

(ii) D.P. Thompson and L.J. Gauckler, "Further study of the Be-Si-O-N polytypes", J. Amer. Ceram. Soc.

(iii) D.P. Thompson, "Note on silicon cerium oxynitride", J. Mat. Sci.

(iv) A.W.J.M. Rae, D.P. Thompson and K.H. Jack, "The role of additives in the densification of nitrogen ceramics", Proceedings of the Fifth AMMRC Materials Technology Conference 1977.

(v) K.H. Jack, "The relationship of phase diagrams to research and development of sialons" in "Phase Diagrams: Materials Science and Technology, volume 5", edited by A.M. Alper

REFERENCES

1. S. Wild, P. Grieveson, K.H. Jack and M.J. Latimer, Special Ceramics, 5, 377, (1972).

2. G.R. Terwilliger and F.F. Lange, J. Amer. Ceram. Soc. 57, 25, (1974).

3. P. Drew and M.H. Lewis, J. Mat. Sci. 9, 261, (1974).

4. K.H. Jack, 2nd Army Materials Technology Conference, "Ceramics for High-Performance Applications", Hyannis 1973, p. 265, Brook Hill Pub. Co. (1974).

5. W.D. Kingery, J. Appl. Phys. 30, 301, (1959).

6. R.J. Weston and T.G. Carruthers, Proc. Brit. Ceram. Soc. 22, 197, (1973).

7. R.J. Brook, T.G. Carruthers, L.J. Bowen and R.J. Weston, Proc. NATO Advanced Study Institute, "Nitrogen Ceramics", Canterbury 1976, to be published.

8. G.E. Gazza, Bul. Amer. Ceram. Soc. 54, 778, (1975).

9. A.W.J.M. Rae, D.P. Thompson, N.J. Pipkin and K.H. Jack, Special Ceramics, 6, 347, (1975).

10. F.F. Lange, S.C. Singhal and R.C. Kuznicki, J. Amer. Ceram. Soc. 60, 249, (1977).

11. R.R. Wills, J.A. Cunningham, J.M. Wimmer and R.W. Stewart, J. Amer. Ceram. Soc. 59, 269, (1976).

12. A.W.J.M. Rae, Ph.D. Thesis, The University of Newcastle upon Tyne, 1976.

13. W.D. Kingery, J.M. Woulbroun and F.R. Charvat, J. Amer. Ceram. Soc. 46, 391, (1963).

14. I. Colquhoun, D.P. Thompson, W.I. Wilson, P. Grieveson and K.H. Jack, Proc. Brit. Ceram. Soc. 22, 181, (1973).

15. R.R. Wills, R.W. Steward and J.M. Wimmer, Amer. Ceram. Soc. Bull. 56, 194, (1977).

16. J.P. Torre and A. Mocellin, Proc. NATO Advanced Study Institute, "Nitrogen Ceramics", Canterbury 1976, to be published.

17. P.H.A. Roebuck, Ph.D. Thesis, The University of Newcastle upon Tyne, 1977.

18. L.J. Gauckler, H.L. Lukas and G. Petzow, J. Amer. Ceram. Soc. 58, 346, (1975).

19. D.P. Thompson, Proc. NATO Advanced Study Institute, "Nitrogen Ceramics", Canterbury 1976, to be published.

20. K.H. Jack, J. Mat. Sci. 11, 1135, (1976).

21. D.R. Clarke, T.M. Shaw and D.P. Thompson, J. Mat. Sci. 13, (1978), to be published.

22. G.K. Layden, 1976, Paper presented at the Basic Science Fall Meeting of the American Ceramic Society, San Francisco.

23. J.D. Venables, D.K. McNamara and R.G. Lye, Proc. NATO Advanced Study Institute, "Nitrogen Ceramics", Canterbury 1976, to be published.

24. R.J. Lumby, B. North and A.J. Taylor, Proc. 5th Army Materials Technology Conference "Ceramics for High-Performance Applications II", Newport 1977, to be published.

25. L.J. Gauckler, S. Boskovic, G. Petzow and T.Y. Tien, to be published.

26. A. Kant and K. Moon, 1977. Private communication.

27. L.J. Gauckler, Proc. 5th Army Materials Technology Conference "Ceramics for High-Performance Applications II", Newport 1977, to be published.

28. Y. Oyama and O. Kamigaito, Japan J. Appl. Phys. 10, 1637, (1971).

29. K.H. Jack and W.I. Wilson, Nature Phys. Sci. (London), 238, 28, (1972).

30. K.H. Jack, Trans. J. Brit. Ceram. Soc. 72, 376, (1973).

31. P. Drew and M.H. Lewis, J. Mat. Sci. 9, 261, (1974).

32. S. Wild, Special Ceramics, 6, 309, (1975).

33. E. Gugel, I. Petzenhauser and A. Fickel, Powder Met. Int. 7, 66, (1975).

34. D.P. Thompson, J. Mat. Sci. 11, 1377, (1976).

35. D.P. Thompson and L.J. Gauckler, J. Mat. Sci. 13, (1978), to be published.

36. K. Komeya, H. Inoue and A. Tsuge, J. Amer. Ceram. Soc. 57, 411, (1974).

37. K. Komeya, Doctoral thesis. Private communication (1977).

38. A. Hendry, D.S. Perera, D.P. Thompson and K.H. Jack, Special Ceramics, 6, 321, (1975).

39. S. Wild, Private communication, (1976).

40. L.J. Gauckler, H.L. Lukas and T.Y. Tien, Mat. Res. Bull. 11, 503, (1976).

41. I. Oda, Proc. NATO Advanced Study Institute, "Nitrogen Ceramics", Canterbury 1976, to be published.

42. A.W.J.M. Rae, D.P. Thompson and K.H. Jack, Proc. 5th Army Materials Technology Conference, "Ceramics for High-Performance Applications II", Newport 1977, to be published.

43. R.R. Wills, S. Holmquist, J.M. Wimmer and J.A. Cunningham, J. Mat. Sci. 11, 1305, (1976).

44. A. Tsuge, K. Komeya, H. Hashimato, K. Nishida and T. Ishii, Toshiba Review 30, 580, (1975).

45. R.R. Wills and J.A. Cunningham, J. Mat. Sci. 12, 208, (1977).

46. D.P. Thompson, J. Mat. Sci. 13, (1978).

47. R.R. Wills, R.W. Stewart, J.A. Cunningham and J.M. Wimmer, J. Mat. Sci. 11, 749, (1976).

48. P.E.D. Morgan and P.J. Carroll, Mat. Res. Bull. 12, 251, (1977).

49. M. Mizumo, R. Berjoun, J.P. Coutures and M. Foex, Yogyo-Kyokai-Shi, 83, 90, (1975).

50. G. Cevales, Ceramurgia, 11, 159, (1972).

51. Y. Inomata, Y. Hasegawa, T. Matsuyama and Y. Yajima, Yogyo-Kyokai-Shi, 84, 600, (1976).

52. N. Claussen, R. Wagner, L.J. Gauckler and G. Petzow, Paper presented at meeting of American Ceramic Society, Chicago, April 1977. To be published.

53. P.F. Becher and S.A. Halen, Proc. 5th Army Materials Technology Conference, "Ceramics for High-Performance Applications II", Newport 1977. to be published.

54. G.A. Jeffrey and V.Y. Wu, Acta Cryst. 16, 566, (1963).

55. G.A. Jeffrey and V.Y. Wu, Acta Cryst. 20, 538, (1966).

56. J.L. Henry, J.H. Russell and H.J. Kelly, 1969 U.S. Bureau of Mines Report No. 7320.

57. T.H. Elmer and M.E. Nordberg, J. Amer. Ceram. Soc. 50, 275, (1967).

58. K.H. Jack and D.P. Thompson, 1973 Progress Report No. 11 on "The Crystal Chemistry of Ceramic Phases in the Si-N-O and Related Systems", Ministry of Defence Contract AT/2043/028AML.

59. M. Mitomo, J. Mat. Sci. 11, 1103, (1976).

60. W.C. Tripp and H.C. Graham, J. Amer. Ceram. Soc. 59, 399, (1976).

61. G.R. Terwilliger and F.F. Lange, J. Mat. Sci. 10, 1169, (1975).

62. I. Colquhoun, S. Wild, P. Grieveson and K.H. Jack, 1973 Proc. Brit. Ceram. Soc. 22, 207.

63. A. Hendry, Proc. NATO Advanced Study Institute, "Nitrogen Ceramics", Canterbury 1976, to be published.

64. R.L. Coble, J. Appl. Phys. 41, 4798, (1970).

65. L.J. Bowen, R.J. Weston, T.G. Carruthers and R.J. Brook. Private communication 1977; to be published in Ceramurgia.

66. G.R. Terwilliger and F.F. Lange, J. Amer. Ceram. Soc. 57, 25, (1974).

67. M. Mitomo, J. Mat. Sci. 11, 1103, (1976).

68. F.F. Lange (1976). Paper presented at the Basic Science Fall Meeting of the American Ceramic Society, San Francisco.